NTNU – Trondheim
Norwegian University of
Science and Technology

Linear and Nonlinear Analysis of a High-rise Building Excited by Earthquake

Lineær og ikke-lineær analyse av høyhus utsatt for jordskjelveksitasjon

Bård Hagberg Stana

Civil and Environmental Engineering
Submission date: June 2014
Supervisor: Svein N Remseth, KT
Co-supervisor: Amir Kaynia, KT

Norwegian University of Science and Technology
Department of Structural Engineering

Department of Structural Engineering
Faculty of Engineering Science and Technology
NTNU- Norwegian University of Science and Technology

ACCESSIBILITY

OPEN

MASTER THESIS 2014

SUBJECT AREA:	DATE:	NO. OF PAGES: 132
Structural dynamics	02.06.2014	(20 + 86 + 26)

TITLE:

Linear and Nonlinear Analysis of a High-rise Building Excited by Earthquake

Lineær og ikke-lineær analyse av høyhus utsatt for jordskjelveksitasjon

BY:

Bård Hagberg Stana

SUMMARY:

The purpose of this thesis is to evaluate the linear and nonlinear response of a high-rise building located in Norway. The Oslo Plaza building, located in Oslo, has been chosen for this purpose. A finite element model of the structure was created in the structural analysis program SAP2000 with emphasis on representing the nonlinear behavior as correctly as possible. Modifications of ground motion data was performed to better represent a typical earthquake in a Norwegian environment, and the seismic response of the building was investigated using several different analysis methods.

Oslo Plaza was found to behave linearly for earthquakes with an expected return period of 475 years, while for a 3000-year earthquake major nonlinear effects are expected to occur, especially in the longitudinal direction. Oslo Plaza should however still not collapse during an earthquake of this magnitude, even though it is expected to experience permanent deformations. While dimensioning high-rise buildings for 475-year earthquakes the response spectrum method described in EC8 was found to be adequate.

RESPONSIBLE TEACHER: Svein N. Remseth

SUPERVISOR(S): Svein N. Remseth

CARRIED OUT AT: Department of Structural Engineering

Department of Structural Engineering
Faculty of Engineering Science and Technology
NTNU - The Norwegian University of Science and Technology

MASTER THESIS SPRING 2014

For

Bård Hagberg Stana

Linear and Nonlinear Analysis of a High-rise Building Excited by Earthquake

Lineær og ikke-lineær analyse av høyhus utsatt for jordskjelveksitasjon

High-rise buildings do not necessarily have to be the structures that are the most exposed to damage during earthquakes. The risk for damages occurring will depend largely on which mode shapes get dynamically amplified. This thesis will focus on different conditions associated with modeling and analysis of a high-rise building.

The purpose of the thesis is to:

- achieve an understanding of the fundamental principles for the dynamic modeling of a high-rise building and utilize the structure's ductility
- perform modeling and analysis of a building and discuss the results compared to simplified modeling and possible calculations according to Eurocode 8

The report should include the following topics:

- theory for ductile behavior of structures including the creation of plastic hinges
- theory about earthquakes with a focus on earthquakes in Norway
- descriptions of damping, stiffness and active mass during dynamic analysis of constructions
- analysis of natural periods of a typical high-rise building

- perform dynamic analysis with excitation on the foundation level and compare and discuss the results including the effects of uncertainties in the model
- compare to simplified analysis described by Eurocode 8
- conclusions

The thesis should be performed according to the guidelines for theses provided by The Department of Structural Engineering. Changes in the design have to be considered according to the nature of the thesis.

Supervisor: Professor Svein Remseth

The thesis must be submitted to The Department of Structural Engineering at NTNU by June 10, 2014.

Preface

This thesis was completed the spring semester 2014 at The Norwegian University of Science and Technology, NTNU, at the Department of Structural Engineering, which is part of The Faculty of Engineering Science and Technology.

The thesis is a continuation of the project *Earthquake design after Eurocode 8* carried out in the fall semester 2013 in the field of structural dynamics and earthquake engineering.

First I would like to give a huge thanks to my supervisor Professor Svein N. Remseth for providing theoretical basis, weekly follow-up, discussions and always being able to answer any questions I might have. I would also like to thank Adjunct Professor Amir M. Kaynia for great follow-up, helpful discussions and for providing me with valuable ideas for my thesis. Next I would like to thank Associate Professor Anders Rønnquist for providing theoretical basis about tuned liquid dampers.

I would like to thank MSc Øystein Flakk at EDRMedeso AS for providing me with a licence for SAP2000, always being available for answering questions about the software and valuable help with my FEM model. Last, I would like to thank MSc Bjørn Svendsen for providing me with background information regarding the master thesis *The Effects of Near-fault Earthquakes On a High-rise Structure In The Oslo Area* completed the spring semester 2012.

Trondheim, June 2, 2014

Bård Hagberg Stana

Abstract

The purpose of this thesis is to evaluate the linear and nonlinear response of a high-rise building located in Norway. The Oslo Plaza building, located in Oslo, has been chosen for this purpose. A finite element model of the structure was created in the structural analysis program SAP2000 with emphasis on representing the nonlinear behavior as correctly as possible. Modifications of ground motion data was performed to better represent a typical earthquake in a Norwegian environment, and the seismic response of the building was investigated using several different analysis methods.

Oslo Plaza was found to behave linearly for earthquakes with an expected return period of 475 years, while for a 3000-year earthquake major nonlinear effects are expected to occur especially in the longitudinal direction. Oslo Plaza should however still not collapse during an earthquake of this size, even though it is expected to experience permanent deformations.

While dimensioning high-rise buildings for 475-year earthquakes the response spectrum method described in EC8 was found to be adequate. For most engineering firms this is by far be the easiest method for analysing a high-rise building considering its simplicity and the fact that nonlinear direct integration time history analyses require significantly more computational power and calculation times.

An interesting point found during the work with this thesis is that the swimming pool located in the top-stories of Oslo Plaza might work as a tuned liquid damper during the building's linear seismic response. This damping effect was found to have the potential to be significant if the dimensions of the swimming pool had been altered by only a few meters.

Keywords: Ground-motion; High-rise structure; Oslo; Nonlinear; Tuned liquid damper; Dynamic analysis

Sammendrag

I denne rapporten er den lineære og ikke-lineære responsen til en høy bygning i Norge evaluert. Oslo Plaza har blitt valgt til dette formålet, og en numerisk element-modell av bygningen har blitt laget i analyseprogrammet SAP2000. I denne modellen har hovedfokuset vært på å modellere den ikke-lineære responsen til bygningen så korrekt som mulig. Tidsserier fra tidligere jordskjelv har blitt modifisert for å bedre representere norske forhold, og den seismiske responsen til bygningen har deretter blitt kalkulert ved å bruke flere forskjellige analysemetoder.

Resultatene av analysene viser at Oslo Plaza oppfører seg elastisk for jordskjelv med forventet returperiode på 475 år, mens for 3000-års jordskjelv er det forventet at betydelige ikke-lineære effekter oppstår, spesielt i lengderetningen av bygget. Det er derimot ikke forventet at Oslo Plaza kollapser under et jordskjelv av denne størrelsen, selv om bygget vil oppleve permanente deformasjoner.

Respons-spektrum metoden som er beskrevet i Eurokode 8 viser seg å være tilstrekkelig ved dimensjonering av høyhus med tanke på 475-års jordskjelv. For de fleste firmaer vil dette være den mest relevante analysemetoden å bruke, grunnet dens enkelhet og det faktum at andre analysemetoder, som ikke-lineære direkte integrasjons tidsserieanalyser, krever betraktelig mer regnekraft og bruker mange ganger så stor regnetid.

Et interessant poeng som ble funnet under arbeidet med denne oppgaven var at svømmebassenget i Oslo Plaza har potensiale til å virke som en demper under byggets lineære seismiske respons og drastisk redusere forskyvninger og krefter i systemet. For å få noen nytte av denne effekten burde dimensjonene til bassenget vært forandret med noen få meter.

Nøkkelord: Jordskjelv; Høy bygning; Oslo; Ikke-linear; Tuned liquid damper; Dynamisk analyse

Contents

List of Tables

List of Figures

Nomenclature

Latin letters

A	Maximum ground displacement
A_{fault}	Area of fault
a	Acceleration
$a_0(t)$	Original time history
$a_1(t)$	Adjusted time history
a_{g40Hz}	Acceleration of bedrock normalized to 1 g
a_{gR}	Peak ground acceleration
a_{vg}	Vertical ground acceleration
b_j	Set of coefficients
B	Width of water tank
$\mathbf{b}$	Vector pf coefficients
c	The damping of a SDOF system
c_{ij}	Components in $\mathbf{C}_b$
c_v	Damping of equivalent TMD
C^*	Modal damping
$\mathbf{C}$	Damping matrix
$\mathbf{C}_b$	Coefficient matrix
$\mathbf{M}^*$	Modal damping matrix
D_{fault}	Average displacement of fault
E_{Edx}	Time history component in x-direction
E_{Edy}	Time history component in y-direction
E_{Edz}	Time history component in z-direction
$f_j(t)$	Set of adjustment functions
f_v	Frequency of equivalent TMD
$\mathbf{F}$	Nodal force matrix
g	Gravity, 9.81 m/s^2
h_i	Acceleration impusle response
h_0	Water depth in tank
k	The stiffness of a SDOF system
k_n	Number of modes used in analysis
k_v	Stiffness of equivalent TMD
K^*	Modal stiffness
$\mathbf{K}$	Stiffness matrix
$\mathbf{K}^*$	Modal stiffness matrix

$\mathbf{K_E}$	Elastic stiffness matrix
$\mathbf{K_G}$	Geometric stiffness matrix
L	Length of water tank
L^*	Modal load
$\mathbf{L}^*$	Modal load matrix
m	The mass of a SDOF system
m_L	Mass of liquid in TLD
m_v	Mass of equivalent TMD
M_0	Seismic moment
M_L	Richter local magnitude
M_S	Surface wave magnitude
M_W	Moment magnitude
M^*	Modal mass
$\mathbf{m}^*$	Modal mass vector
$\mathbf{M}$	Mass matrix
$\mathbf{M}^*$	Modal mass matrix
n	Number of degrees-of-freedom
N	Total number of floors in structure / Number of spectral points
$p(t)$	Forcing function
$p_e(t)$	External loading
$p_v(t)$	Fluid force
P	Axial load
P_i	Polarity of response
$\mathbf{P(t)}$	Load vector
q	Modal amplitude displacement
$\dot{q}$	Modal amplitude velocity
$\ddot{q}$	Modal amplitude acceleration
$\mathbf{q}$	Modal amplitude displacement vector
$\dot{\mathbf{q}}$	Modal amplitude velocity vector
$\ddot{\mathbf{q}}$	Modal amplitude acceleration vector
Q_i	Target spectrum
r_{no}	Peak modal response
R	Estimation of eigenfrequency
R_i	Absolute value of peak response
r_o	Peak response
S	Soil amplification factor

S_a	Pseudo spectral acceleration
S_d	Pseudo spectral displacement
S_v	Pseudo spectral velocity
t	Time
T	Eigenperiod of system
$\mathbf{T}$	Size of displacement or rotation from each mode to displacement or rotation in the total system
u	Relative displacement of a SDOF system
$\ddot{u}_g$	Ground acceleration
$\mathbf{u}$	Displacement vector
$\dot{u}$	Relative velocity of a SDOF system
$\ddot{u}$	Relative acceleration of a SDOF system
$\ddot{u}_g$	Ground acceleration
$\ddot{u}_t$	Absolute acceleration of a SDOF system
$\ddot{u}_v$	Acceleration of equivalent TMD
$\dot{\mathbf{u}}$	Velocity vector
$\ddot{\mathbf{u}}$	Acceleration vector
v	Assumed fundamental mode shape
V	Base shear force

Greek letters

α	Rayleigh damping scale factor
β	Rayleigh damping scale factor
β_i	Damping for a given frequency
Δ	Interstory drift
Δ_e	Distance from seismometer to epicenter in degrees
ϵ	Water depth ratio
ϕ_j	The eigenvector of the j-th eigenfrequency
$\mathbf{\Phi}$	Modal matrix
γ	Relaxation factor
Γ	Participation factor
μ_r	Shear strength of fractured rock
μ_v	Mass ratio
ν	Liquid kinematic viscosity
ω_0	Angular frequency of a SDOF system
ω_D	Damped angular frequency
ω_v	Angular frequency of equivalent TMD

ρ	Correlation factor
τ	Time integration factor
ξ	Damping ratio
ξ_v	Damping ratio of equivalent TMD

Combination of latin and greek letters

$P-\Delta$	Second order effect of gravity loads on laterally deformed structures
$P-\theta$	Relationship between forces and moments
$\delta a(t)$	Adjustment time history
δR	Difference between target spectrum and computed spectrum
$\delta \mathbf{R}$	Vector containing difference between target spectrum and computed spectrum

Abbrevations

AMD	Active mass damper
CQC	Complete quadratic combination
DOF	Degree-of-freedom
EW	East-West
FEM	Finite Element Method
HHT	Hilber-Hughes-Taylor alpha
MDOF	Multiple-degree-of-freedom
NS	North-South
NORSAR	Norwegian Seismic Array
NTNU	The Norwegian University of Science and Technology
PGA	Peak ground acceleration
SDOF	Single-degree-of-freedom
SRSS	Square-root-sum-of-squares
TLD	Tuned liquid damper
TMD	Tuned mass damper

1 Introduction

Norway is considered a low-seismicity area and seismic design has historically not been highly prioritized. However, both the Oslo area and especially the seabed west of Norway have experienced some major earthquakes throughout history. The best example of this is perhaps the 1904 Oslo earthquake which had a magnitude of 5.4 and occurred 100 km south of Oslo [1]. Parts of Oslo have a foundation of deep clay deposits, which can severely amplify the seismic response. This, in addition to the tendency to build higher buildings and the increased use of high-performance materials makes seismic design more important than ever.

The objective of the presented research is to create and analyse a fine element model of a high-rise structure located in the Oslo-area. For this purpose, the Oslo Plaza building has been chosen, and a model of this building has been created in the structural analysis program SAP2000. This model has then been exposed to acceleration time histories to calculate the dynamic behavior of a high-rise building during earthquakes.

This thesis is divided into 7 chapters and 7 appendices. Following is a short description of each chapter.

Chapter 2 gives a theoretical background for the rest of the thesis. Basic seismology is presented in addition to discussions about the history of earthquakes in Norway. Next, dynamics for a single-degree-of-freedom system and a multiple-degree-of-freedom system are introduced in addition earthquake response analysis and damping used in these. There is also a short section on estimation of natural periods in systems. Thereafter, the nonlinear response of buildings are discussed, before finally, a method for calculating the effect of tuned liquid dampers are outlined.

Chapter 3 provides an explanation of the FEM-model used for analyses, in addition to the acceleration time histories used. This chapter also contains an explanation of how these time histories are modified to better represent Norwegian conditions.

Chapter 4 describes the different analyses performed in addition to containing the results obtained from these analyses and brief discussions of these results.

Chapter 5 contains discussions and comparisons of the results obtained in chapter 4.

Chapter 6 provides conclusions and summarizes the work with this thesis.

Chapter 7 presents suggestions for further work in this area.

2 Theoretical background

2.1 Seismology

2.1.1 Plate tectonics

The understanding of earthquakes starts with the understanding of the physical structure of the earth. The earth consists of several different plates, and there are three different boundaries between these plates: convergent, divergent and transform plate boundaries. The earth consists of six continental-sized plates and about 14 subcontinental plates [2]. These plates are illustrated in Figure 2.1.

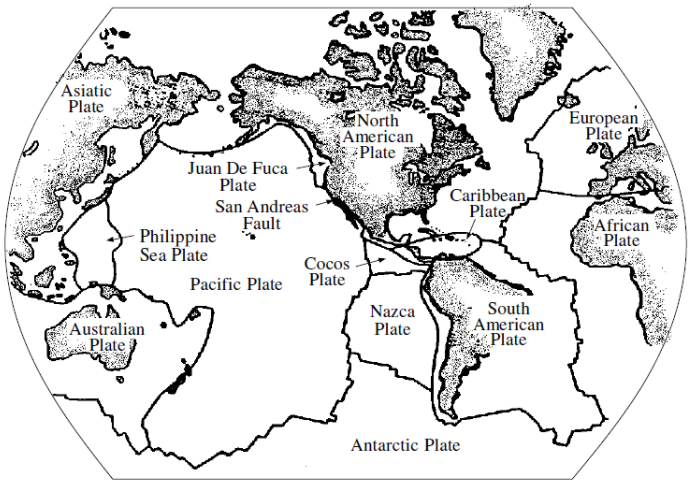

Figure 2.1: Simplified map of the Earth's crustal plates [3]

Earthquakes mainly occur on the boundary between two plates, especially along convergent plate boundaries where one plate slides beneath another. The area with most seismic activity is called the circum-Pacific belt. This area includes the coastal regions of North- and Central America, Chile, Indonesia and Japan [4]. This area, along with the other most active areas, is shown in Figure 2.2. It is possible to see the correlation between plate boundaries and earthquake activity by comparing Figure 2.2 to Figure 2.1.

2.1.2 Earthquake terminology

Earthquakes occur when massive amounts of elastic energy is released as seismic waves. This happens as a result of rupture and slippage along faults, fractures in Earth's crust. The focus, or hypocenter, of an earthquake is the point where the earthquake originates,

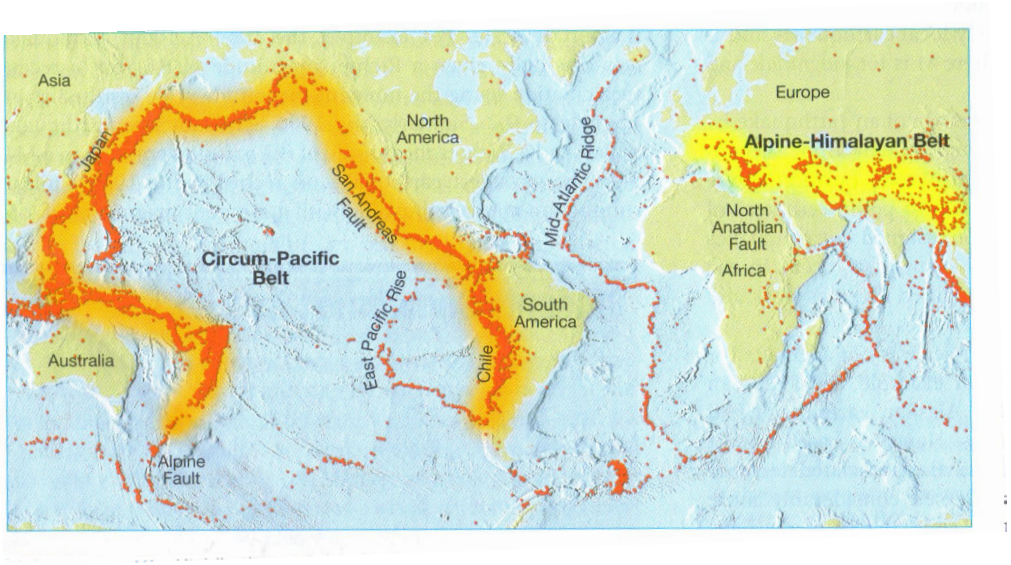

Figure 2.2: Distribution of earthquakes with magnitude of 5 or more for a 10-year period [4]

mostly at depths between 5 and 700 kilometers. The epicenter is the point at the surface directly above the focus [4]. These definitions are shown visually in Figure 2.3.

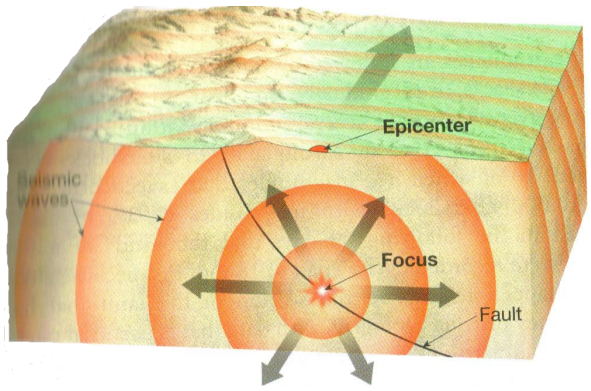

Figure 2.3: Definition of earthquake terms [4]

2.1.3 Seismic waves

The seismic waves can be divided into two categories; waves traveling through the ground, and waves traveling on the surface of the earth. There are two different types of waves traveling through the ground; P-waves and S-waves. P-waves are pressure waves, while S-waves are shear waves. The S-waves travel slower than the P-waves and can only travel through solid material [5]. Figure 2.4 illustrates these two wave types.

The two normal most types of waves traveling on the surface are Love-waves and Rayleigh-waves. Love-waves travel parallel to the surface, while in a Rayleigh-wave the points on

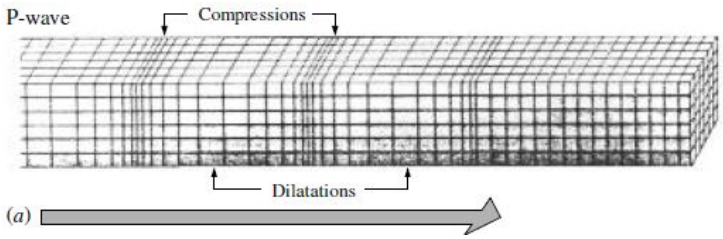

(a) Illustration of P-waves

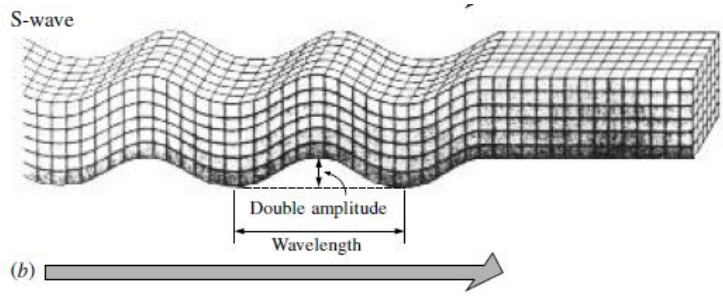

(b) Illustration of S-waves

Figure 2.4: Diagram illustrating the two types of seismic waves traveling through the ground [3]

the surface move in a vertical oval motion. The best illustration of this is water waves, which are Rayleigh-waves. These two types of waves propagate even slower than S-waves, with Rayleigh-waves being the slowest [5]. Figure 2.5 illustrates these two types of surface waves.

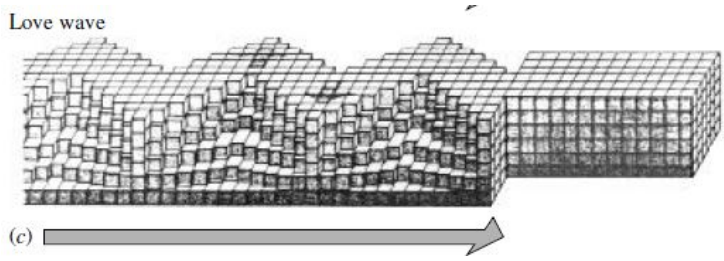

(a) Illustration of Love-waves

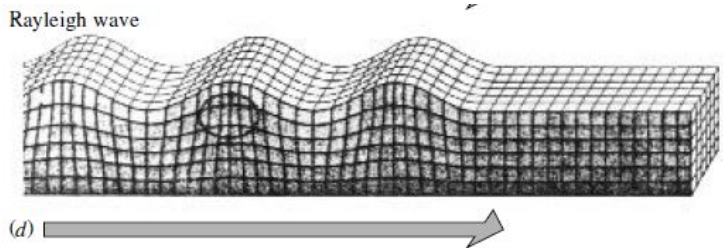

(b) Illustration of Rayleigh-waves

Figure 2.5: Diagram illustrating two of the seismic wave types that travel on the ground surface [3]

2.1.4 Size of earthquakes

Historically, descriptions of the size of earthquakes have been based on qualitative experiences of the effects of the experience. During the past 80 years however, modern instruments have been developed to measure the ground motions during an earthquake [2]. In 1935, Charles Richter developed what is now the most famous magnitude scale for shallow, local earthquakes; the Richter local magnitude (M_L). The Richter magnitude uses the base logarithm of the earthquake's maximum amplitude measured by a Wood-Anderson seismograph and correct it to a distance of 100 km [3]. In general, an earthquake with magnitude of 5 or larger can be expected to produce damaging ground motions. Even though the Richter scale is the best known amplitude description, it is not always the best way to describe earthquakes. This is because it is not suitable to describe earthquakes with magnitude larger than 7.5, or those which are located more than 1000 km away.

To describe moderate and large earthquakes more than 1000 km away, with a focal depth of less than about 70 km it is normal to use the surface wave magnitude. The reason for this is that at this distance the motion is dominated by surface waves as most of the body waves have been attenuated. The formula for the surface wave magnitude is shown in formula 2.1

$$M_S = logA + 1.66log\Delta_e + 2.0 \tag{2.1}$$

where A is the maximum ground displacement measured in micrometers and Δ is the distance from the seismometer to the epicentral measured in degrees. The surface wave magnitude is however not suitable to describe earthquakes with a magnitude larger than 8.

A magnitude scale that is suitable to describe very large earthquakes is the moment magnitude. This amplitude is based on the seismic moment instead of the ground shaking. The moment magnitude is given by equation 2.2

$$M_W = \frac{logM_0}{1.5} - 10.7 \tag{2.2}$$

where M_0 is given by

$$M_0 = \mu_r A_{fault} D_{fault} \tag{2.3}$$

M_0 is the seismic moment, μ_r is the shear strength of the fractured rock, A is the area of the fault and D_{fault} is the average displacement of the fault [2].

2.2 Earthquakes in Norway

During an earthquake, the ground moves rapidly back and forth and this can potentially cause large deformations and damage to structures. Buildings must therefore be designed in order to withstand the effects of earthquakes, both to spare human lives and material assets. On the Norwegian mainland, there has not been very many large earthquakes historically, but all structures (with a few exceptions) still have to be designed for earthquake loads. This is especially important when it comes to structures for the petroleum industry, along the western coast and on the continental shelf, in addition to new types of structures and designs constructed and materials used. Throughout the last 30 years it has also become clear that we can expect higher seismic activity in Norway and on the continental shelf in the future [1].

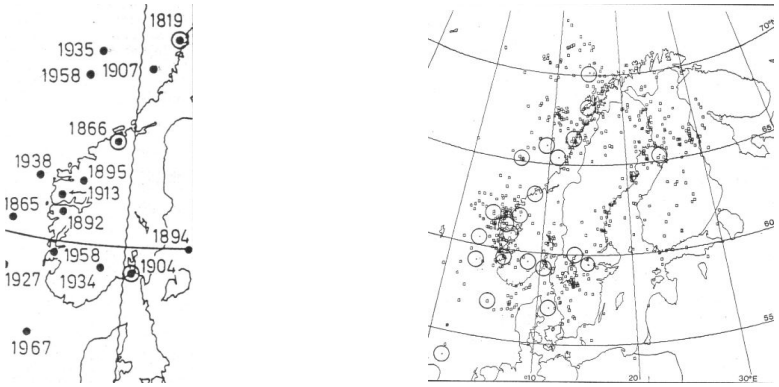

(a) Earthquakes larger than a magnitude of 5 on the Richter scale since year 1800. Double circles show earthquakes with a magnitude of 6.0-6.5

(b) Instrumentally recorded earthquakes in Scandinavia between 1951 and 1975. Large circles show magnitude greater than 5.0.

Figure 2.6: Earthquakes in Norway and Scandinavia [6]

Figure 2.6 shows the distribution of earthquakes recorded in Norway and in Scandinavia. As shown, there have been several earthquakes with a magnitude of 5.0 or higher on the Richter scale. This can be a contrast to the publicly accepted opinion that "We do not experience earthquakes in Norway". Even if an earthquake has an epicenter either on the seabed of the Atlantic or outside of Norway's borders, it can still affect Norwegian cities. Figure 2.7 shows an example of how far away the effects of an earthquake in Oslo can be felt.

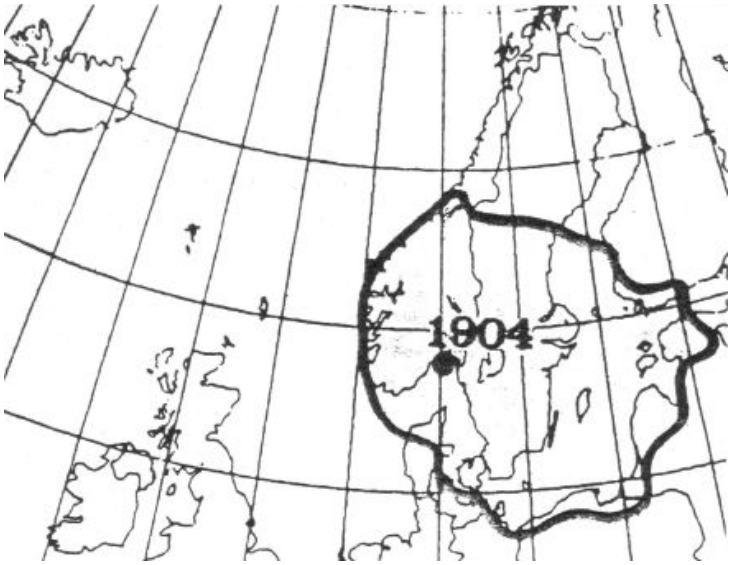

Figure 2.7: The area where the earthquake in the Oslo Fjord in 1904 could be felt [6]

The peak ground acceleration, or PGA, of an earthquake is the largest acceleration recorded by a seismograph. NORSAR and Norwegian Geotechnical Institute have created maps with contour lines showing which PGAs for earthquakes can be expected in Norway for different annual exceedance probabilities [1]. Figure 2.8 shows an example for the annual exceedance probability of $2.1 \cdot 10^{-3}$, which corresponds with a return period of 475 years. These values are a_{g40Hz}, which means they are values for the acceleration of the bedrock normalized to 1 g for the frequency $f = 40\ Hz$. For the Oslo region, where Oslo Plaza is located, the figure gives an expected a_{g40Hz} between 0.5 m/s^2 and 0.6 m/s^2 with an annual exceedance probability of $2.1 \cdot 10^{-3}$. According to EC8 [7] NA.3.2.1 the PGA a_{gR} can be found from the formula

$$a_{gR} = 0.8 \cdot a_{g40Hz} \tag{2.4}$$

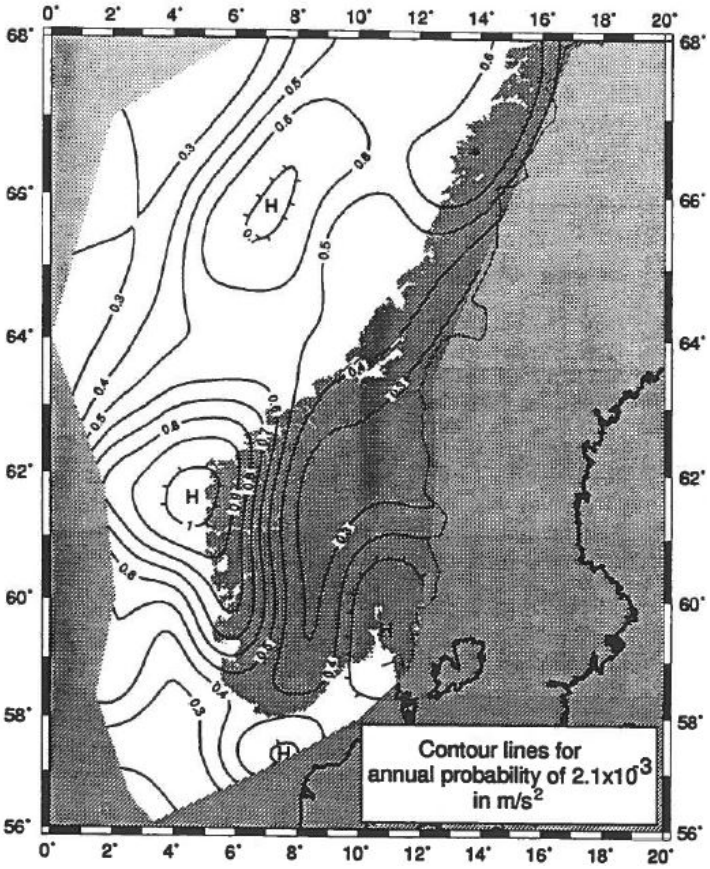

Figure 2.8: a_{g40Hz} contours in m/s^2 for annual exceedance probability of $2.1 \cdot 10^{-3}$ (return period 475 years) [1]

2.3 Dynamics for a single-degree-of-freedom system

When a building is subjected to an earthquake, both the motion from the earthquake and the building's response is time-dependent. A dynamical approach must therefore be applied when dealing with problems involving earthquakes [1].

For a simple single-degree-of-freedom system (shown in Figure 2.9), hereafter referred to as SDOF system, the characteristic equation of motion is

$$m\ddot{u}_t + c\dot{u} + ku = p(t) \tag{2.5}$$

where

$$\ddot{u}_t = \ddot{u} + \ddot{u}_g \tag{2.6}$$

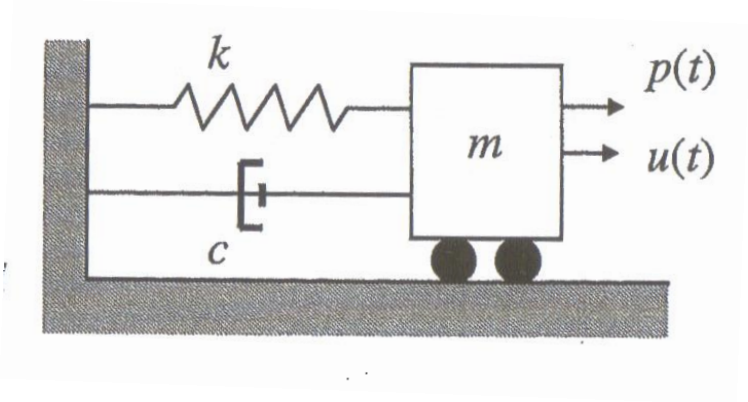

Figure 2.9: A typical SDOF system [8]

$$\ddot{u} = \frac{d^2u}{dt^2} \tag{2.7}$$

$$\dot{u} = \frac{du}{dt} \tag{2.8}$$

u_g is the ground motion, u is the motion of the SDOF system, m, c and k are the mass, damping and stiffness of the system, and $p(t)$ is the forcing function. Combining equation 2.5 and 2.6 with the dynamic equilibrium requirement $p(t) = 0$, we end up with the following equation of motion for a 1-DOF system subjected to a ground acceleration [3]

$$m\ddot{u} + c\dot{u} + ku = -m\ddot{u}_g \tag{2.9}$$

For an undamped system, the angular frequency is given by $\omega_0 = \sqrt{(k/m)}$. If damping is then introduced, the damping ratio is $\xi = c/(2km)$, and the damped angular frequency is $\omega_D = \omega_0\sqrt{(1-\xi^2)}$ [8]. A normal assumption is to set the damping ratio ξ equal to 0.05.

The relationship between a system's eigenperiod and frequency is describer by equation 2.10.

$$T = \frac{1}{f} = \frac{2\pi}{\omega} \tag{2.10}$$

where T is the eigenperiod of the system and f is the eigenfrequency.

2.4 Dynamics for a multi-degree-of-freedom system

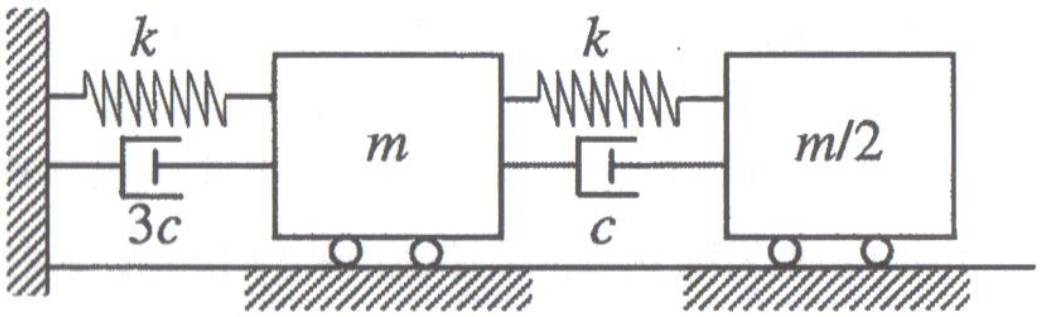

Figure 2.10: A simple 2-DOF system [8]

For most systems, the response cannot be described be a SDOF model, but rather by a multi-degree-of-freedom system. Hereafter referred to as a MDOF system. A typical 2-DOF system is shown in Figure 2.10. With several degrees of freedom, the system will now be described by equations containing vectors and matrices, where the size of the vectors and matrices depends on the numbers of degrees of freedom, n. A linear MDOF system is characterized by

$$\mathbf{M\ddot{u}} + \mathbf{C\dot{u}} + \mathbf{Ku} = \mathbf{P}(t) \tag{2.11}$$

where $\mathbf{M}$ is the mass matrix, $\mathbf{C}$ the damping matrix, $\mathbf{K}$ the stiffness matrix, $\mathbf{u}(t)$ the displacement vector and $\mathbf{P}(t)$ the load vector [8]. Solving equation 2.11 is harder than solving equation 2.5 not only because it is a matrix equation, but also because the damping matrix $\mathbf{C}$ introduces complications. The stiffness matrix might contain not only the elastic stiffness of the system, but also its geometric stiffness [3]. The stiffness matrix will then be given by

$$\mathbf{K} = \mathbf{K_E} + \mathbf{K_G} \tag{2.12}$$

where $\mathbf{K_E}$ is the elastic stiffness matrix and $\mathbf{K_G}$ the geometric stiffness.

When considering the free vibration of an undamped system , equation 2.11 becomes

$$\mathbf{M\ddot{u}} + \mathbf{Ku} = \mathbf{0} \tag{2.13}$$

This equation can be tranformed into the linear eigenvalue problem for ω_0 shown in equation 2.14 [8].

$$\mathbf{K}\phi_j = \omega_j^2 \mathbf{M}\phi_j \tag{2.14}$$

ϕ_j is the eigenvector corresponding to the j-th eigenfrequency. For a MDOF system with n degrees of freedom this equation has n solutions, where the lowest eigenfrequency and its corresponding eigenmode is called the fundamental mode.

The vector $\mathbf{m}^*$ is called the modal mass vector. It describes the distribution of the structure's mass matrix over the different modes. The model mass of mode n is given by

$$m_n^* = \phi_n^T \mathbf{M}\phi_n \tag{2.15}$$

The matrix $\mathbf{T}$ defines the size of the displacement or rotation from each mode to the displacement or rotation in the total system's degrees of freedom. $\mathbf{\Gamma}$ is called the participation factor and describes the contribution from the different modes to the displacement or rotation in the i degrees of freedom. The participation factor for mode n to displacement i is given by

$$\Gamma_n = \frac{\phi_n^T \mathbf{M}\mathbf{T}_i}{m_n^*} \tag{2.16}$$

2.5 Earthquake response analysis

2.5.1 Modal analysis of earthquake response

A commonly used procedure to determine the dynamic response of a system is the modal analysis. As seen in Section 2.4 the equation of motion for a MDOF system can be written as

$$\mathbf{M}\ddot{\mathbf{u}} + \mathbf{C}\dot{\mathbf{u}} + \mathbf{K}\mathbf{u} = \mathbf{P}(t) \tag{2.17}$$

$\mathbf{P}(t)$ can be rewritten as $\mathbf{P}(t) = -\mathbf{M}\mathbf{T}\ddot{u}_g(t)$ where $\mathbf{T}$ is the strain matrix derived from the shape functions used in the finite element formulation and $\ddot{u}_g$ is the ground acceleration [9]. Equation 2.17 thus becomes

$$\mathbf{M\ddot{u}} + \mathbf{C\dot{u}} + \mathbf{Ku} = -\mathbf{MT}\ddot{u}_g(t) \tag{2.18}$$

Using the mode shapes of the system, $\mathbf{u}$ can be written as

$$\mathbf{u} = \mathbf{\Phi q} \tag{2.19}$$

where $\mathbf{\Phi}$ is the modal matrix containing the mode shapes of the system and $\mathbf{q}$ is the modal coordinates. When combining equation 2.18 and equation 2.19 the following equation is obtained.

$$\mathbf{M}^*\ddot{\mathbf{q}} + \mathbf{C}^*\dot{\mathbf{q}} + \mathbf{K}^*\mathbf{q} = -\mathbf{L}^*\ddot{u}_g(t) \tag{2.20}$$

where

$$\mathbf{M}^* = \mathbf{\Phi}^T\mathbf{M\Phi} \tag{2.21}$$

$$\mathbf{C}^* = \mathbf{\Phi}^T\mathbf{C\Phi} \tag{2.22}$$

$$\mathbf{K}^* = \mathbf{\Phi}^T\mathbf{K\Phi} \tag{2.23}$$

$$\mathbf{L}^* = \mathbf{\Phi}^T\mathbf{MT} \tag{2.24}$$

Equation 2.20 can be written as n uncoupled equations

$$M_i^*\ddot{q}_i + C_i^*\dot{q}_i + K_i^*q_i = -L_i^*\ddot{u}_g(t), \quad i = 1, 2, ..., n \tag{2.25}$$

Dividing through with M_i^* the following equation is obtained for each mode i

$$\ddot{q}_i + 2\xi_i\omega_i\dot{q}_i + \omega_i^2 q_i = \frac{-L_i^*}{M_i^*}\ddot{u}_g(t) \tag{2.26}$$

where ξ_i is the damping ratio of the ith mode, defined as

$$\xi_i = \frac{C_i^*}{2M_i^*\omega_i} \tag{2.27}$$

Equation 2.26 for each mode can be solved either by using the Duhamel Integral or by using step-by-step methods like the Newmark method. A Matlab script using the Newmark method can be found in appendix B, while the Duhamel Integral is

$$q_i(t) = \frac{-L_i^*}{M_i^*}\frac{1}{\omega_i}\int_0^t \ddot{u}_g(\tau)e^{-\xi_i\omega_i^2(t-\tau)}sin\ \omega_{Di}(t-\tau)d\tau, \quad i = 1, 2, ..., n \tag{2.28}$$

The total displacement of the structure can then be found from equation 2.19. After the total displacements are found, the forces acting on the structure, the nodal forces, can be found from

$$\mathbf{F} = \mathbf{Ku} \tag{2.29}$$

Using the equation for an undamped free vibration system, $\mathbf{K}\phi_i = \omega_i^2\mathbf{M}\phi_i$, equation 2.29 can be rewritten as

$$\mathbf{F} = \mathbf{K\Phi q} = \mathbf{M\Phi}\omega^2\mathbf{q} \tag{2.30}$$

2.5.2 Response spectra

A response spectrum shows the maximum acceleration, velocity or displacement of a SDOF system as a function of period when subjected to an earthquake. This can be a very convenient way to obtain maximum responses, as no response history analysis have to be carried out [9]. Response spectra are easily available and can be found in Eurocode 8 [7] or other standards.

Response spectra can be derived from a single ground motion record. If this is done for several different ground motions, one can draw a smoothed response spectrum curve with straight lines. This is the type of spectrum found in EC8 [7] and other standards.

The pseudo spectral displacement, S_d, pseudo spectral velocity, S_v, and pseudo spectral acceleration, S_a, are defined as [3]

$$S_{v_i}(\xi_i, \omega_i) = [\int_0^t \ddot{u}_g(\tau)sin(\omega_{Di}(t-\tau)e^{-\xi_i\omega_i^2(t-\tau)}d\tau]_{max} \tag{2.31}$$

$$S_{d_i}(\xi_i, \omega_i) = \frac{1}{\omega_i} S_{v_i}(\xi_i, \omega_i) \tag{2.32}$$

$$S_{a_i}(\xi_i, \omega_i) = \omega_i S_{v_i}(\xi_i, \omega_i) \tag{2.33}$$

Response spectra use the approximation that *the absolute acceleration is at all times proportional to the relative displacement* [8], and the following simplifications can be used for a SDOF system with moderate to small damping

$$S_d = Max.\ relative\ displacement \tag{2.34}$$

$$S_a \approx Max.\ absolute\ acceleration \tag{2.35}$$

The most normal response spectra are plots of the pseudo acceleration plotted against either the frequency or the period of the SDOF system. This is the kind of response spectrum that can be found in Eurocode 8 [7].

For the i-th mode the maximum modal response is defined as

$$q_{i,max} = \frac{L_i^*}{M_i^*} S_{d_i} = \frac{L_i^*}{M_i^*} \frac{1}{\omega_i} S_{v_i} = \frac{L_i^*}{M_i^*} \frac{1}{\omega_i^2} S_{a_i} \tag{2.36}$$

Using the pseudo spectral acceleration the displacement and nodal forces can then be written as

$$\mathbf{u}_{i,max} = \phi_i q_{i,max} = \phi_i \frac{L_i^*}{M_i^*} \frac{1}{\omega_i^2} S_{a_i} \tag{2.37}$$

$$\mathbf{F}_{i,max} = \mathbf{K}\mathbf{u}_{i,max} = \mathbf{K}\phi_i q_{i,max} = \mathbf{K}\phi_i \frac{L_i^*}{M_i^*} \frac{1}{\omega_i^2} S_{a_i} \tag{2.38}$$

and combining with equation 2.30

$$\mathbf{F}_{i,max} = \mathbf{M}\phi_i \frac{L_i^*}{M_i^*} \frac{1}{\omega_i^2} S_{a_i} \tag{2.39}$$

The base shear force of the structure is often of interest, and using virtual work it can be shown that the base shear in a specific direction can be written as

$$V_{i,max} = \mathbf{T}\mathbf{F}_{i,max} = \mathbf{T}\mathbf{M}\phi_i \frac{L_i^*}{M_i^*} \frac{1}{\omega_i^2} S_{a_i} = \frac{(L_i^*)^2}{M_i^*} S_{a_i} \tag{2.40}$$

To obtain inelastic design spectra the elastic response spectra are scaled by a structural behavior factor, $q > 1$, which accounts for the building's ability to deform elastically and dissipate energy in that way. It is important to make sure that the value for q used in the analysis correctly matches the ductility properties of the building. The scaled response spectrum reduces the inelastic problem to an equivalent elastic problem which is much easier to handle.

2.5.3 Modal combination rules

The responses from the modal analysis will attain their peaks at different times, so these peak modal responses can therefore not be summed to achieve the peak value of the total response. A simple summation will give an answer that is overly conservative. Therefore there exists several modal combination rules, and two of the normal most ones will be explained here: the *square-root-of-sum-of-squares* rule and the *complete quadratic combination* rule. The peak value of the total response is here denoted r_o, while the peak modal response of mode n is denoted $r_{no}, (n = 1, 2, \ldots, N)$ where N is the total number of modes used.

In the square-root-of-sum-of-squares (SRSS) rule the total peak response is given by

$$r_o \approx (\sum_{n=1}^{N} r_{no}^2)^{1/2} \tag{2.41}$$

This modal combination rule gives good estimates for structures with well-separated eigenperiods, but does not take into account coupling between terms [9].

The complete quadratic combination (CQC) rule on the other hand overcomes this limitation. The peak of the total response according to the CQC rule is given by

$$r_0 \approx (\sum_{i=1}^{N} \sum_{n=1}^{N} \rho_{in} r_{io} r_{no})^{1/2} \tag{2.42}$$

where ρ_{in} is the correlation factor for modes i and n, varying between 0 and 1. Equation 2.42 can also be written as

$$r_o \approx (\sum_{n=1}^{N} r_{no}^2 + \underbrace{\sum_{i=1}^{N} \sum_{n=1}^{N}}_{i \neq n} \rho_{in} r_{io} r_{no})^{1/2} \tag{2.43}$$

since $\rho_{in} = 1$ for $i = n$.

2.6 Damping

For nonlinear analyses the damping matrix, $\mathbf{C}$, of a system has to be defined completely. For a multistory building with a similar structural system and materials over its height classical damping is an appropriate idealization. The classical damping matrix can be found by using either Rayleigh damping or Caughey damping [9]. In the following section the Rayleigh procedure will be outlined.

2.6.1 Rayleigh damping

As seen in Section 2.11, the dynamic response of a MDOF-system can be written as

$$\mathbf{M\ddot{u}} + \mathbf{C\dot{u}} + \mathbf{Ku} = \mathbf{P}(t) \tag{2.44}$$

The damping term in this equation can be be calculated by Rayleigh damping, using the following equation [10]:

$$\mathbf{C} = \alpha\mathbf{M} + \beta\mathbf{K} \tag{2.45}$$

where α and β are scale factors calculated from

$$\alpha = \frac{2(\xi_i\omega_j - \xi_j\omega_i)\omega_i\omega_j}{\omega_j^2 - \omega_i^2} \tag{2.46}$$

$$\beta = \frac{2(\xi_j\omega_j - \xi_i\omega_i)}{\omega_j^2 - \omega_i^2} \tag{2.47}$$

where ω_i and ω_j are two of the eigenfrequencies of the system and ξ_i and ξ_j are their corresponding damping ratios, approximately equal to 0.02.

The damping ratio for each mode i can thereafter be calculated from [11]:

$$\xi_i = \frac{1}{2\omega_i}\alpha + \frac{\omega_i}{2}\beta \tag{2.48}$$

2.7 Estimation of eigenfrequencies

An upper bound to the fundamental eigenfrequency can be estimated by using the Rayleigh Quotient method. Assuming a fundamental mode shape v, this approximation is given by

$$\omega_1^2 \approx R = \frac{\mathbf{v}^T\mathbf{K}\mathbf{v}}{\mathbf{v}^T\mathbf{M}\mathbf{v}} \tag{2.49}$$

For a system with n modes, R must lie in the interval $\omega_1^2 \leq R \leq \omega_n^2$ [8].

Using the Dunkerley-Mikhlin method, it is possible to find a lower bound to the fundamental eigenfrequency. Used together with the Rayleigh Quotient method this gives a range for the fundamental eigenfrequency. The Dunkerley-Mikhlin method is given by

$$\omega_1 \approx \frac{1}{\sqrt{tr(\mathbf{K}^{-1}\mathbf{M})}} \tag{2.50}$$

where tr means the trace of a matrix, in other words the sum of its diagonal values. The disadvantage of this method is that it requires the diagonal values of $\mathbf{K}^{-1}$, which might be computationally expensive to find [8].

2.8 Nonlinear response of buildings

In earthquake engineering the inelastic earthquake response of buildings is of great importance, as most buildings, when subjected to strong earthquakes, are expected to deform past the limit point for elastic behavior. This chapter will cover nonlinear phenomena and how these are handled in both the Eurocodes and in the FEM-program SAP2000.

2.8.1 The $P-\Delta$ effect

The $P-\Delta$ effect is a name for the second-order effect of gravity loads acting on a laterally deformed structure. This create an overturning moment in the building, which in some cases can have big impacts on its response. This effect has been termed the $P-\Delta$ effect because this additional overturning moment is equal to the sum of P, the story weight, times Δ, the lateral displacement [11]. Figure 2.11 illustrate the $P-\Delta$ effect for a frame structure. This effect only reduce a structure's initial elastic stiffness slightly, and will

therefore have small influence if a building is subjected to an earthquake small enough that it remains in the elastic range. On the post-yield response of a structure however, the $P-\Delta$ effect can make a difference. The influence of $P-\Delta$ effects will be analysed in Section 4.4.

For a well-designed building the changes in displacements and member forces when including $P-\Delta$ effects compared to not including them are normally less than 10 %. When it comes to the effects on eigenperiods, the $P-\Delta$ effect can affect both translational and torsional modes, and will generally have more impact on a mode the higher its eigenperiod is [12].

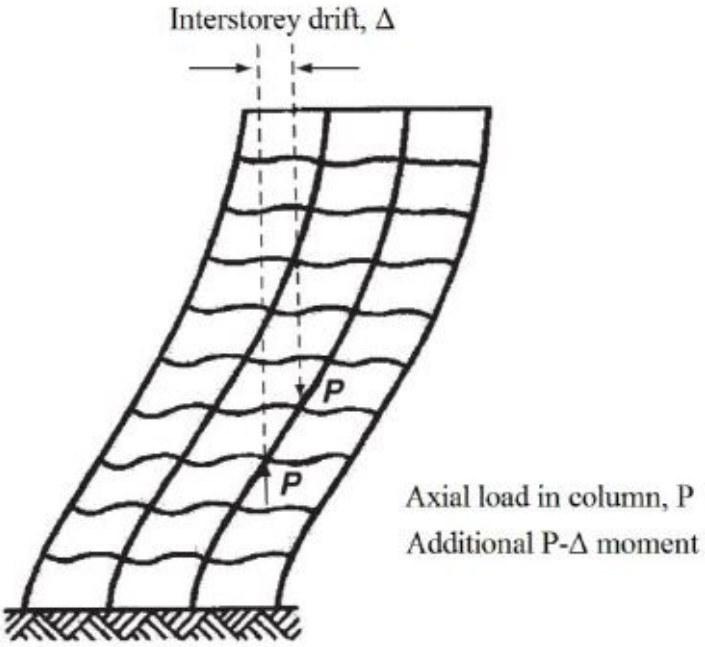

Figure 2.11: Illustration of the $P-\Delta$ effect [13]

2.8.2 Plastic hinge mechanism

A plastic hinge is rigid until the forces reach the yield point. After that, its stiffness is a fraction of the elastic stiffness. The plastic hinge mechanism is a model that is appropriate if the maximum moment occurs at the ends of members [6]. A frame structure where the hinges form at the end of the beams first is called a beam-hinge model. If the hinges however form in the columns first, it is called a column-hinge model [9]. The difference between these two models are shown in Figure 2.12.

When using the plastic hinge model, there is no coupling between yield at one end with yield at the other end. Cracking can however be allowed for in hysteresis curves [6].

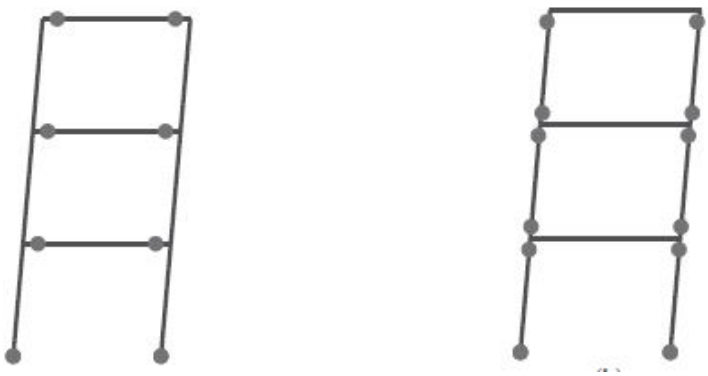

(a) Beam-hinge model **(b)** Column-hinge model

Figure 2.12: The difference between the beam-hinge and the column-hinge model for a frame structure [9]

2.8.3 Soft-story models

If plastic hinges form in the columns first, there is a risk of developing a soft-story mechanism. This happens when one of the stories develops a horizontal stiffness that is a lot smaller than the horizontal stiffness of the other floors. This often happens because of shear walls or other bracing elements that are omitted in one floor. Historically, a typical mistake when designing a building has been to use columns in the bottom floor and stiffer bracing elements in the other stories [14]. Figure 2.13 illustrates the soft-story effect for a frame structure.

Figure 2.13: Illustration of the soft-story effect for a frame structure [9]

When a soft-story mechanism is developed, the result is often a dangerous sway mechanism and finally collapse. An example of this is shown in Figure 2.14.

(a) Izmit, Turkey 1999 **(b)** Kobe, Japan 1995

Figure 2.14: Examples of the effect of soft-story mechanism [14]

2.8.4 Handling of nonlinearity in Eurocode 8

According to EC8 5.2.2.1 [7] concrete structures should be classified as one out of six types of load carrying systems depending on its behavior during horizontal seismic excitation. Section 5.2.2.2 in EC8 then describes a method for calculating the ductility factor q used for response spectrum analysis. q is given by

$$q = q_0 \cdot k_w \geq 1.5 \tag{2.51}$$

where q_0 is the base value for the ductility factor found in EC8 Table 5.1 and k_w is a factor that depends on the fracture form of the building. k_w is calculated as

$$k_w = \begin{cases} 1.00, & \text{for frames and frame equivalent double systems} \\ (1 + \alpha_0)/3 \leq 1, & \text{but not less than 0.5 for other systems} \end{cases}$$

where α_0 is calculated as

$$\alpha_0 = \sum h_{wi} / \sum l_{wi} \tag{2.52}$$

where h_{wi} is the height of wall i and l_{wi} is the length of wall i.

2.9 Tuned liquid dampers

In today's society, structures are built higher and higher as a result of shortage of land space, the use of high-strength materials and modern construction techniques. These buildings are often built relatively light and flexible. One of the main challenges with these structures is to find effective means of protecting them from environmental hazards such as earthquakes and wind loadings. This is a more serious problem for these structures than for earlier buildings, and neglecting to address this in a good manner can lead to discomfort for occupants and possibly structural failure.

Some of the methods developed for handling these problems are tuned mass dampers (TMDs), active mass dampers (AMDs) and tuned liquid dampers (TLDs). The TLDs use sloshing motion of liquids to absorb energy, and have several advantages such as low initial cost, easy maintenance and no limit of vibration amplitude. A tuned liquid damper in the shape of a water tank can also serve other purposes including water supply, firefighting and swimming pools [15] [16] [17].

2.9.1 Modeling of TLD-structure systems as equivalent TMD-structure systems

A TLD-structure system can be modeled as an equivalent TMD-structure system as shown in Figure 2.15

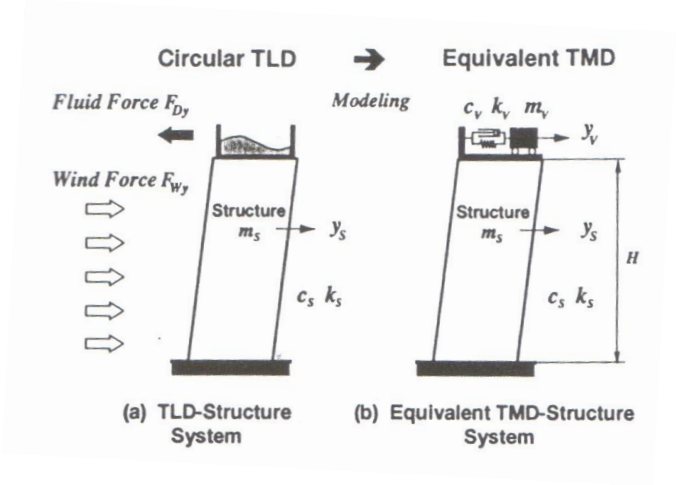

Figure 2.15: Equivalent TMD-structure model [18]

As seen in Section 2.3 the characteristic equation of motion for a 1-DOF system can be written as

$$m\ddot{u} + c\dot{u} + ku = p(t) \tag{2.53}$$

for the TMD-structure model the forcing function $p(t)$ is given by [18]

$$p(t) = p_e(t) + p_v(t) \tag{2.54}$$

where $p_e(t)$ is the external loading, wind or earthquake, and $p_v(t)$ is the fluid force. $p_v(t)$ can be written as

$$p_v(t) = -m_v(\ddot{u} + \ddot{u}_v) \tag{2.55}$$

where $\ddot{u}_v$ is the acceleration of the equivalent TMD and m_v is the mass of the equivalent TMD given by

$$m_v = \mu_v m_L \tag{2.56}$$

m_L is the mass of the liquid in the TLD and μ_v is the mass ratio. This ratio can be estimated from potential flow theory as [19]

$$\mu_v = \frac{8tanh(\pi\epsilon)}{\pi^3\epsilon} \tag{2.57}$$

where h_0 is the water depth in the tank and where ϵ is the water depth ratio given by $\epsilon = \frac{h_0}{L}$. L is the length of the tank.

The equation of motion for the TMD-system can be written as

$$m_v\ddot{u}_v + c_v\dot{u}_v + k_v u_v = -m_v\ddot{u} \tag{2.58}$$

where c_v and k_v are the damping and stiffness of the equivalent TMD, given by

$$c_v = 2\mu_v m_L \omega_v \xi_v \tag{2.59}$$

$$k_v = \mu_v m_L \omega_v^2 \tag{2.60}$$

where ω_v is the fundamental natural frequency of the water sloshing motion. For a TLD shaped as a rectangular tank, according to linear water wave theory, this is given by [20]

$$\omega_v = \sqrt{\frac{\pi g}{L} tanh(\pi\epsilon)} \tag{2.61}$$

ξ_v is the damping ratio for the TMD which can be estimated by [21]

$$\xi_v = \frac{1}{2h_0}\sqrt{\frac{\nu}{\pi f_v}(1 + \frac{h_0}{B})} \tag{2.62}$$

where ν is the liquid kinematic viscosity ($\approx 10^{-6}\ m^2/s$ for water), $f_v = \frac{\omega_v}{2\pi}$ and B is the width of the water tank.

When combining equation 2.53 and equation 2.58 the equations of motion for the TMD-system can be written as

$$\mathbf{M\ddot{u}} + \mathbf{C\dot{u}} + \mathbf{Ku} = \mathbf{P} \tag{2.63}$$

where

$$\mathbf{M} = \begin{bmatrix} m & 0 \\ \mu_v m_L & \mu_v m_L \end{bmatrix} \tag{2.64}$$

$$\mathbf{C} = \begin{bmatrix} 2m\omega_n\xi & -2\mu_v m_L \omega_v \xi_v \\ 0 & 2\mu_v m_L \omega_v \xi_v \end{bmatrix} \tag{2.65}$$

$$\mathbf{K} = \begin{bmatrix} m\omega_n^2 & -\mu_v m_L \omega_v^2 \\ 0 & \mu_v m_L \omega_v^2 \end{bmatrix} \tag{2.66}$$

$$\mathbf{u} = \begin{bmatrix} u \\ u_v \end{bmatrix} \tag{2.67}$$

$$\mathbf{P} = \begin{bmatrix} p(t) \\ 0 \end{bmatrix} \tag{2.68}$$

3 Modeling of Oslo Plaza

3.1 Oslo Plaza

(a) The complete building **(b)** The tower of Oslo Plaza

Figure 3.1: Oslo Plaza [13]

Radisson Blu Plaza Hotel Oslo, often just called Oslo Plaza, is with its 117 m and 37 floors the second tallest building in Norway. The main building has an area of around 3 800 m^2 and consists of a tower part, an administration part and a conference part. The tower part has a ground surface of approximately 975 m^2 and rises up from the 4^{th}. It was officially opened the 14^{th} of March 1990 and was designed by White Architects.

The building has a structural system consisting of concrete walls. Torsional resistance in the tower is provided by four concrete walls in addition to the elevator cores. The shear walls support both lateral loads in the transverse direction and lateral loads. The elevator cores also support gravity loads in addition to lateral loads in the longitudinal direction. On the first five floors the shear walls are supported on concrete columns. The exterior glass facade are supported on steel columns. The floors are made out of cast in situ concrete slabs of variyng thickness. The described concrete structure reaches to the 34^{th} floor. The top floors are made up by a steel frame structure.

3.2 Ground conditions

The ground on which Oslo Plaza is built consists mostly of silty clay which in turn rests on solid rock. This layer of silty clay is normally between 15 m and 20 m, but increases rapidly to between 25 m and 28 m on the south-east side of the building. The shear strength of the clay is mostly between 30 kPa and 45 kPa.

Under the tower part of the building, there are piles cast in the clay, while under the rest of the building the piles go all the way to the solid rock. These piles were dimensioned very conservativly when the structure was built. The underground railroad in Oslo goes directly underneath Oslo Plaza, and parts of the building rests on the railroad tunnel.

Taking these factors into account, the foundation is chosen to be represented as ground type D according to EC8 Table NA.3.1, which gives a soil amplification factor $S = 1.6$ according to EC8 Table NA.3.3.

3.3 Acceleration time histories

According to Eurocode 8 [7]3.2.3.1.1(2)P the seismic action during a time history analysis should consist of three simultaneously acting accelerograms, and the same accelerogram cannot be used in both horizontal directions at the same time. EC8 3.2.3.1.3(3) demands that at least three recorded accelerograms are used. The three accelerograms used in this project are shown in Figure 3.2 and Figure 3.3, each with a component in the North-South, East-West and Vertical direction. These are the recorded acceleration time histories for the following three earthquakes:

Table 3.1: Information about the recorded acceleration time histories used

Earthquake	Recording site	Date	Component	PGA $[m/s^2]$	Sampling interval $[s]$
Nahanni, Canada	Site 3	23.12.1985	N-S	1.558	0.02
			E-W	1.267	0.02
			Vertical	1.212	0.02
Whittier, California	Mt. Wilson	01.10.1987	N-S	1.289	0.02
			E-W	1.611	0.02
			Vertical	1.012	0.02
Friuly, Italy	Breginj	11.09.1976	N-S	1.222	0.01
			E-W	1.510	0.01
			Vertical	0.592	0.01

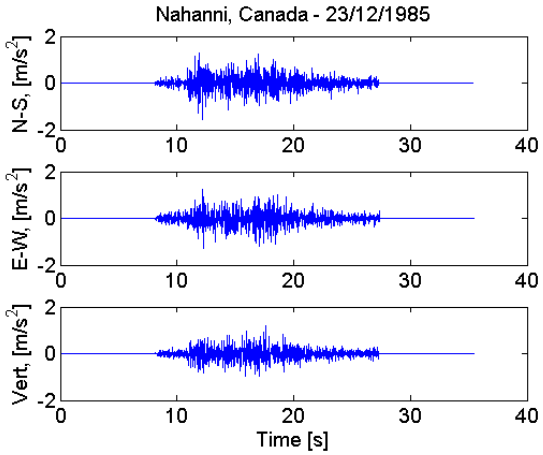

Figure 3.2: Acceleration time history for the earthquake in Nahanni, Canada

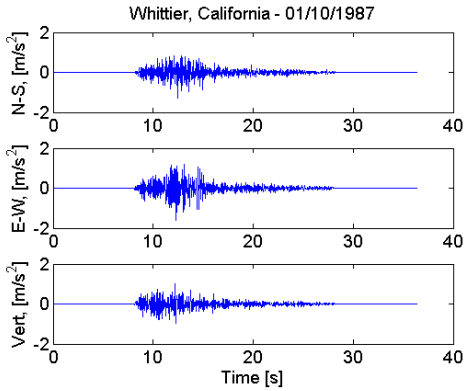

(a) Acceleration time history for the earthquake in Whittier, California

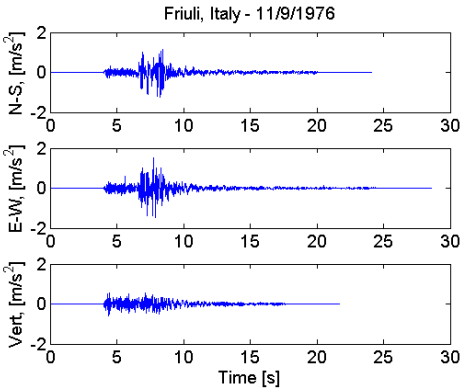

(b) Acceleration time history for the earthquake in Friuly, Italy

Figure 3.3: Acceleration time histories

3.3.1 Combination of acceleration time history components

EC8 [7] 4.3.3.5.2(4) gives rules for combining the acceleration time history components in the North-South, East-West and Vertical components. The rules given are:

$$E_{Edx} + 0.30\ E_{Edy} + 0.30\ E_{Edz} \tag{3.1}$$

$$0.30\ E_{Edx} + E_{Edy} + 0.30\ E_{Edz} \tag{3.2}$$

$$0.30\ E_{Edx} + 0.30\ E_{Edy} + E_{Edz} \tag{3.3}$$

where E_{Edx}, E_{Edy} and E_{Edz} are the components of the acceleration time histories in the x, y and z-direction, and "+" means combined with. EC8 [7] 4.3.3.5.2(1) does however state that the vertical component can be neglected if the following criteria is satisfied:

$$a_{vg} \leq 0.25\ g \approx 2.45\ m/s^2 \tag{3.4}$$

where a_{vg} is the ground acceleration in the vertical direction. If the vertical component is neglected, the combination rules become:

$$E_{Edx} + 0.30\ E_{Edy} \tag{3.5}$$

$$0.30\ E_{Edx} + E_{Edy} \tag{3.6}$$

In the simulations the North-South component has to be applied in both the x and y-direction, and similarly the East-West component has to be applied in both the y and x-direction. This gives the following load combinations for each of the recorded earthquakes:

Table 3.2: Load combinations used in analyses

Combination name	Load in x-direction	Load in y-direction
NS+0.30EW	N-S component	0.30 E-W component
0.30NS+EW	0.30 N-S component	E-W component
EW+0.30NS	E-W component	0.30 N-S component
0.30EW+NS	0.30 E-W component	N-S component

3.3.2 Response spectra for the earthquakes

In this section, the calculated response spectra for the three recorded earthquakes are plotted and compared to the Eurocode 8 [7] response spectrum. In Section 3.3.3, the time histories will be modified and the calculated response spectra will be plotted again for comparison.

Figure 3.4 and Figure 3.5 show response spectra generated for the Nahanni earthquake

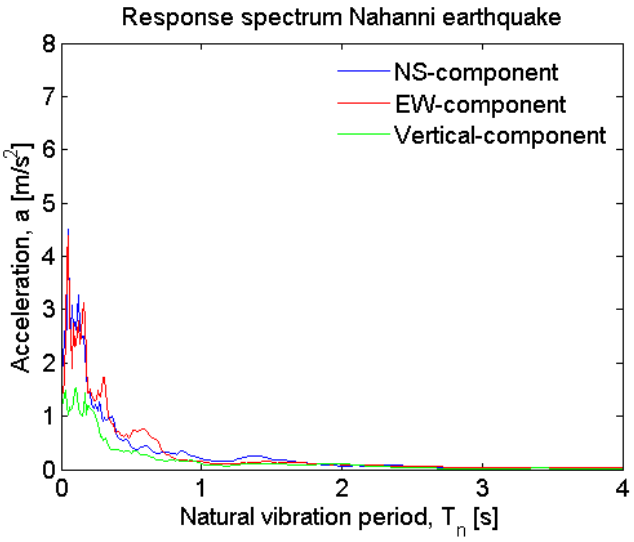

Figure 3.4: Response spectrum generated for the earthquake in Nahanni, Canada in 1985

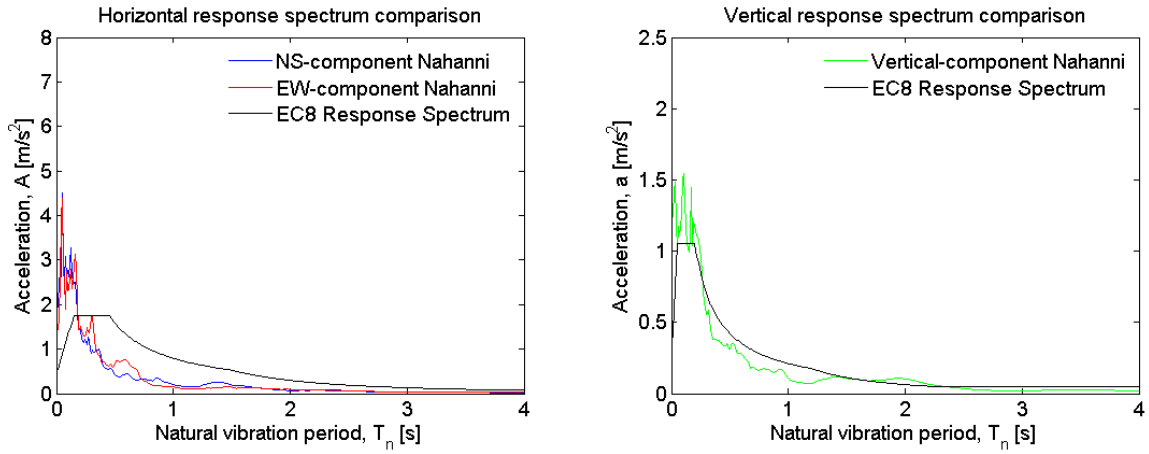

(a) Horizontal component

(b) Vertical component

Figure 3.5: Comparison of the response spectrum generated for the earthquake in Nahanni, Canada in 1985 to the EC8 elastic response spectrum

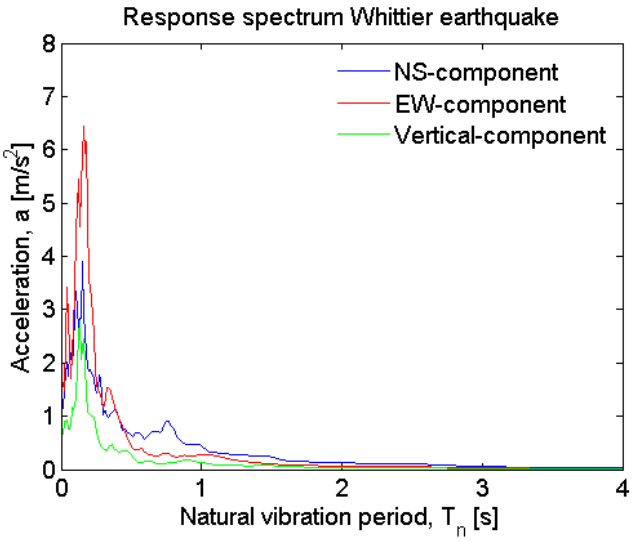

Figure 3.6: Response spectrum generated for the earthquake in Whittier, California in 1987

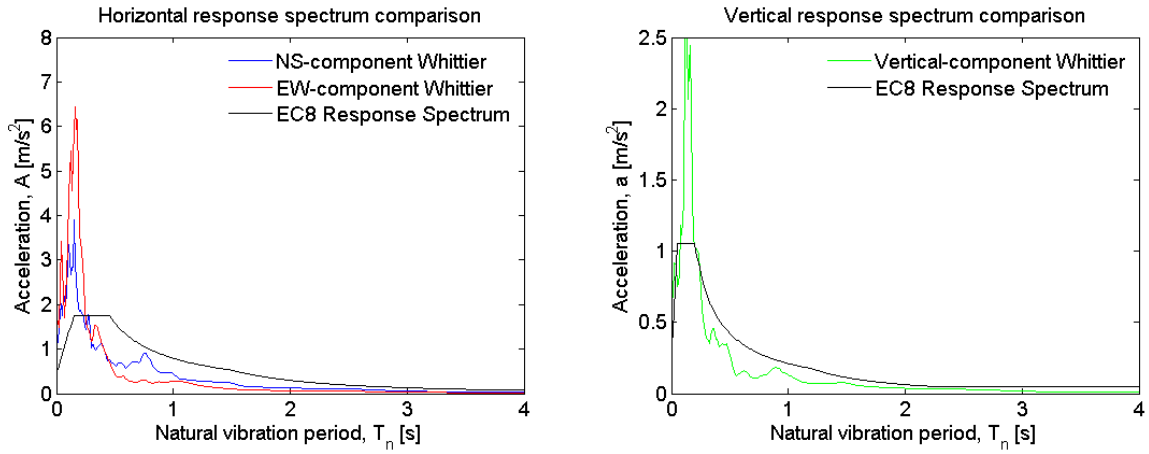

(a) Horizontal component

(b) Vertical component

Figure 3.7: Comparison of the response spectrum generated for the earthquake in Whittier, California in 1987 to the EC8 elastic response spectrum

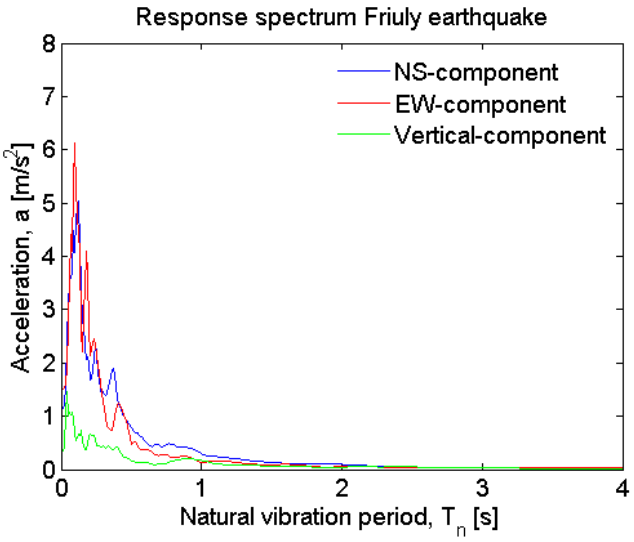

Figure 3.8: Response spectrum generated for the earthquake in Friuly, Italy in 1976

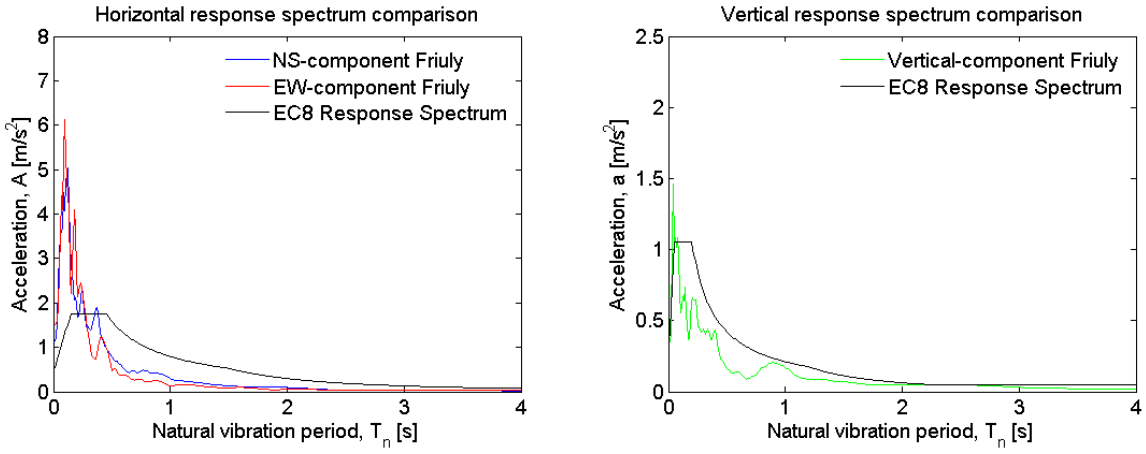

(a) Horizontal component **(b)** Vertical component

Figure 3.9: Comparison of the response spectrum generated for the earthquake in Friuly, Italy in 1976 to the EC8 elastic response spectrum

3.3.3 Modifications of the acceleration time histories

There exists primarily two methods to modify recorded acceleration time histories to obtain design time series. These are scaling and spectral matching [22]. When scaling a time series, one multiplies the initial accelerogram with a constant factor, while spectral matching modifies the frequency content of the time series to match a design spectrum at all spectral periods.

According to EC8 [7] 3.2.3.1.3(1)P the recorded accelerograms used have to be scaled to the value of $a_g S$ for the relevant site, where a_g is the design ground acceleration for

ground type A and S is an amplification factor that depends on the ground conditions. It is assumed that the records given represent ground type A. As shown in Section 2.2, the expected a_{g40Hz} for Oslo with a return period of 475 years is between 0.5 m/s^2 and 0.6 m/s^2, hereafter assumed to be 0.55 m/s^2. This gives a PGA of:

$$a_{gR} = 0.8 \cdot 0.55\ m/s^2 = 0.44\ m/s^2 \tag{3.7}$$

In Oslo, the ground conditions can be classified as type D according to EC8 [7] Table NA.3.1, which gives a value of S equal to 1.6 according to EC8 Table NA.3.3. The recorded acceleration time histories should therefore be scaled to the following PGA:

$$a_g S = 0.44\ m/s^2 \cdot 1.6 \approx 0.70\ m/s^2 \tag{3.8}$$

The acceleration time histories are thereafter adjusted to match the Eurocode 8 [7] response spectrum. This is done using the software SeismoMatch version 2.1.0 by SeismoSoft. This software uses the wavelets algorithm for spectral matching to make the recorded accelerograms match the conditions at the actual place. This procedure is outlined below. This theory is obtained from Abrahamson [1992] [23].

The difference between the target spectrum, in this case the Eurocode 8 [7] spectrum, and the computed spectrum from a time history for frequency ω_i and damping β_i is given by

$$\delta R_i = (Q_i - R_i)P_i \tag{3.9}$$

where Q_i is the target spectrum for ω_i and β_i, R_i is the absolute value of the peak response and P_i is the polarity of the peak response. δR_i includes the polarity of the response.

Also let an adjustment time history be given by

$$\delta a(t) = \sum_{j=1}^{N} b_j f_j(t) \tag{3.10}$$

where $f_j(t)$ is a set of adjustment functions, b_j is a set of coefficients to be determined and N is the number of spectral points (pairs of frequency and damping) to match. The purpose of this procedure is to determine $\delta a(t)$ such that its response at time t_i is equal to δR_i for all i. The acceleration response of $\delta a(t)$ at time t_i is given by

$$\delta R_i = \sum_{j=1}^{N} b_j \int_0^{\infty} f_j(\tau) h_i(t_i - \tau) d\tau \tag{3.11}$$

where $h_i(t)$ is the acceleration impulse response of the oscillator for ω_i and β_i given by

$$h_i(t) = \frac{-\omega_i}{\sqrt{1-\beta_i^2}} e^{-\omega_i \beta_i t} [(2\beta_i^2 - 1) sin(\omega_i' t) - 2\beta_i \sqrt{1-\beta_i^2} cos(\omega_i' t)] \tag{3.12}$$

where

$$\omega_i' = \omega_i \sqrt{1-\beta_i^2} \tag{3.13}$$

and $h_i(t) = 0$ for $t < 0$.

Then the values for b_j can be found from the equation (in matrix form)

$$\mathbf{b} = \mathbf{C}_b^{-1} \delta \mathbf{R} \tag{3.14}$$

where the components in the matrix $\mathbf{C}_b$ are given by

$$c_{ij} = \int_0^{t_i} f_j(\tau) h_i(t_i - \tau) d\tau \tag{3.15}$$

Given b_j, $\delta a(t)$ can be found from equation 3.10, and finally the adjusted time history is given by

$$a_1(t) = a_0(t) + \gamma \delta a(t) \tag{3.16}$$

where $a_0(t)$ is the original time history and γ is a relaxation parameter (between 0 and 1) to damp the adjustments. The entire procedure is then repeated for the adjusted time history until the desired spectral match is achieved.

The selection of the adjustment function $f_j(t)$ is important for this procedure, but will not be covered here. Readers are referred to Abrahamson [1992] [23] for discussions about the selection of $f_j(t)$.

The final acceleration time histories will then match the expected PGA, ground conditions

and frequency content at the target location. Figure 3.10, Figure 3.11 and Figure 3.12 shows the calculated response spectra for the modified acceleration time histories.

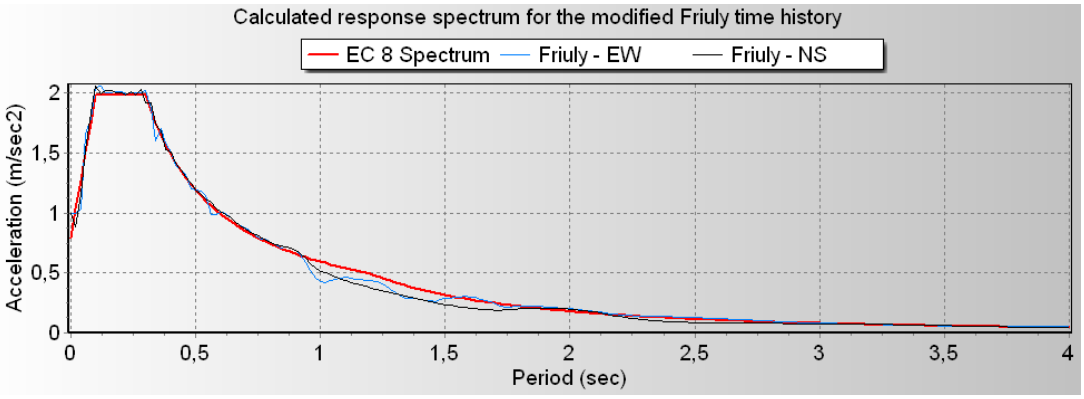

Figure 3.10: Response spectrum generated for the modified Friuly time histories compared to the Eurocode 8 response spectrum

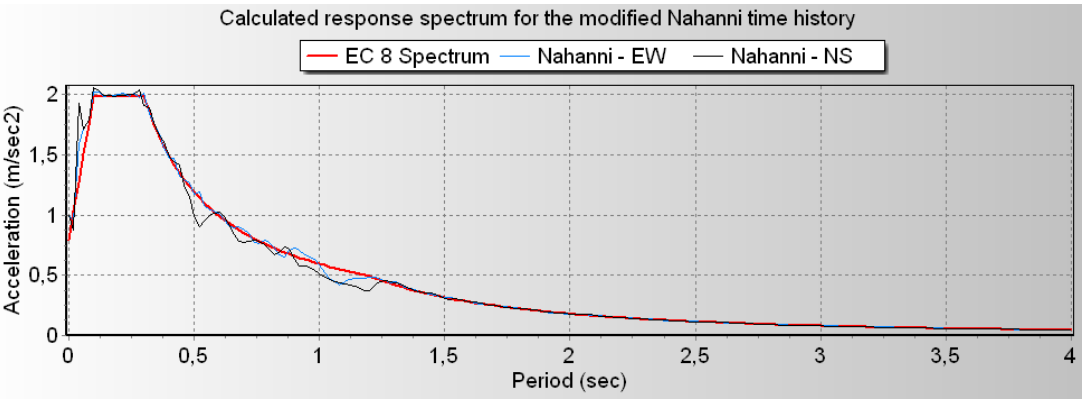

Figure 3.11: Response spectrum generated for the modified Nahanni time histories compared to the Eurocode 8 response spectrum

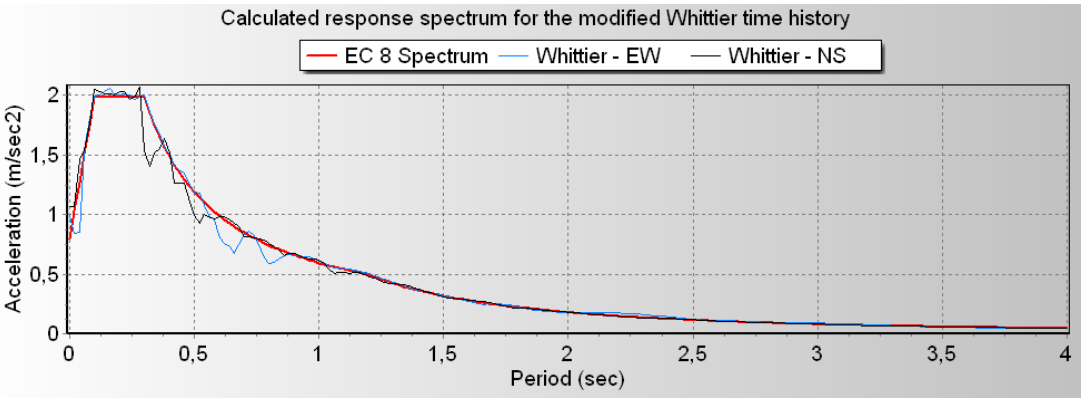

Figure 3.12: Response spectrum generated for the modified Whittier time histories compared to the Eurocode 8 response spectrum

3.4 FEM-model

For the analyses, Oslo Plaza is modeled in the FEM-program SAP2000 v15.2.1 Ultimate developed by Computers & Structures Inc. This section will describe the model, including materials and components used, in addition to loads and modeling of ground conditions. Also described are simplifications done and uncertainties in the model. The objective of creating this 3D-model was to obtain information about the dynamic behavior of the building and to be able to perform seismic analyses and compare the response obtained from different types of seismic analyses.

The geometry of the structure has been obtained from an extensive amount of construction and architectural drawings. These have been obtained from supervisor Svein Remseth and from email conversations with Bjørn Svendsen. They have both obtained the drawings from Oslo Municipal Planning & Building Services and from the Oslo Plaza management.

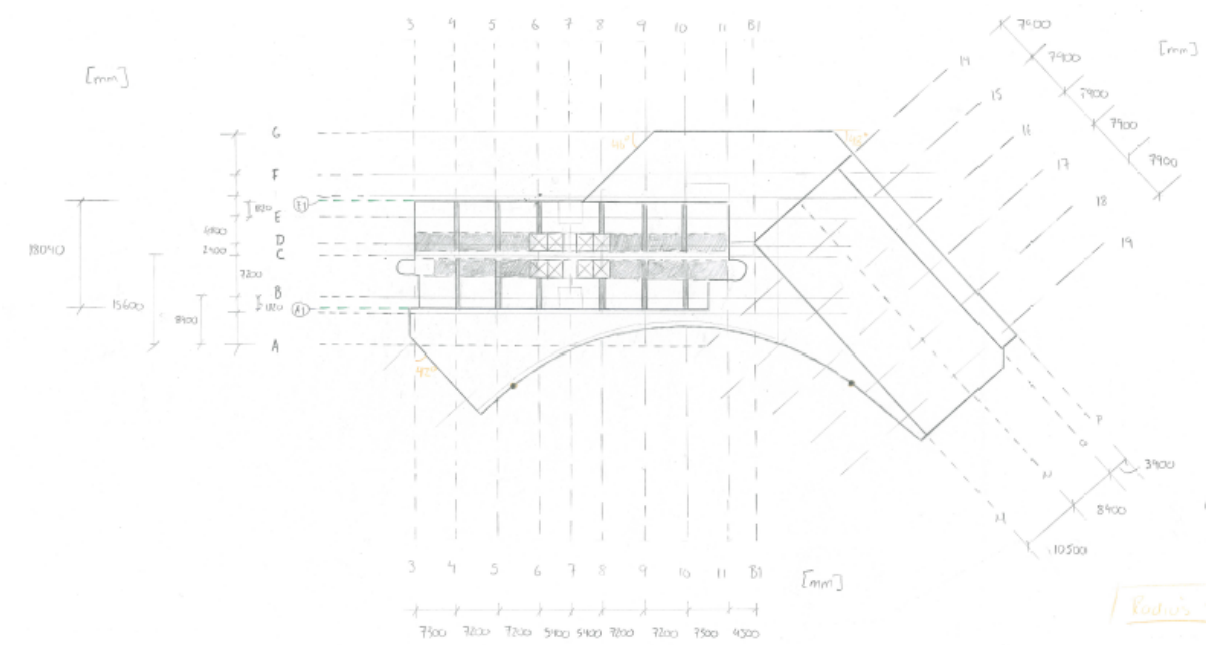

Figure 3.13: Overview of the Oslo Plaza floor plan

3.4.1 Materials

Table 3.3 shows the materials used in the FEM-model. This table shows only the linear properties of the materials. When it comes to material nonlinearity, data for several materials are included in SAP2000. Figure 3.14 and Figure 3.15 show the nonlinear stress-strain curves for C35 concrete, S355 steel and a typical rebar steel used in SAP2000.

Table 3.3: Material properties used in the FEM-model

Material	Young's modulus, E $[MPa]$	Poisson ratio, ν	Weight $[kN/m^3]$	Mass $[kg/m^3]$	Yield stress $[Mpa]$
Concrete C35	35 000	0.25	25	2548	28
Steel S355	210 000	0.3	77	7849	355
Rebar	200 000	0	25	2548	483

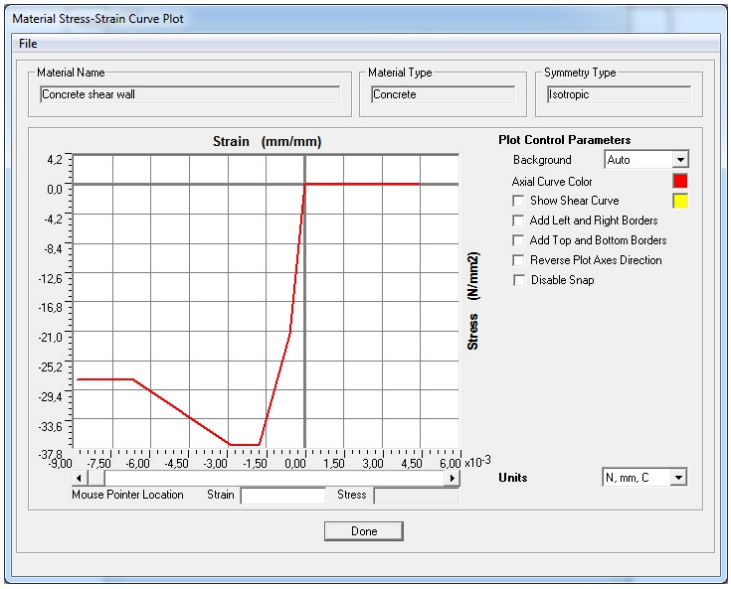

Figure 3.14: Nonlinear stress-strain curve for concrete used in SAP2000

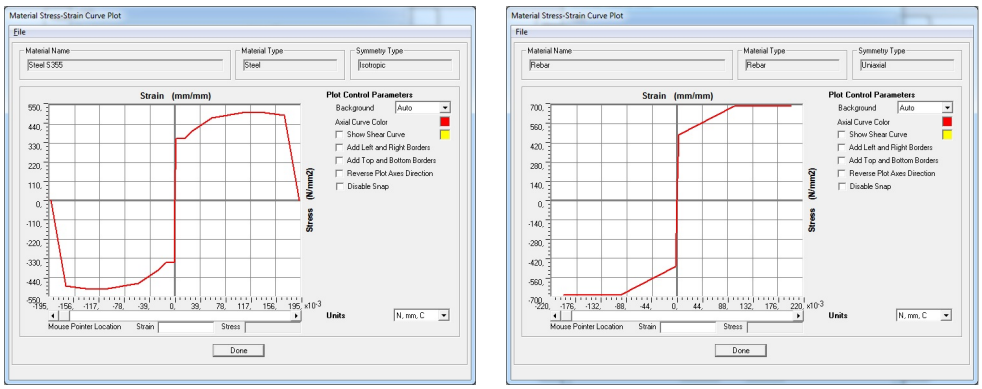

(a) Nonlinear stress-strain curve for steel used in SAP2000

(b) Nonlinear stress-strain curve for rebars used in SAP2000

Figure 3.15: Nonlinear stress-strain curves used for construction steel and reinforcing bars used in SAP2000

There are three hysteresis models for the user to choose between in SAP2000. These are elastic, kinematic and Takeda models. Figure 3.16a shows a typical elastic hysteresis model for a rubber material. This model is not interesting for the analyses in this report.

Figure 3.16b shows a typical kinematic hysteresis model. In SAP2000, this is the default model used for steel members and for reinforcing bars.

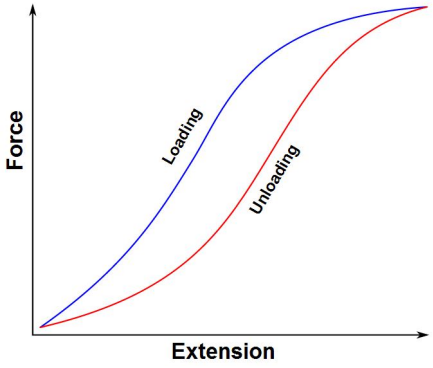

(a) Elastic hysteresis model for a typical rubber material

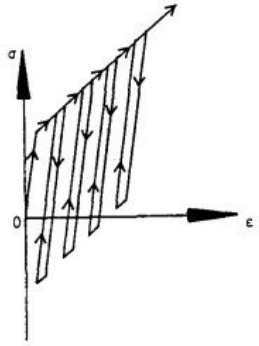

(b) A typical kinematic hysteresis model generally used for steel members and reinforcing bars in SAP2000 [24]

The Takeda model for hysteresis is shown in Figure 3.17. This is considered to be one of the best hysteretic rules introduced to present nonlinear behavior [25]. In SAP2000 this model is the default for concrete members.

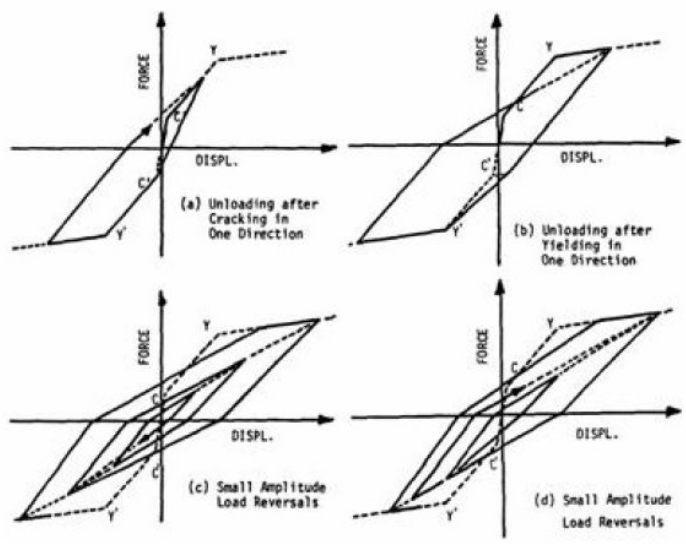

Figure 3.17: The Takeda hysteresis model generally used for concrete members in SAP2000 [25]

3.4.2 Components

Table 3.4 shows the structural elements used in the model.

Table 3.4: Components used in the FEM-model

Structural element	Material	Element type	Dimensions
Columns	Concrete C35	Frame	Circular 600 mm diameter
			Circular 1200 mm diameter
			Rectangular 300 mm x 400 mm
			Rectangular 400 mm x 400 mm
			Rectangular 600 mm x 500 mm
			Rectangular 600 mm x 600 mm
			Rectangular 800 mm x 1200 mm
	Steel S355	Frame	Tube 200 mm x 100 mm x 10 mm
			Tube 250 mm x 450 mm x 40 mm
Beams	Steel S355	Frame	Flange beam 600 mm x 1300 mm
Shear walls	Concrete C35	Layered reinforced shell	250 mm thickness
			300 mm thickness
			800 mm thickness
Elevator shaft	Concrete C35	Layered reinforced shell	200 mm thickness
			250 mm thickness
Slabs	Concrete C35	Layered reinforced shell	220 mm thickness
			250 mm thickness
			270 mm thickness
			290 mm thickness
			340 mm thickness
Foundation walls	Concrete C35	Layered reinforced shell	500 mm thickness

A frame element is modeled as a straight line connecting two points, and uses a three-dimensional beam-column formulation including biaxial beding, torsion, axial deformation and biaxial shear deformations [26].

In SAP2000, material nonlinearity in frames are handled by the creation of concentrated plastic hinges [27]. The possible location of these hinges have to be appointed manually by the user. SAP2000 lets the user choose between two different types of plastic hinges, P-M2-M3 hinges and fiber hinges.

For P-M2-M3 hinges the post-yield behavior is interpolated from user-defined $P-\theta$ curves, where θ represents the relationship between M2 and M3. As the analysis is running, an energy-equivalent moment-rotation curve is generated relative to the input $P-\theta$ curves and the interaction-surface yield point. This moment-rotation curve describes the post-yield behavior of a beam-column element subjected to combined axial and bending conditions. P-M2-M3 hinges are mostly used for static analyses, like the nonlinear

pushover analysis described in Section 4.4.2. P-M2-M3 hinges should however be avoided in analyses where significant hysteresis is expected, like nonlinear dynamic time history analyses.

When fiber hinges are used, the cross section is discretized into a series of axial fibers which extends along the hinge length. Each of these fibers has a stress-strain relationship, and together these give the force-deformation and moment-rotation relationships for the frame section. The fiber hinge is more accurate than the P-M2-M3 hinge, but the drawback is that using fiber hinges is more computationally expensive. They do however capture nonlinear hysteretic effects and are therefore ideal for nonlinear dynamic analyses.

Shell elements combine membrane and plate-bending behavior, using a three- or four-node formulation [28]. For linear analyses, homogeneous shell elements are sufficient, while to model nonlinear behavior multi-layered shell elements are the most normal method [27]. For this method, the concrete and reinforcement are modeled respectively with different layers. This is based on the concept of composite material mechanics. The axial strain and curvature of the middle layer can be obtained in one element during the finite element calculation, and thereafter the strains and curvatures of the other layers can be calculated according to the assumption that plane remains plane [29]. Figure 3.18 shows a typical multi-layer shell element

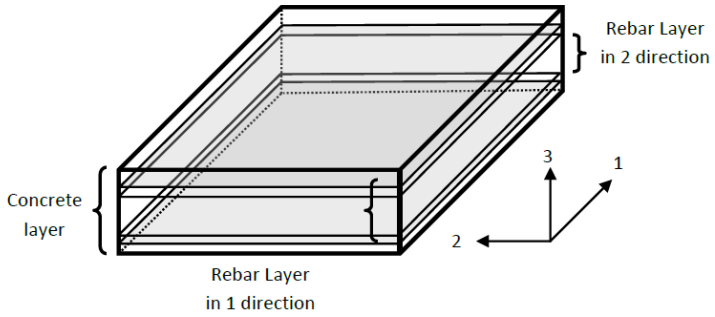

Figure 3.18: Multi layer shell elements [29]

3.4.3 Loads

A combination of dead loads, live loads and snow loads have been used during the analyses of the model in addition to the acceleration loads. The dead loads are calculated by SAP2000 from the assigned material weights, while the live loads and snow loads have been assigned manually. Table 3.5 shows the dead loads, live loads and snow loads used according to Eurocode.

Table 3.5: Loads used during the analyses of the FEM-model

Floor	Dead load $[kN/m^2]$	Live load $[kN/m^2]$	Snow load $[kN/m^2]$
1-4	Calculated in SAP2000	5	2.8 (4^{th} floor)
5-33	Calculated in SAP2000	2	
34-37	Calculated in SAP2000	3	2.8 (34^{th} floor)

The roof area where the snow load is applied is so small that the snow load in reality is negligible. A load combination of

$$Total\ load = 1.0 \cdot Dead\ load + 0.3 \cdot Live\ load + 0.2 \cdot Snow\ load \tag{3.17}$$

has been used for the element model.

3.4.4 Simplifications and uncertainties

The section plans and drawings used as a basis for modeling Oslo Plaza have been somewhat incomplete, so in some cases assumptions have been made. This includes some stories having been assumed to be similar to the stories above or below. In other parts of the model some floors have been simplified to look more like the rest of the building to create a simpler model while not changing the behavior of the model significantly.

Another uncertainty is that the model has been modeled as standing directly on bed rock and the effect of the soil foundation have only been included in the soil amplification factor S used to scale the acceleration time histories. Modeling the soil as part of the FEM-model is a topic that would be interesting to analyse further, as discussed in Section 7

4 Analysis of Oslo Plaza

4.1 Natural periods and mode shapes

The first analysis run is to obtain the natural periods and mode shapes of the building using eigenvectors. Table 4.1 shows the ten first eigenperiods and their participating mass ratios and participation factors as defined in Section 2.4. Note that the participating mass ratios given for each mode are the sums of the participating mass ratios of that mode and all the modes with a higher natural period than it. If all the modes of the building were used, the total participating mass ratios would be equal to 1.0.

Table 4.1: Modal analysis results obtained from SAP2000 for the element model

Mode	Mode shape	Eigenperiod	Participating mass ratio			Participation factor $[Ns^2]$		
#	Description	T[s]	Sum X	Sum Y	Sum Z	X	Y	Z
1	Translation in x-direction	3.993599	0.62	0.0005248	0.00001959	255.354948	7.451971	1.439788
2	Translation in y-direction	3.359992	0.62	0.58	0.0001229	-7.686824	248.193689	3.306652
3	Rotation about z-axis	2.442929	0.62	0.58	0.0001255	2.410444	-3.247066	0.523649
4	Deformation in x-direction along z-axis	1.086345	0.73	0.58	0.0007554	-108.565728	1.120413	-8.164239
5	Deformation in y-direction along z-axis	0.730281	0.73	0.74	0.0007684	-1.315312	128.82465	-1.173427
6	Twisting about z-axis	0.625829	0.73	0.76	0.001895	-1.016054	46.966076	10.916484
7	Deformation in z-direction	0.555806	0.73	0.76	0.07705	6.024021	3.308497	89.178257
8	2nd deformation in x-direction along z-axis	0.518859	0.78	0.76	0.08639	71.407298	2.735657	-31.447474
9	Local mode	0.38841	0.78	0.76	0.58	2.373646	-1.207325	229.490426
10	Local mode	0.383773	0.78	0.78	0.59	2.292196	-39.151364	10.851161

Figure 4.1 shows the first 6 mode shapes of the model.

Eurocode 8 4.3.3.3.1(3) [7] states that for a modal response spectrum analysis one of the following criteria has to be fulfilled when it comes to number of modes used:

- the sum of the participating mass ratios for the modes used exceeds 90 % of the total mass of the building
- all modes with a participating mass ratio larger than 5 % of the total mass of the building are included

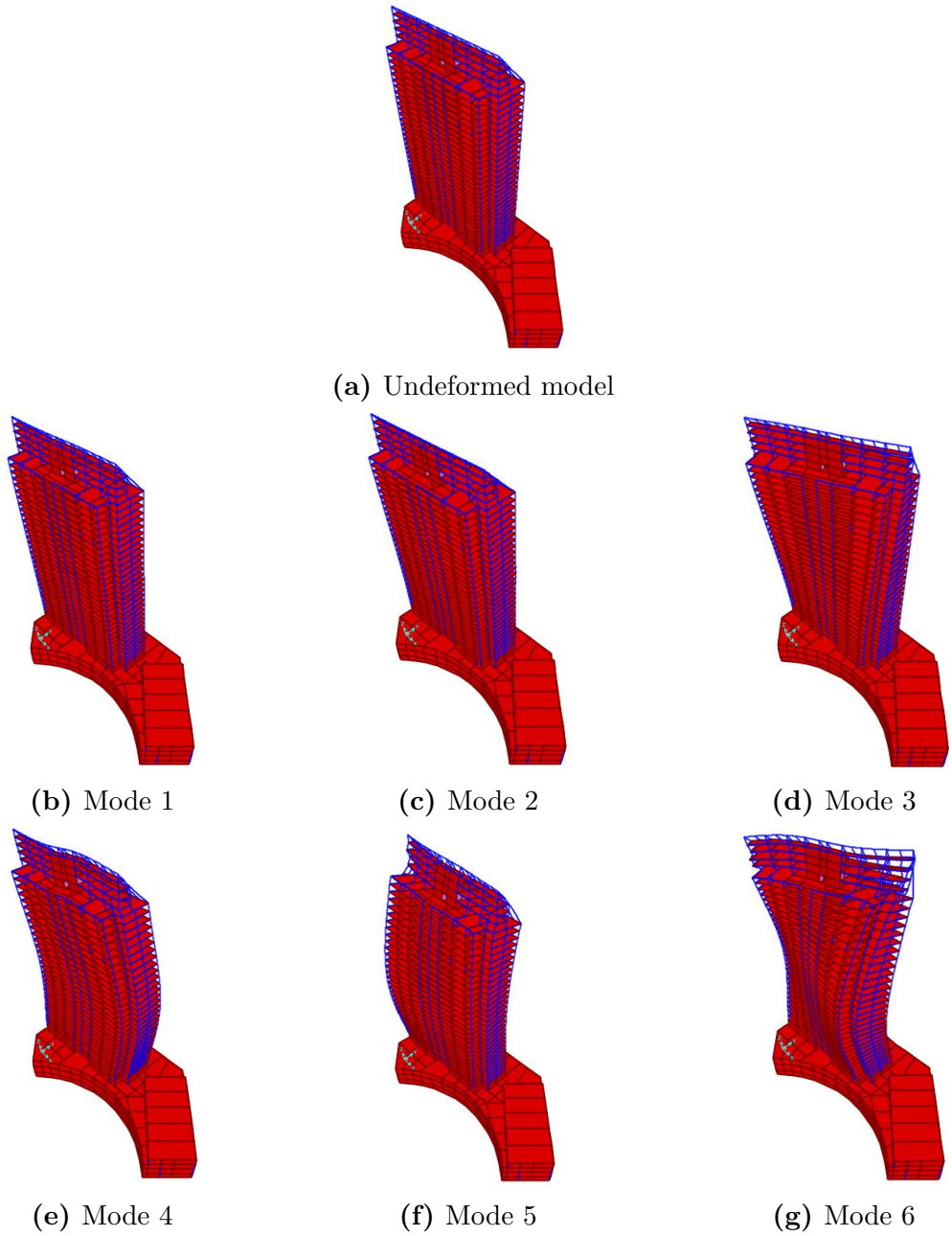

(a) Undeformed model

(b) Mode 1 **(c)** Mode 2 **(d)** Mode 3

(e) Mode 4 **(f)** Mode 5 **(g)** Mode 6

Figure 4.1: The first six mode shapes of the Oslo Plaza

However, Eurocode 8 4.3.3.3.1(5) [7] gives an exception to the aforementioned criteria for buildings with significant contributions from torsional modes. If this is the case, like for the Oslo Plaza, then both of the two following criteria have to be fulfilled:

- $k_n \geq 3\sqrt{N}$
- $T_k \leq 0.20s$

where k_n is the number of modes used in the analysis, N is the total number of stories in

the building and T_k is the eigenperiod of mode k. Using these criteria, at least the first 19 modes have to be used in the analysis. For the rest of the analyses in this project, around 20 modes could therefore be used. This does however give very low mass participation ratios, and it has instead been chosen to use the 200 first modes, to obtain more accurate results.

4.2 Estimates of eigenperiod

As described in Section 2.7, an upper and lower bound for the natural angular frequency can be estimated by the Rayleigh quotient method and the Dunkerley-Mikhlin method. The Rayleigh quotient method gives an upper bound for the angular frequency, and it will therefore provide a lower bound for the natural period of the building. The Dunkerley-Mikhlin method gives a lower bound for the angular frequency, and therefore provides an upper bound to the natural period.

Table 4.2 shows the mass for each story in addition to the calculated 2nd moment of inertia about the x- and y-axis. The calculations are shown in appendix C.

Table 4.2: Estimates of mass per story and second moments of inertia

Mass, m	2nd moment of inertia about x-axis, I_x	2nd moment of inertia about y-axis, I_y
815 000 kg	1100 m^4	5950 m^4

The building is considered as a MDOF cantilever beam with one degree of freedom for each story with a mode shape following the function

$$v_i = 1 - cos(\frac{i\pi}{2N}), i = 1 \dots N \tag{4.1}$$

where N is the total number of stories. The mass and stiffness matrix are calculated from the values in Table 4.2 for one direction at the time. Thereafter, the Rayleigh quotient method and Dunkerley-Mikhlin method are used to estimate the following lower and upper bounds to the two first natural periods

$$3.23 \leq T_1 \leq 9.19 \tag{4.2}$$

$$1.85 \leq T_2 \leq 4.82 \tag{4.3}$$

In the mass and stiffness matrices it has been taken into account that the stories are lighter and have less stiffness towards the top of the building. These numbers are still crude estimates, as the building is modeled as a MDOF system with very few degrees of freedom, and masses and stiffness are considered to only have two different values; one for the lower parts of the building and one for the upper part of the building. The masses and the 2nd moments of inertia are also estimates.

However, even though the calculated natural periods are very rough estimates, they give an upper and lower bound for the naturral period of the building, and both the 1st and 2nd periods found in section 4.1 lie between these values, and it can therefore be assumed that the natural periods used for analysing the model are in the right order and will give satisfying results.

4.3 Linear time history analyses

After having determined the natural periods and mode shapes of the model in Section 4.1 linear model acceleration time history analyses are performed for the three earthquakes and the load cases described in Section 3.3. Modal time history analyses are much faster and usually reliable for linear analyses, so this is done first to get an idea of which load cases gives the largest response. Thereafter linear and nonlinear direct integration time history analyses are performed for these load cases.

4.3.1 Linear Modal Time History Analyses

The damping in the modal analyses is modeled as Rayleigh damping as described in Section 2.6. Assuming the modal damping equal to 0.02 for the two first modes obtained in Section 4.1 the following Rayleigh scale factors are obtained:

$$\alpha = \frac{2(\xi_i\omega_j - \xi_j\omega_i)\omega_i\omega_j}{\omega_j^2 - \omega_i^2} = 0.03509 \tag{4.4}$$

$$\beta = \frac{2(\xi_j\omega_j - \xi_i\omega_i)}{\omega_j^2 - \omega_i^2} = 0.01132 \tag{4.5}$$

Figure 4.2, Figure 4.3 and Figure 4.4 show the displacement of the top-story in the x- and y-direction for the time history analyses of the three different earthquakes (plot a-b), in addition to the maximum displacement of each story in the x- and y-direction (plots c-d). The displacement is plotted for 50 seconds from the start of the earthquake recordings. The length of the earthquake recordings are approximately 25-35 seconds. The reason the response is plotted for a longer time period is to be able to look at the response of the building after the excitations have ended. This will be discussed further in Section 4.7.

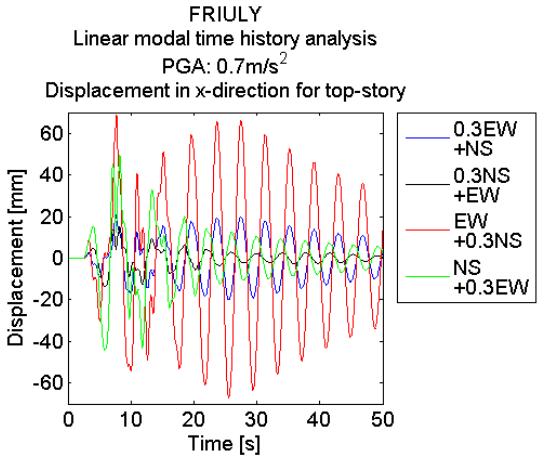

(a) x-direction displacement of the top story over time

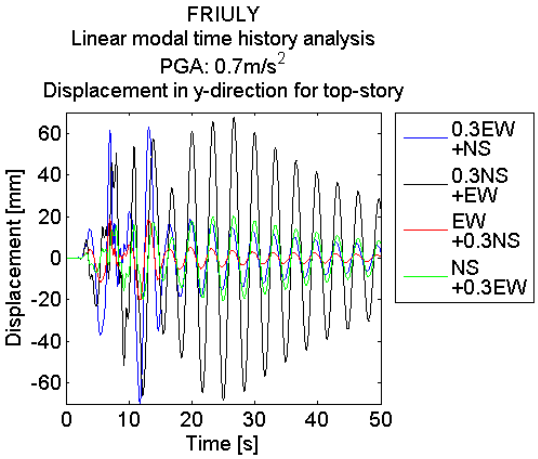

(b) y-direction displacement of the top story over time

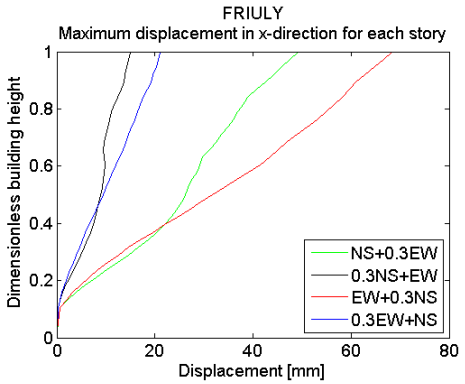

(c) Maximum displacement of each story in the x-direction

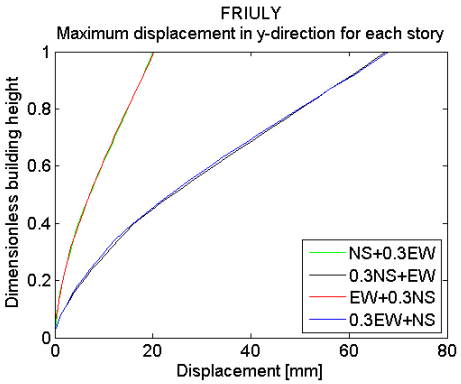

(d) Maximum displacement of each story in the y-direction

Figure 4.2: Displacements in the x- and y-direction for the Friuly earthquake

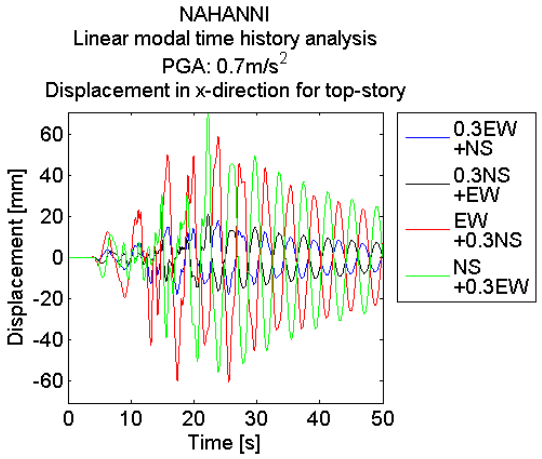

(a) x-direction displacement of the top story over time

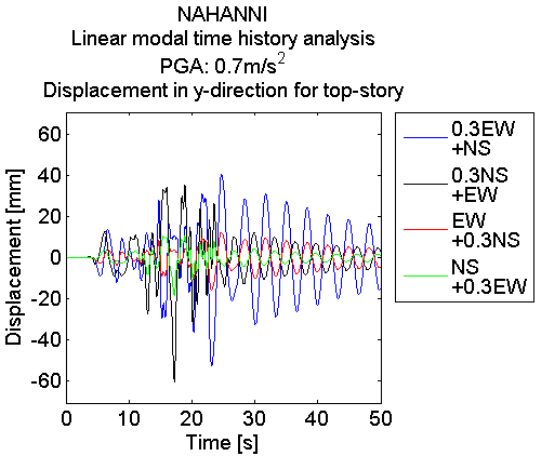

(b) y-direction displacement of the top story over time

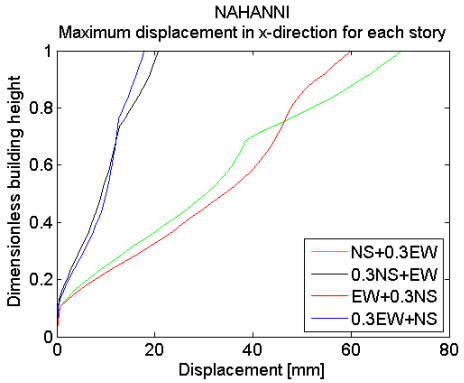

(c) Maximum displacement of each story in the x-direction

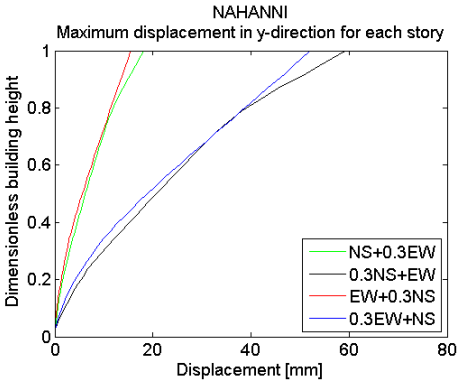

(d) Maximum displacement of each story in the y-direction

Figure 4.3: Displacements in the x- and y-direction for the Nahanni earthquake

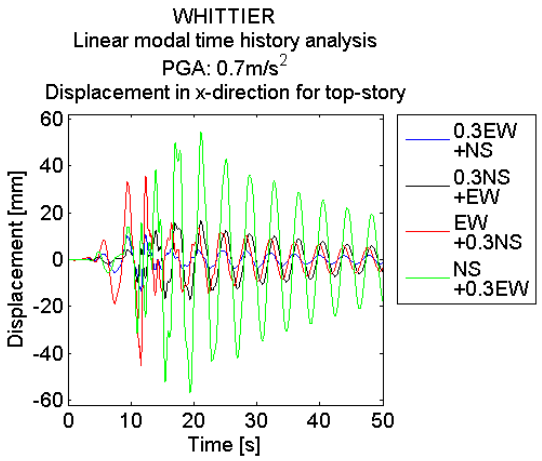

(a) x-direction displacement of the top story over time

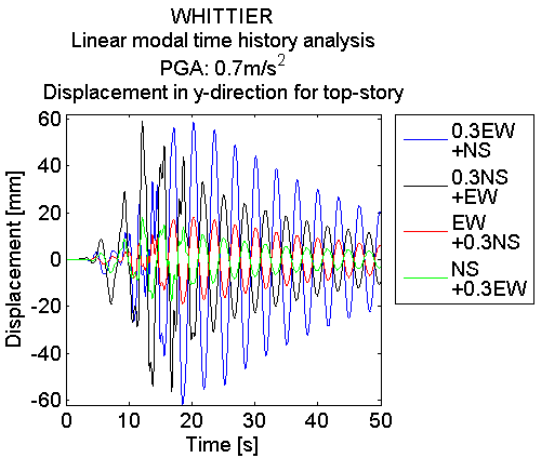

(b) y-direction displacement of the top story over time

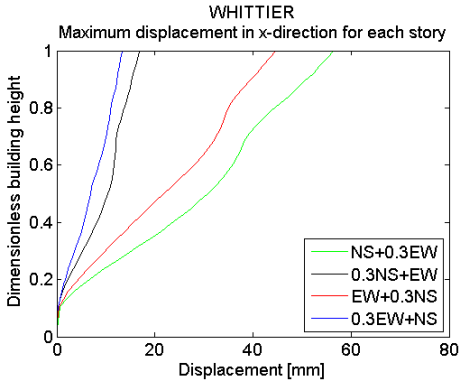

(c) Maximum displacement of each story in the x-direction

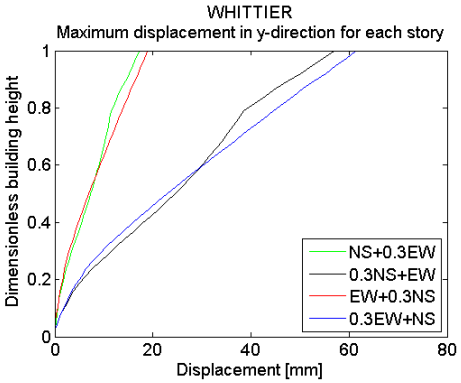

(d) Maximum displacement of each story in the y-direction

Figure 4.4: Displacements in the x- and y-direction for the Whittier earthquake

From these plots it is possible to see that the Friuly earthquake gives the largest response, especially the loadcases EW+0.3NS for displacement in the x-direction and 0.3NS+EW for displacement in the y-direction. Table 4.3 shows the maximum displacements, base moments and base shear forces for the different load cases. It is also possible here to see that the Friuly earthquake gives some of the largest responses. For the rest of the earthquake analyses, the Friuly EW+0.3NS and Friuly 0.3NS+EW load cases will therefore be focused on, unless otherwise specified.

Table 4.3: Results from linear modal acceleration time history analyses with PGA 0.7 m/s^2

Earthquake	Load case	Max base shear		Max base moment about axis			Max displacement	
		x-dir. $[N]$	y-dir. $[N]$	x-axis $[Nmm]$	y-axis $[Nmm]$	z-axis $[Nmm]$	x-dir. $[mm]$	y-dir. $[mm]$
Friuly	0.3EW+NS	6.28E+06	2.84E+07	8.44E+11	2.84E+11	7.93E+11	23.7	65.7
Friuly	0.3NS+EW	5.62E+06	2.64E+07	9.11E+11	2.08E+11	7.38E+11	17.8	63.7
Friuly	EW+0.3NS	1.77E+07	8.66E+06	2.55E+11	8.34E+11	2.61E+11	81.2	18.5
Friuly	NS+0.3EW	1.84E+07	7.82E+06	2.49E+11	6.16E+11	3.75E+11	56.7	18.5
Nahanni	0.3EW+NS	4.77E+06	2.35E+07	6.35E+11	1.90E+11	6.82E+11	20.0	52.3
Nahanni	0.3NS+EW	3.91E+06	3.07E+07	8.49E+11	1.43E+11	8.25E+11	19.3	59.2
Nahanni	EW+0.3NS	1.61E+07	6.97E+06	1.97E+11	6.45E+11	2.68E+11	69.0	15.2
Nahanni	NS+0.3EW	1.34E+07	9.17E+06	2.82E+11	4.98E+11	2.64E+11	69.0	18.4
Whittier	0.3EW+NS	4.16E+06	2.63E+07	7.42E+11	1.40E+11	6.51E+11	14.2	59.1
Whittier	0.3NS+EW	4.56E+06	2.34E+07	8.32E+11	1.72E+11	6.33E+11	16.6	54.6
Whittier	EW+0.3NS	1.32E+07	7.98E+06	2.36E+11	4.75E+11	2.57E+11	46.6	18.8
Whittier	NS+0.3EW	1.47E+07	7.10E+06	2.56E+11	5.18E+11	3.48E+11	52.9	16.3

The fact that the Friuly EW+0.3NS and Friuly 0.3NS+EW load cases give the largest responses in respectively the x- and y-direction can be explained from the response spectra for the time history components. One can notice that the EW component of the Friuly earthquake is the main component in both of these load cases. Table 4.1 shows that mode 1 is the most important for response in the x-direction, while mode 2 is the most important for response in the y-direction. Figure 4.5 shows plots of the response spectra for the acceleration time history components with the natural periods of the aforementioned modes shown as dotted lines.

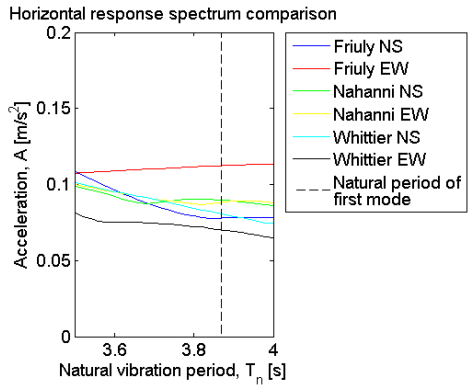

(a) Response spectrum comparison for the first natural period of the structure

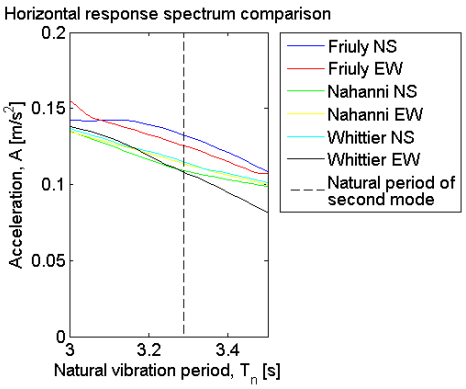

(b) Response spectrum comparison for the second natural period of the structure

Figure 4.5: Response spectrum comparisons for the first and second natural period of the building

From these plots, it is clear that for mode 1 and 2, components of the Friuly earthquake are the ones who give the largest response. This explains why the Friuly load cases are the ones who give the largest responses the the building as seen in Table 4.3.

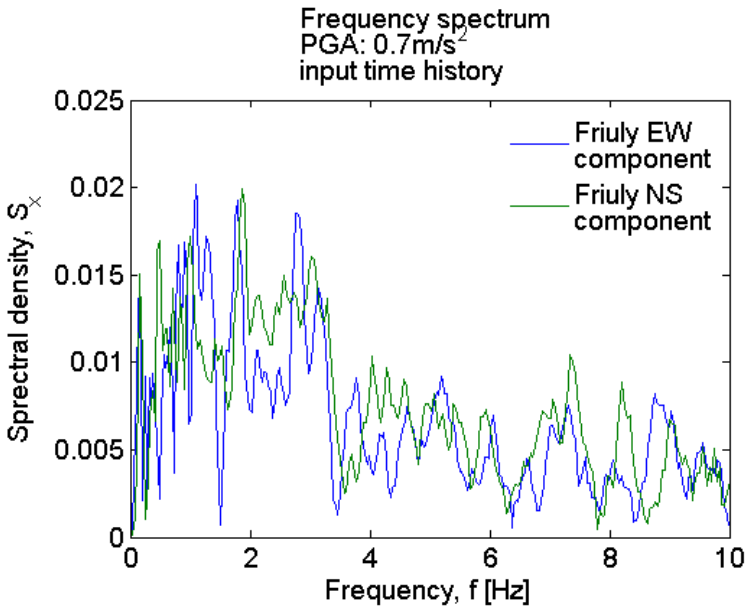

Figure 4.6: Fourier transform of the EW and NS components of the Friuly acceleration time history

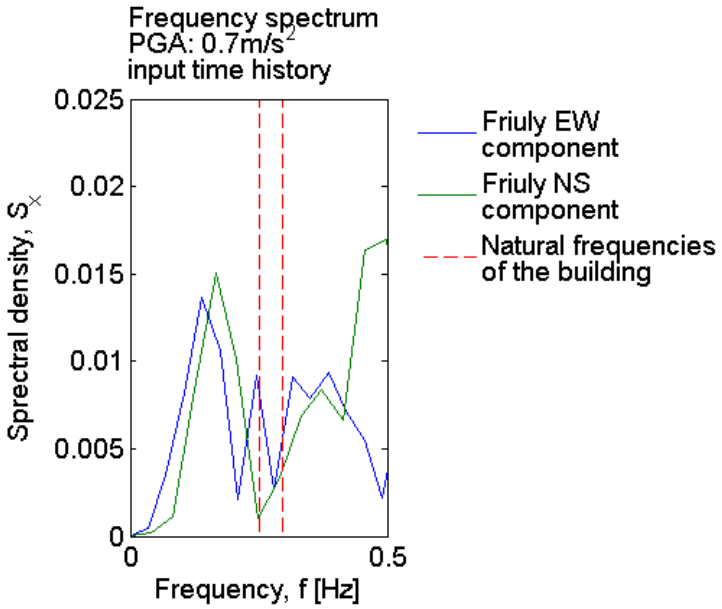

Figure 4.7: Fourier transform of the EW and NS components of the Friuly acceleration time history zoomed in and compared to the first two natural frequencies of the building

Figure 4.6 shows the frequency content of the modified Friuly acceleration time history records obtained by performing a Fourier transform of the records. The matlab script used for this operation is shown in appendix E. Figure 4.7 is a zoomed-in version of the same plot. From this plot, it is clear that the EW component of the Friuly record has a higher frequency content in the frequency range of the first two natural frequencies for

the building than the NS component does. This explains why the Friuly EW+0.3NS and Friuly 0.3NS+EW load cases are the ones who give the largest responses, since both of these load cases includes the EW component multiplied with a factor of 1 and the NS component multiplied with a factor of 0.3.

Figure 4.8 shows the inter-story drift in the x- and y-direction for the Friuly EW+0.3NS and Friuly 0.3NS+EW load cases. It is interesting to notice that for the first stories the inter-story drift is very low, both in the x-direction and the y-direction. This is as expected, as these floors are constructed with mainly concrete walls and concrete columns and are therefore very rigid. Also worth noticing, is the way the inter-story drift varies throughout the building height for the two different directions. In the x-direction the inter-story drift is at its peak around halfway up the building and thereafter decreases towards the top, while in the y-direction the inter-story drift varies almost linearly throughout the building height, with its maximum close to the top story. The reason for this is that area of the floors decreases towards the top of the building. This leads to a smaller mass per story. The stiffness in the x-direction does however remain almost the same in these stories as in the rest of the building, while the stiffness in the y-direction decreases. Thus, the mass-stiffness ratio will remain almost constant in the y-direction but change in the x-direction.

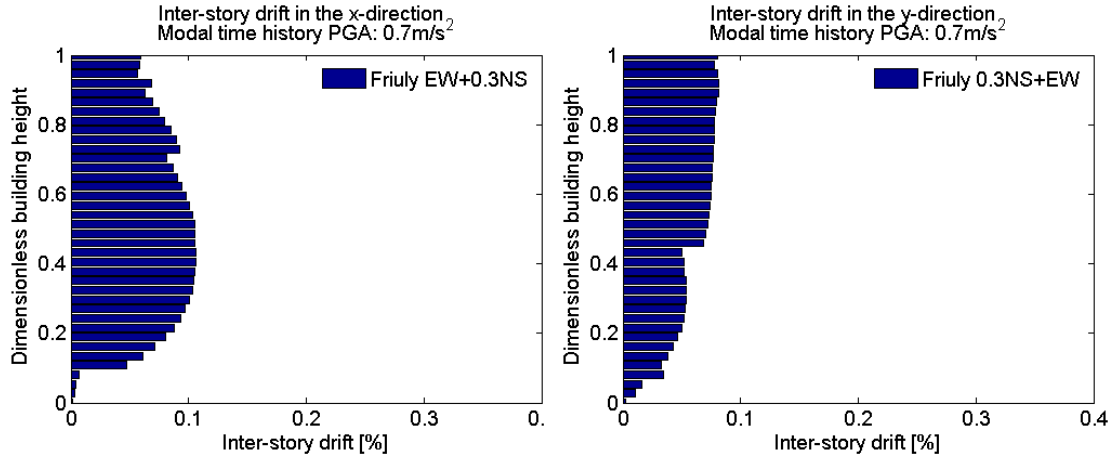

(a) Inter-story drift in the x-direction **(b)** Inter-story drift in the y-direction

Figure 4.8: Inter-story drift in the x- and y-direction for the most dominant modal time history load cases

4.3.2 Linear direct integration time history analysis

The other option for performing time history analyses in SAP2000 is direct integration time history analyses. These analyses solve the full equations of motion for each time-

step without the use of modal superposition [27]. Direct integration generally gives more accurate results than modal time history analyses for nonlinear analyses, but are more computationally expensive. For the following analyses, the *Hilber-Hughes-Taylor alpha* (HHT) method is used. Linear direct integration time history analyses are run for the two load cases discussed in the previous section. These linear direct integration analyses will be used to compare with the later nonlinear analyses, and are generally considered more accurate than the modal analyses. Table 4.4 compares the results obtained by modal and direct integration analyses.

Table 4.4: Results from linear direct integration acceleration time history analyses with PGA 0.7 m/s^2

			Modal time history	Direct integration time history	Difference
Max base shear	x-direction	$[N]$	1.77E+07	1.80E+07	1.5 %
	y-direction	$[N]$	2.64E+07	2.16E+07	-18.2 %
Max base moment	About x	$[Nmm]$	9.11E+11	6.81E+11	-25.2 %
	About y	$[Nmm]$	8.34E+11	7.36E+11	-11.7 %
	About z	$[Nmm]$	7.38E+11	5.76E+11	-22.0 %
Max displacement	x-direction	$[mm]$	81.2	83.9	3.4 %
	y-direction	$[mm]$	63.7	93.9	47.4 %

As seen in this table, there are some large differences between the results obtained from linear modal time history analysis and direct integration time history analysis. The largest differences occur for the base shear in the y-direction, the base moments and especially the displacement in the y-direction. The reason for these differences might be that 200 modes is not enough for the modal time history analyses, since the sums of the modal participating mass factor for the first 200 modes are respectively 0.92, 0.78, 0.69 and 0.66 for y-direction and rotation about the x-axis, y-axis and z-axis. Even though they are this different, the results from both types of analyses will be used as bases for comparison with other analyses; the results from the modal analysis will be compared to results from response spectrum analyses and to discuss the effects of tuned liquid dampers, while the results from the direct integration analysis will be compared to nonlinear direct integration time history analyses.

Figure 4.9 shows the maximum displacement of each story in the x- and y-direction for the linear direct integration time history analysis.

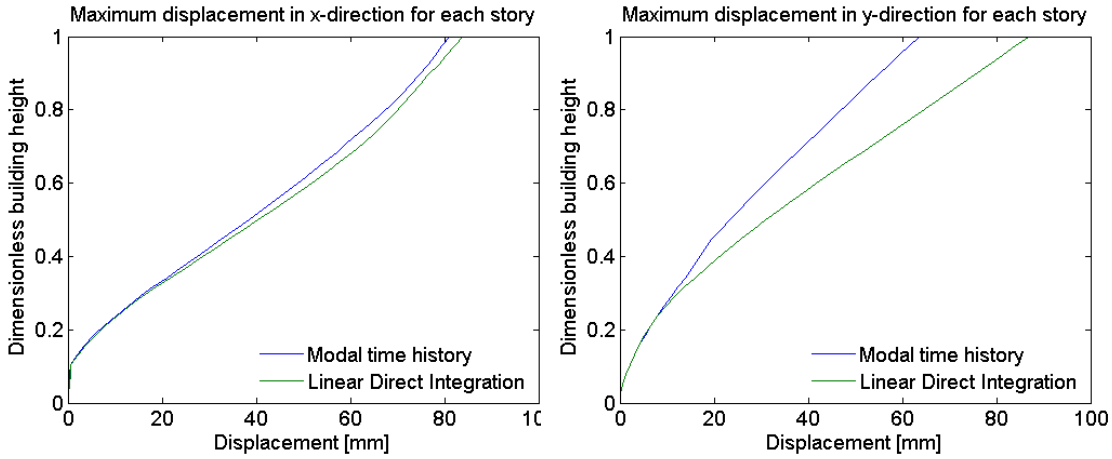

(a) Maximum displacement of each story in the x-direction

(b) Maximum displacement of each story in the y-direction

Figure 4.9: Maximum displacement of each story in the x- and y-direction for linear direct integration time history analysis compared to modal time history analysis with PGA 0.7 m/s^2

As seen in this figure, the maximum displacement in the x-direction is almost identical for the modal time history analysis and the linear direct integration time history analysis. For the displacement in the y-direction however, the displacement is nearly identical for the first stories, before the displacement obtained from the direct integration analysis increases more rapidly from around 20 % to 30 % up the height of the building. This tendency can also be observed in Figure 4.11, which shows the inter-story drift of each story for the two analysis methods plotted in the same plot. This indicates that when running direct integration analyses the top 70 % - 80 % of the building is considered more flexible in the y-direction than it does with modal analyses.

Figure 4.10 shows the inter-story drift of the stories for the linear direct integration time history analysis. When compared to Figure 4.8, it can be seen that the inter-story drift in the y-direction has a shape that looks more like the start of a sin-wave, while for the modal analysis the inter-story drift has an almost linear shape.

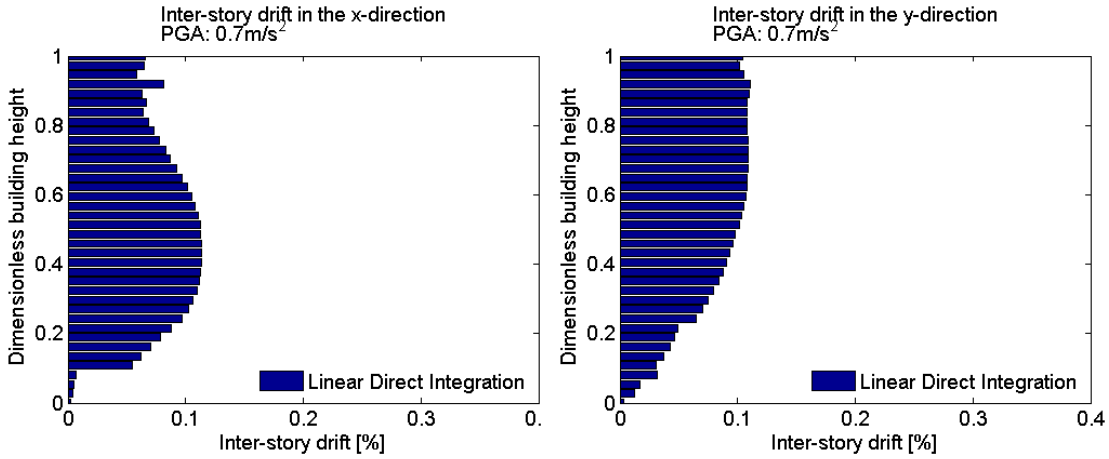

(a) Inter-story drift in the x-direction **(b)** Inter-story drift in the y-direction

Figure 4.10: Inter-story drift in the x- and y-direction for linear direct integration time history analysis with PGA 0.7 m/s^2

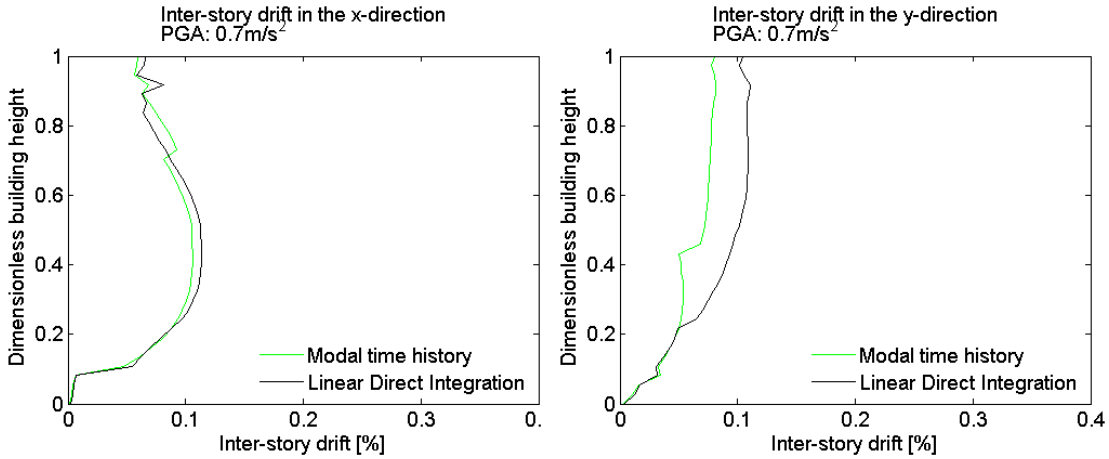

(a) Inter-story drift in the x-direction **(b)** Inter-story drift in the y-direction

Figure 4.11: Inter-story drift in the x- and y-direction for linear direct integration time history analysis compared to modal time history analysis with PGA 0.7 m/s^2

4.4 Quasi-static onlinear analyses

4.4.1 Initial $P-\Delta$ Analysis

For several analysis methods SAP2000 does not use the traditional iteration-based methods for incorporating $P-\Delta$ effects when analysing structures. Since the masses that causes the $P-\Delta$ effects, the masses of each floor, are constant, SAP2000 instead linearize the $P-\Delta$ effect and satisfy equilibrium in the deformed position without iterations. The $P-\Delta$ effects are incorporated into the structural stiffness matrix as a geometric

stiffness correction and will account for the change in eigenperiods and mode shapes used for static and dynamic analyses [11].

The method to incorporate this in SAP2000 is to use a so-called *initial* $P-\Delta$ *analysis*. This is a load-controlled nonlinear quasi-static load case that use the load case including dead-load, live-load and snow-load as loading. This load case creates a stiffness matrix for the building that takes the $P-\Delta$ effect into account. This stiffness can then be used as the initial conditions for other analyses, for instance linear direct-integration time-history analyses, and enables these analyses to be considered as linear and the results of these can be superposed [27].

The stiffness matrix obtained from the initial $P-\Delta$ analysis can also be used as an initial condition for a modal analysis. This way one can obtain the natural periods and mode shapes of a building including the $P-\Delta$ effect. These mode shapes can thereafter be used as a basis for other analyses like modal time-history analyses and response spectrum analyses. Table 4.5 shows the change in the ten first eigenperiods when including the $P-\Delta$ effects as described.

Table 4.5: Comparison of eigenperiods obtained with and without $P-\Delta$ effects

Mode	Natural period of vibration, T[s]		Difference
#	Without $P-\Delta$ effects	Including $P-\Delta$ effects	
1	3.993599	4.138586	3.63%
2	3.359992	3.458160	2.92%
3	2.442929	2.474102	1.28%
4	1.086345	1.102833	1.52%
5	0.730281	0.735822	0.76%
6	0.625829	0.628516	0.43%
7	0.555806	0.556117	0.06%
8	0.518859	0.523605	0.91%
9	0.388410	0.388995	0.15%
10	0.383773	0.386748	0.78%

These results are as expected, since the addition of $P-\Delta$ effects reduce the stiffness of the system, and a reduced stiffness will result in higher natural periods. As discussed in Section 2.8.1 the addition of $P-\Delta$ effects will generally have a higher impact on the modes with higher eigenperiods, and this corresponds well with the results in Table 4.5.

Table 4.6: Results from modal time history analysis with and without $P-\Delta$ effects included with PGA 0.7 m/s^2

			Modal time history w/o $P-\Delta$	Modal time history w/ $P-\Delta$	Difference
Max base shear	x-direction	$[N]$	1.77E+07	1.86E+07	4.8 %
	y-direction	$[N]$	2.64E+07	2.70E+07	2.2 %
Max base moment	About x	$[Nmm]$	9.11E+11	9.52E+11	4.5 %
	About y	$[Nmm]$	8.34E+11	8.67E+11	4.0 %
	About z	$[Nmm]$	7.38E+11	7.44E+11	0.8 %
Max displacement	x-direction	$[mm]$	81.2	80.3	-1.1 %
	y-direction	$[mm]$	63.7	61.6	-3.3 %

Table 4.6 shows the maximum base shear, base moment and displacement obtained from modal time history analyses using the modes obtained with initial $P-\Delta$ analysis compared to the results obtained from modal time history analyses using the modes obtained in Section 4.1. Section 2.8.1 states that for a well-designed building the differences in forces and displacements when including or excluding $P-\Delta$ effects should be less than 10 %. This corresponds well with the results in Table 4.6 where all the differences are less than 5 %. Using an initial $P-\Delta$ analysis to obtain modes and then using these in a modal time history analysis is however not the most accurate analysis method, and the influence of $P-\Delta$ effects will be further discussed in Section 4.5 where nonlinear direct integration time history analyses are performed with and without including $P-\Delta$ effects.

4.4.2 Modal Pushover Analysis

Pushover analyses are quasi-static nonlinear analyses where the lateral displacement is incrementally increased in order to find the weak links and failure modes of a structure [30]. These lateral displacements are most often compatible with a specified mode shape [29] , and in this project the modes described in Section 4.1 will be used; mode 1 for analysis in the x-direction and mode 2 for analysis in the y-direction. When performing pushover analyses in SAP2000, frame hinge locations first have to be defined manually as described in Section 3.4.2, along with the nonlinear properties of shell elements. The first load case defined for a pushover analysis should be a load-controlled nonlinear quasi-static load case similar to the initial $P-\Delta$ load case, although whether this load case includes $P-\Delta$ effects or not depend on whether $P-\Delta$ effects are going to be included in the pushover analysis or not. The main pushover load case will then be a displacement-controlled quasi-static nonlinear case which uses the stiffness at the end of the previous load case [27].

After the pushover analysis is finished, the pushover curve can be plotted. This is a plot of the base shear force versus the displacement of the top-story of the building. An idealized example of this type of curve is shown in Figure 4.12

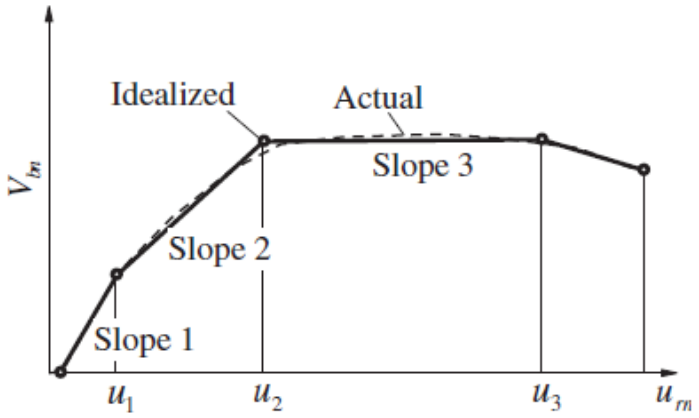

Figure 4.12: Pushover curve idealized as a tri-linear curve [31]

Figure 4.13 shows the pushover curves for the building in the x-direction and y-direction. Note that these analyses are done without taking into account $P - \Delta$ effects. From the plots, it is obvious that plasticity occurs for smaller displacements in the y-direction than for the x-direction. This is as expected from the geometry, since x-axis is the longitudinal axis, while the y-axis is the transverse axis, and the building is therefore expected to be "weaker" in that direction. From these plots, it is possible to see that the maximum displacement in the x-direction has to reach approximately 600 mm before any nonlinearity occurs, while for the y-direction nonlinearity is expected to start occuring at a maximum displacement of around 350 mm.

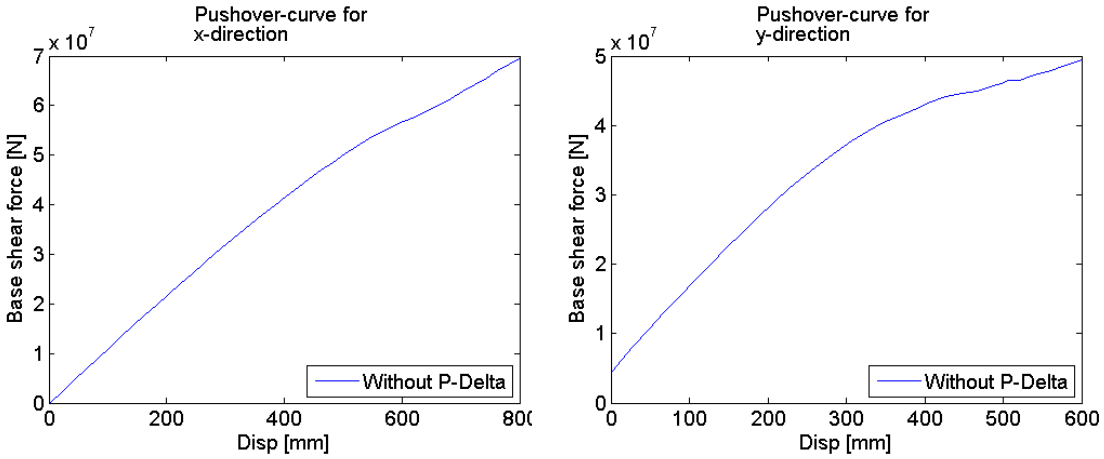

(a) Pushover curve for x-direction **(b)** Pushover curve for the y-direction

Figure 4.13: Pushover curves for the building in the x- and y-direction not including $P - \Delta$ effects

Appendix F shows plots of the maximum and minimum stresses in the concrete and rebar layers of the shear walls and elevator shafts for pushover analyses in the x- and y-direction. Figure 4.14 shows two plots of the rebar stresses that are representative for the plot in appendix F.3. As seen in this figure, the largest stresses occur in the lower stories of the shear walls and elevator shafts alike. This will therefore be where plasticity will first occur and can be considered the "weak points" of the building. The elevator shafts in the x-direction in Figure 4.14 have a 'gap' for a few stories. This has to do with the fact that not all of the elevator shafts go all the way to the top of the building. What looks like an elevator shaft that 'hangs' from the top of the building is in fact a part of a wall system for the top stories. There are consistent wall systems throughout the building's height just a few meters from the section shown in Figure 4.14, so what seem like a strange construction is in fact just a result of where the section cut has been chosen.

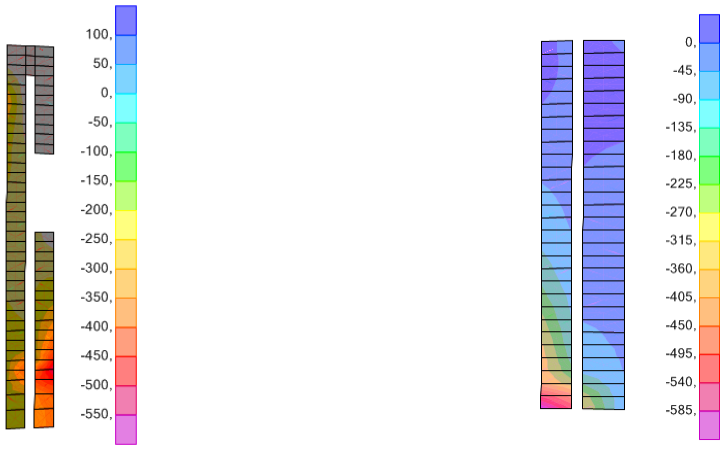

(a) Stresses in x-direction $[MPa]$ **(b)** Stresses in y-direction $[MPa]$

Figure 4.14: Minimum stresses in the rebar layer for pushover analyses in the x- and y-direction

4.4.3 Pushover Analysis Including $P-\Delta$ effects

When performing pushover analyses, the $P-\Delta$ effects can also be taken into account. Figure 4.15 shows the result of this plotted against the pushover curve without considering $P-\Delta$ effects.

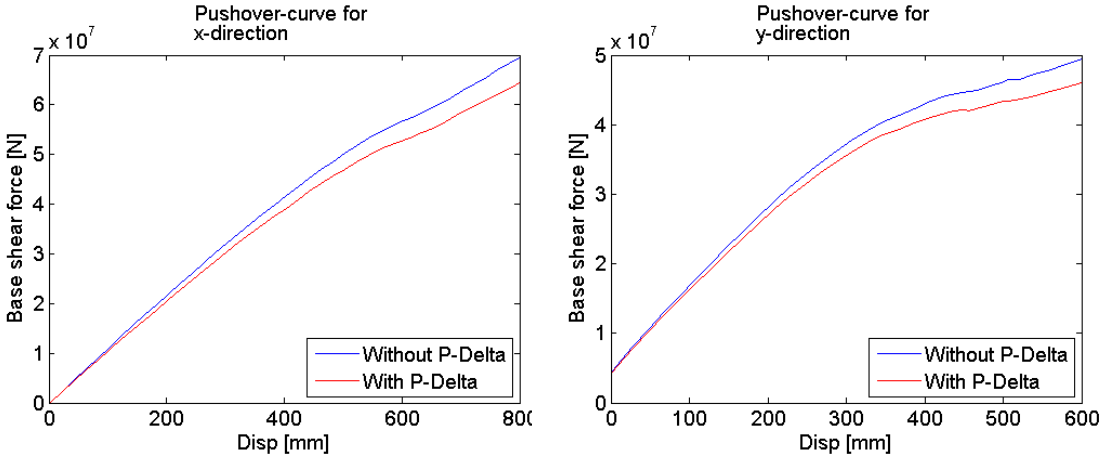

(a) Pushover curve for x-direction **(b)** Pushover curve for y.direction

Figure 4.15: Pushover curves for the building in the x- and y-direction including $P-\Delta$ effects

These plots show that the pushover curve for the analysis including $P-\Delta$ effects are similar to the pushover curve for the analysis that does not include $P-\Delta$ effects for small displacements. As the maximum displacement of the building increases however, the analysis that includes $P-\Delta$ effects shows smaller base shear forces for the same top-story displacement. This is as expected, since the $P-\Delta$ effects will reduce the stiffness

of the building as the lateral displacement is increased.

4.5 Nonlinear time history analyses

Nonlinear direct integration time history analyses are performed both including and excluding $P-\Delta$ effects. The results of these analyses are shown in Table 4.7, together with the results from the linear direct integration time history analyses.

Table 4.7: Results from linear and nonlinear direct integration acceleration time history analyses with PGA 0.7 m/s^2

			Linear	Nonlinear		Difference	Difference
				w/o $P-\Delta$	w/ $P-\Delta$	Lin. vs Nonlin.	w/o $P-\Delta$ vs. w/ $P-\Delta$
Max base shear	x-direction	$[N]$	1.80E+07	1.81E+07	1.80E+07	0.8 %	-0.9 %
	y-direction	$[N]$	2.16E+07	2.10E+07	2.09E+07	-2.8 %	-0.5 %
Max base moment	About x	$[Nmm]$	6.81E+11	6.78E+11	6.77E+11	-0.5 %	0.0 %
	About y	$[Nmm]$	7.36E+11	7.30E+11	7.22E+11	-0.8 %	-1.0 %
	About z	$[Nmm]$	5.76E+11	5.71E+11	5.68E+11	-0.9 %	-0.5 %
Max displacement	x-direction	$[mm]$	83.9	85.9	84.2	2.4 %	-2.0 %
	y-direction	$[mm]$	93.9	96.3	97.5	2.6 %	1.2 %

As seen in this table, there are basically no differences in the response from the nonlinear analysis compared to the linear analysis. This is as expected, since the PGA of the acceleration time histories used in the analyses is only 0.7 m/s^2, and this therefore represents a fairly small earthquake. In Section 4.9, the model will be subjected to larger earthquake records, and it can therefore be expected that the differences between the linear and nonlinear analyses are larger in Section 4.9.

Table 4.7 also shows that the effects of including $P-\Delta$ effects in the analyses are minimal. This can be asumed to be because the displacements of the stories are small and the overturning moment, because of lateral displacement, is therefore also small. The effect of including the $P-\Delta$ effects are also assumed to increase as the size of the earthquake and therefore the displacements are increased.

Figure 4.16 shows the maximum displacement of each story obtained from the nonlinear analyses compared to the linear analyses. As seen, the maximum displacement of each story is almost identical in the y-direction. For the x-direction however, the displacements are similar for the lower half of the building. For the upper half, the displacements obtained from the linear analysis follows a more linear pattern than the displacements obtained from the nonlinear analyses.

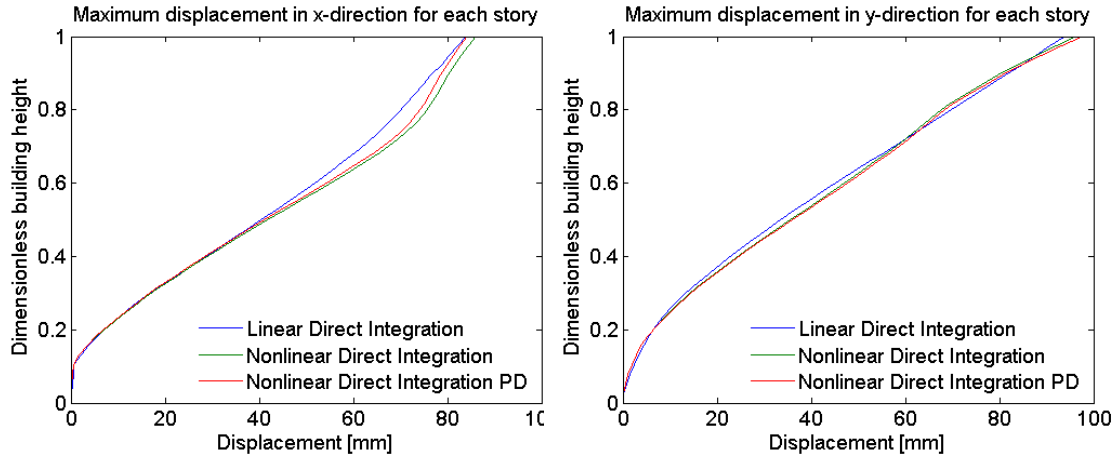

(a) Maximum displacement of each story in the x-direction

(b) Maximum displacement of each story in the y-direction

Figure 4.16: Maximum displacement of each story in the x- and y-direction for nonlinear direct integration time history analysis compared to linear direct integration time history analysis with PGA 0.7 m/s^2. PD in the legend means that $P - \Delta$ effects are included in this analysis

Figure 4.17 shows the inter-story drift obtained from the nonlinear analysis without including $P - \Delta$ effects, while Figure 4.18 plots this together with the inter-story drift obtained from linear analysis. The same trend can be observed here; the inter-story drift throughout the building varies between the linear and nonlinear analyses, but the maximum displacement is approximately the same. The inter-story drift in the y-direction also shows this tendency. This can be a sign that there are in fact nonlinear effects in the bulding even for this small earthquake, but that these effects are too small to have any major impact on the overall behavior of the building.

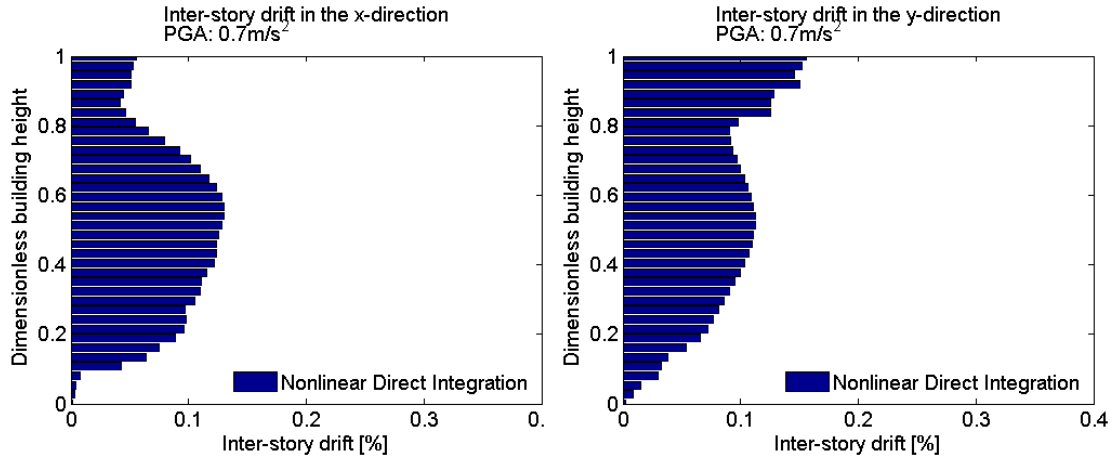

(a) Inter-story drift in the x-direction

(b) Inter-story drift in the y-direction

Figure 4.17: Inter-story drift in the x- and y-direction for nonlinear direct integration time history analysis with PGA 0.7 m/s^2

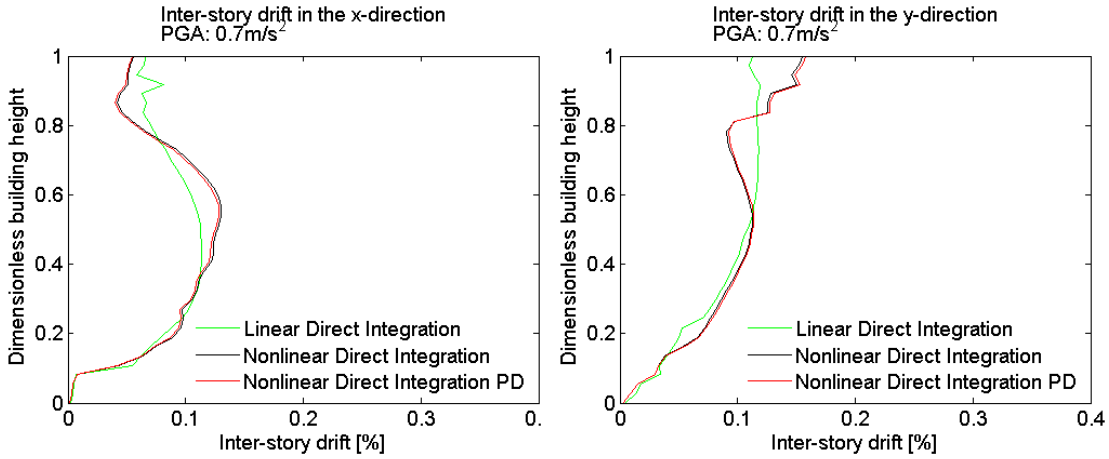

(a) Inter-story drift in the x-direction **(b)** Inter-story drift in the y-direction

Figure 4.18: Inter-story drift in the x- and y-direction for nonlinear direct integration time history analysis compared to linear direct integration time history analysis with PGA 0.7 m/s^2. PD in the legend means that $P - \Delta$ effects are included in this analysis

The stresses in the shear walls and elevator shafts are plotted in appendic F.1. Figure 4.19 shows two of these plots that are representative for the stresses occuring during the nonlinear direct integration analysis; the minimum stresses in the rebar layer in the shear wall and elevator shaft. As seen in these plots, the stresses in the rebar are small compared to the rebar yield stress (483 MPa), and as seen in the plots in appendix F.1, the stresses in the concrete layers are not reaching the yield stress either. It can however be observer that the largest stress magnitudes are obtained in the lower stories of the building, similar to during the pushover analyses discussed in Section 4.4.2, and this confirms the impression that plasticity in the shear walls and elevator shafts will occur in the lower stories first.

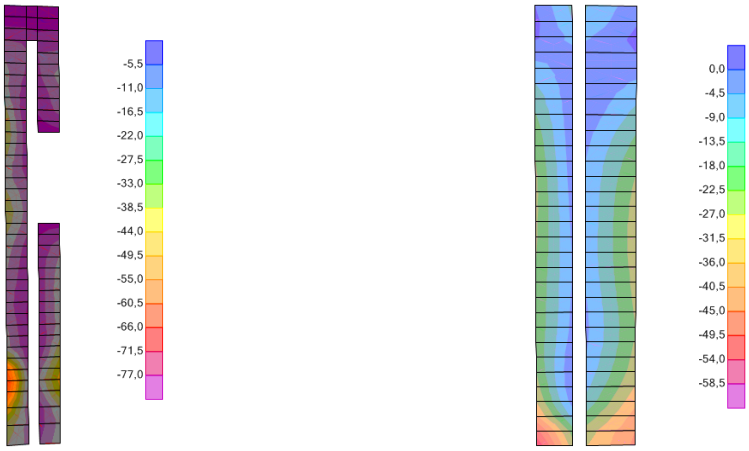

(a) Stresses in x-direction $[MPa]$ **(b)** Stresses in y-direction $[MPa]$

Figure 4.19: Minimum stresses in the rebar obtained from nonlinear direct integration time history analysis with PGA 0.7 m/s^2

4.6 Response spectra

In this section, analyses are performed following the response spectrum method outlined in Section 2.5 using the modes found in Section 4.1. The CQC combination rule, explained in Section 2.5, is used for modal combination, while the SRSS combination rule are used for directional combination.

The ductility factor q for Oslo Plaza can be calculated from the equations described in Section 2.8.4. The load carrying system is classified as an uncoupled ductile wall system. EC8 Table 5.1 then gives $q_0 = 3.0$ for DCM (ductility class medium). For the x-direction α_0 is then calculated as

$$\alpha_0 = \frac{4 * 2.75m}{4 * 5.4m} = 0.51 \tag{4.6}$$

k_w for the x-direction is then calculated as

$$k_w = 0.5 \leq (1 + \alpha_0)/3 \leq 1 \approx 0.5 \tag{4.7}$$

For the y-direction these calculations are

$$\alpha_0 = \frac{4 * 2.75m}{4 * 19m} = 0.14 \tag{4.8}$$

$$k_w = 0.5 \leq (1 + \alpha_0)/3 \leq 1 = 0.5 \tag{4.9}$$

For both the x- and y-direction the ductility factor q is therefore given by

$$q = q_0 k_w = 3.0 \cdot 0.5 = 1.5 \tag{4.10}$$

The response spectrum analysis is first done for a ductility factor of $q = 1.0$ and thereafter for $q = 1.5$.

Table 4.8 shows the result from the response spectrum analysis with $q = 1.0$ compared to the results from the linear modal time history analysis.

Table 4.8: Results from linear modal time history analysis and response spectrum analysis with PGA 0.7 m/s^2 and q = 1.0

			Modal time history	Response spectrum q = 1.0	Difference
Max base shear	x-direction	$[N]$	1.77E+07	2.08E+07	17.1 %
	y-direction	$[N]$	2.64E+07	3.13E+07	18.6 %
Max base moment	About x	$[Nmm]$	9.11E+11	1.05E+12	15.2 %
	About y	$[Nmm]$	8.34E+11	8.06E+11	-3.3 %
	About z	$[Nmm]$	7.38E+11	8.46E+11	14.6 %
Max displacement	x-direction	$[mm]$	81.2	76.6	-5.7 %
	y-direction	$[mm]$	63.7	73.5	15.5 %

Analyses using design spectra are generally meant to give conservative results. From Table 4.8 it is clear that the response from the response spectrum analysis give larger maximum base shear, base moment and displacements than the modal time history analyses with two exceptions. For all of the results, except max base moment about the y-axis and maximum displacement in the x-direction, the response spectrum results are approximately 15 % larger then the results from the modal analyses. The two exceptions might be explained by the fact that the frequency content of the acceleration time histories used for the modal analyses have been altered according to the EC8 response spectrum, as discussed in Section 3.3.3, and for some frequencies the acceleration time histories might therefore have a higher acceleration magnitude than the response spectrum, resulting in the response spectrum not being an envelope for the frequency content of equivalent time histories any more.

Figure 4.20 shows the maximum displacement of each story obtained from the response spectrum analysis compared to the results from modal time history analyses. As seen the shape of the functions are very similar, with the difference mainly being the magnitude of the displacement. This comes from the fact that the two analysis types use the same modes, but the frequency content used is a bit different, although modified to be fairly close.

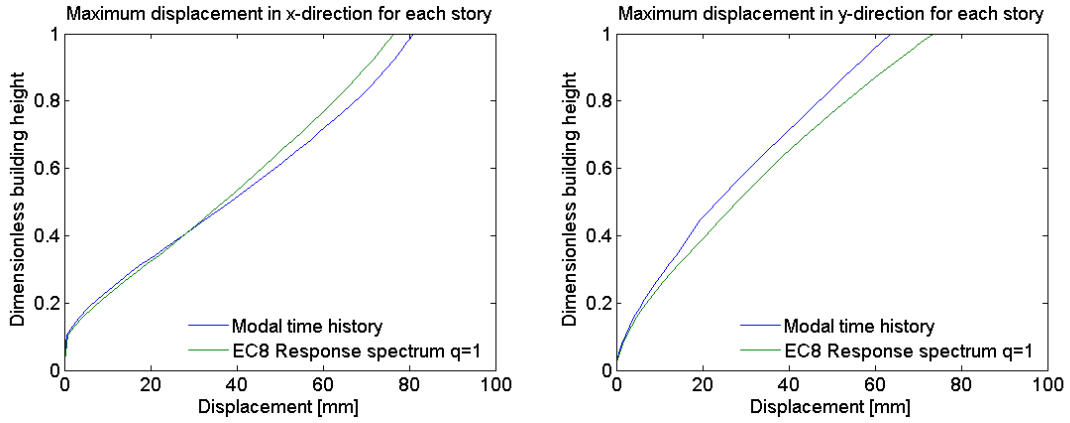

(a) Maximum displacement of each story in the x-direction

(b) Maximum displacement of each story in the y-direction

Figure 4.20: Maximum displacement of each story in the x- and y-direction for modal time history analysis compared to response spectrum analysis with q = 1.0

As shown earlier in this section Eurocode 8 [7] allows the use of a ductility factor $q = 1.5$ that takes into account the energy absorption from plastic effects in the building. Table 4.9 shows the maximum base shear, base moment and displacements obtained with a reponse spectrum analysis with $q = 1.5$ compared to with $q = 1.0$.

Table 4.9: Results from response spectrum analysis with PGA 0.7 m/s^2 and q = 1.5 compared to response spectrum analysis with PGA 0.7 m/s^2 and q = 1.0

			Response spectrum q = 1.0	Response spectrum q = 1.5	Difference
Max base shear	x-direction	$[N]$	2.08E+07	1.48E+07	-29.0 %
	y-direction	$[N]$	3.13E+07	2.12E+07	-32.4 %
Max base moment	About x	$[Nmm]$	1.05E+12	7.44E+11	-29.1 %
	About y	$[Nmm]$	8.06E+11	6.62E+11	-17.9 %
	About z	$[Nmm]$	8.46E+11	5.73E+11	-32.3 %
Max displacement	x-direction	$[mm]$	76.6	67.2	-12.2 %
	y-direction	$[mm]$	73.5	54.3	-26.2 %

As seen, all of the results are significantly lower when $q = 1.5$ is used, where the differences range from 12 % to 32 %. This is due to the factor q reducing the acceleration values of the input response spectrum function; the model is therefore subjected to smaller accelerations.

Figure 4.21 shows plots of the maximum displacements of each story for the response spectrum analyses with $q = 1.0$ and $q = 1.5$ and for the modal analysis. Again, it is clear that the main difference is the magnitude of the displacement, not the shape, as expected since the only difference is that the input magnitude has been reduced.

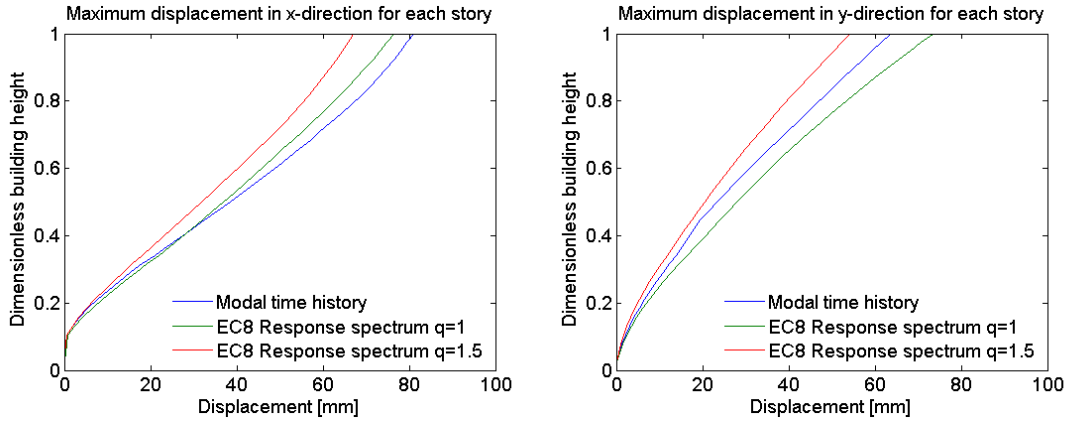

(a) Maximum displacement of each story in the x-direction

(b) Maximum displacement of each story in the y-direction

Figure 4.21: Maximum displacement of each story in the x- and y-direction for modal time history analysis compared to response spectrum analysis with q = 1.5

4.7 Approximation of damping in the building

The fraction of critical damping for a lightly damped system can be estimated by looking at a plot of the displacement over time for the system. In this section, this will be done using the plot of the displacement of the top-story of Oslo Plaza over time for the nonlinear direct integration time history analysis including $P - \Delta$ effects with a PGA of 0.7 m/s^2. Figure 4.22 and Figure 4.23 show these plots for the x- and y-direction displacements. Two peaks in each plot have been chosen and it is these values that will be used in the approximations.

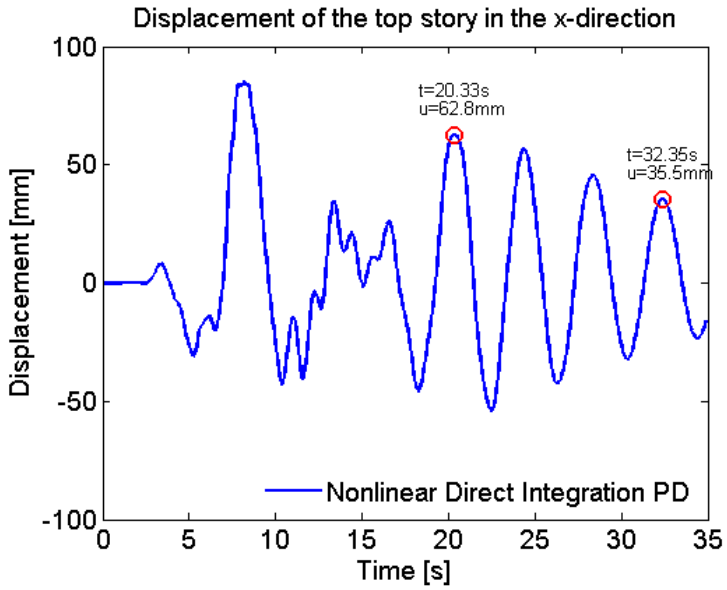

Figure 4.22: Peaks used for approximation of damping in the x-direction. PD in the legend means that $P - \Delta$ effects are included in this analysis

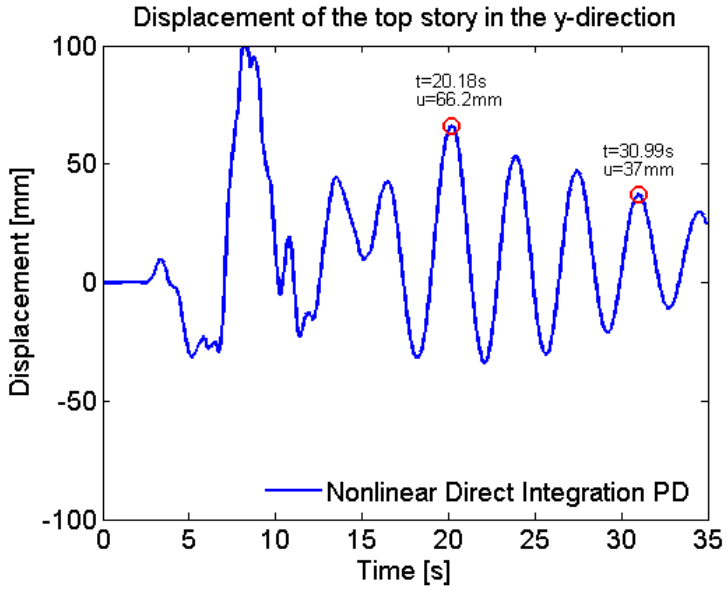

Figure 4.23: Peaks used for approximation of damping in the y-direction. PD in the legend means that $P - \Delta$ effects are included in this analysis

An approximation of the damping in the system can be obtained by using the following equations [8] using the values of two peaks located after the ground motion has ended.

$$\xi = \frac{\Delta_N}{2\pi N} \tag{4.11}$$

where N is the number of damped periods and Δ_N is given by

$$\Delta_N = ln\frac{u_1}{u_2} \tag{4.12}$$

where u_1 and u_2 are the displacements of the two peaks.

For the displacement in the x-direction these values are found to be $u_1 = 62.8mm$, $u_2 = 35.5mm$ and $N = 3$ from Figure 4.22. Using these values in equation 4.11 and equation 4.12 a fraction of critical damping of $\xi = 0.03$ is obtained.

From Figure 4.23 the values $u_1 = 66.2mm$, $u_2 = 37.0mm$ and $N = 3$ are obtained. This gives a fraction of critical damping in the y-direction of $\xi = 0.03$.

These values for the damping $\xi = 0.03$ are larger than the assumed damping of $\xi = 0.02$ used for the modal time history analysis. This can mean that the damping in the system is larger than expected, but this difference can also be due to an uncertainty in the approximation of the damping.

4.8 Tuned liquid damper

In this section, the swimming pool in one of the top stories in Oslo Plaza will be treated as a TLD and modeled as a TMD as described in Section 2.9. After modeling it with the properties of the swimming pool, the dimension of the pool will be altered to see which pool dimesnsions would be optimal for the pool to act as a TLD and reduce the effects of an earthquake on Oslo Plaza.

The TMD is modeled as a pendulum using a 2-node link object in SAP2000. These link objects have the properties found by using the formulas in Section 2.9. Nonlinear modal time history analyses, also called fast nonlinear analysis (FNA), are then used to observe the effect of the TMD. This analysis method is chosen because it is computationally inexpensive and the results can easily be compared to the results obtained by linear modal time history analyses since the only nonlinearity FNAs take into account are link objects, i.e. the only difference between the linear modal time history analysis and the FNA will be the effect of the TMD.

4.8.1 Current swimming pool modeled as a TMD

The dimensions of the pool, located on the 35^{th} floor, is shown in Table 4.10. The length of the pool is considerably longer than its width, and it is therefore expected any possible effects of the TLD is in the x-direction. This is because the dimension of the waves in the y-direction probably are too small to make any impact, while in the x-direction the waves have the potential to slosh back and forth.

Table 4.10: Dimensions of the swimming pool. L is in the x-direction

h_0	L	B
1.85 m	13.80 m	2.60 m

Using the methods described in Section 2.9, the TMD properties shown in Table 4.11 is obtained. The natural period of the TMD in the x- and y-direction are 6.67 s and 1.85 s, while the two first natural periods of the building are 3.99 s and 3.36 s. Because of this big difference in natural periods, the TMD is expected to have close to zero impact on the result.

Table 4.11: Properties of the equivalent TMD for the swimming pool

	m_v $[kg]$	c_v $[Ns/m]$	k_v $[N/m]$	T_v $[s]$
x-dir	50833	49	45172	6.67
y-dir	23525	35	272546	1.85

Table 4.12 shows the base reactions and maximum displacements obtained by FNA including the TMD compared to linear modal time history analysis without the TMD. Figure 4.24 shows the maximum displacement of each story in the x- and y-direction for the two analysis methods. As expected, the results are basically the same and the pool has no damping effect on the building.

Table 4.12: Results from modal time history analysis without TMD and FNA with TMD with PGA 0.7 m/s^2

			Modal time history w/o TMD	FNA with TMD	Difference
Max base shear	x-direction	$[N]$	1.77E+07	1.75E+07	-1.2 %
	y-direction	$[N]$	2.64E+07	2.64E+07	-0.1 %
Max base moment	About x	$[Nmm]$	9.11E+11	9.11E+11	0.0 %
	About y	$[Nmm]$	8.34E+11	8.35E+11	0.1 %
	About z	$[Nmm]$	7.38E+11	7.36E+11	-0.3 %
Max displacement	x-direction	$[mm]$	81.2	80.9	-0.3 %
	y-direction	$[mm]$	63.7	63.2	-0.7 %

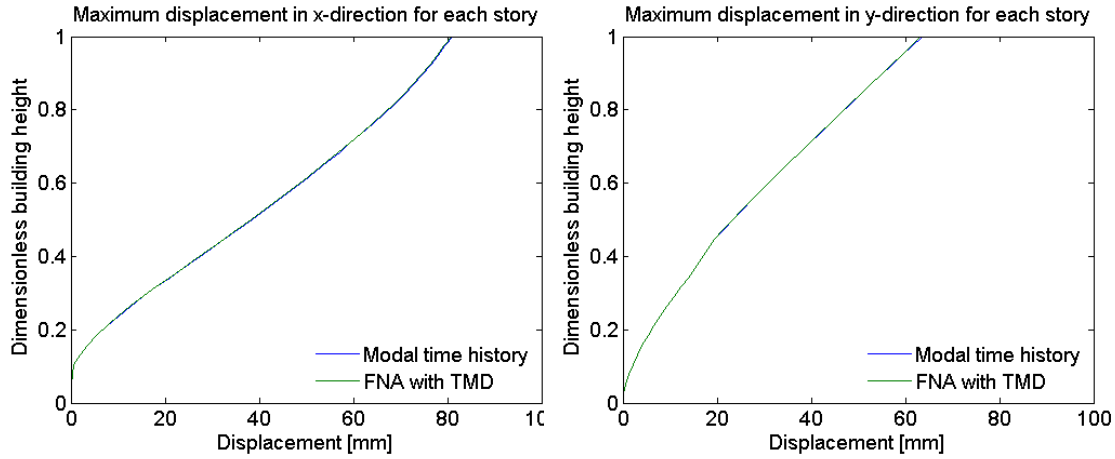

(a) Maximum displacement of each story in the x-direction

(b) Maximum displacement of each story in the y-direction

Figure 4.24: Maximum displacement of each story in the x- and y-direction for FNA with TMD compared to modal time history analysis without TMD

4.8.2 Modified dimensions of swimming pool modeled as a TMD

If the dimensions of the pool had been different, it is expected that it could actually damp some of the response from an earthquake. To be able to work as a TLD, the natural period of the equivalent TMD in one direction should be as close as possible to the first natural period of the building in that direction. By modifying the dimensions of the pool to the values shown in Table 4.13, the natural period of the TMD in the x-direction is changed. With these pool dimensions, the equivalent TMD has the properties shown in Table 4.14.

Table 4.13: Modified dimensions of the swimming pool. L is in the x-direction

h_0	L	B
1.90 m	8.00 m	2.60 m

Table 4.14: Properties of the modified equivalent TMD for the swimming pool

	m_v $[kg]$	c_v $[Ns/m]$	k_v $[N/m]$	T_v $[s]$
x-dir	27170	33	66237	4.02
y-dir	13673	21	158823	1.84

The natural period of the TMD in the x-direction is now 4.02 s, which is a lot closer to the first natural period of the building at 3.99 s. It is therefore expected that the

TMD with these properties will have a large impact on the effects of an earthquake in the x-direction, i.e. base shear and displacement in the x-direction and the base moment about the y-axis. The base reactions and maximum displacements obtained by a FNA including the modified TMD comapred to a linear modal time history analysis without the TMD is shown in Table 4.15 and the maximum displacement of each story in the x- and y-direction of the two analysis methods are shown in Figure 4.25.

Table 4.15: Results from modal time history analysis without TMD and FNA with modified TMD with PGA 0.7 m/s^2

			Modal time history w/o TMD	FNA with TMD	Difference
Max base shear	x-direction	$[N]$	1.77E+07	1.32E+07	-25.7 %
	y-direction	$[N]$	2.64E+07	2.51E+07	-5.2 %
Max base moment	About x	$[Nmm]$	9.11E+11	9.00E+11	-1.1 %
	About y	$[Nmm]$	8.34E+11	7.35E+11	-11.9 %
	About z	$[Nmm]$	7.38E+11	7.35E+11	-0.5 %
Max displacement	x-direction	$[mm]$	81.2	61.6	-24.1 %
	y-direction	$[mm]$	63.7	63.0	-1.1 %

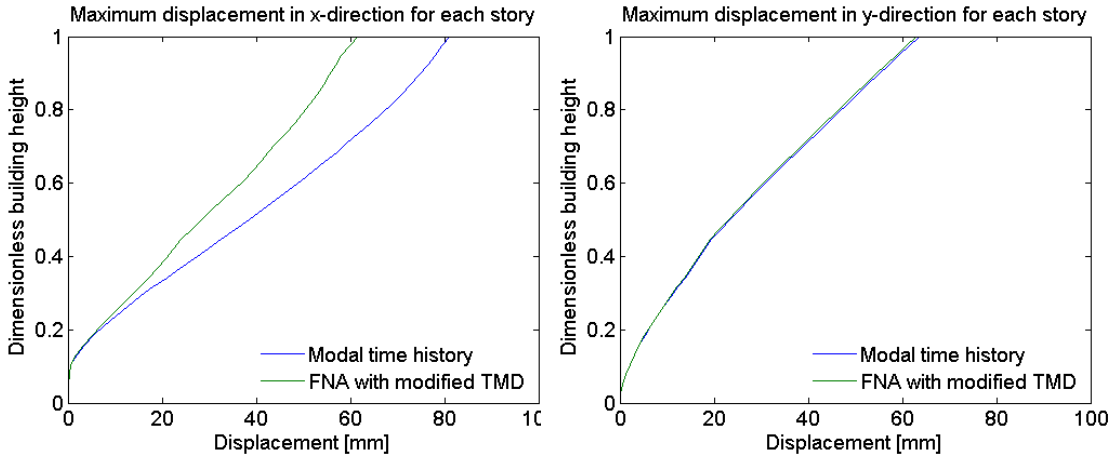

(a) Maximum displacement of each story in the x-direction

(b) Maximum displacement of each story in the y-direction

Figure 4.25: Maximum displacement of each story in the x- and y-direction for FNA with modified TMD compared to modal time history analysis without TMD

As expected, the modified TMD has a significant impact on the base shear and displacement in the x-direction and the base moment about the y-axis. The base shear and maximum displacement in the x-direction is reduced by approximately 25 % and the base moment about the y-axis is reduced by about 12 %. These are significant differences and it can be concluded that if the pool had been 8 m, long instead of 13.8 m, and 0.05 m deeper the building would have experienced an additional damping during earthquakes. This is a damping that could have been obtained with no additional cost, with the only

drawback being the pool would be smaller. This means of course, that fewer guests at the hotel would be able to use it at the same time and it may be less esthetically pleasing, as the current pool dimensions match the dimensions of that story. There would also be less water in the pool and therefore less water that could be used in an emergency, such as a fire. From a purely Earthquake design viewpoint, it is however clear that building the pool with the proposed dimensions, instead of the dimensions it currently has, could be a simple method for improving the behavior of the building during an earthquake.

4.9 Analyses with higher PGA

To look further at the nonlinear behavior of the building during time history analyses, it has been chosen to perform these analyses for a higher PGA also. In this case, the PGA of an earthquake with a return period of 3000 years has been chosen. Seismic Zonation of Norway [1] does not give maps of PGA contour lines for this return period, but it does provide these for return periods of 475, 1000 and 10000 years. If fitting these values to a second order curve and interpolating it is possible to find a PGA for an earthquake with a return period of 3000 years. The matlab script to do this can be seen in appendix D, and the result is shown in Figure 4.26.

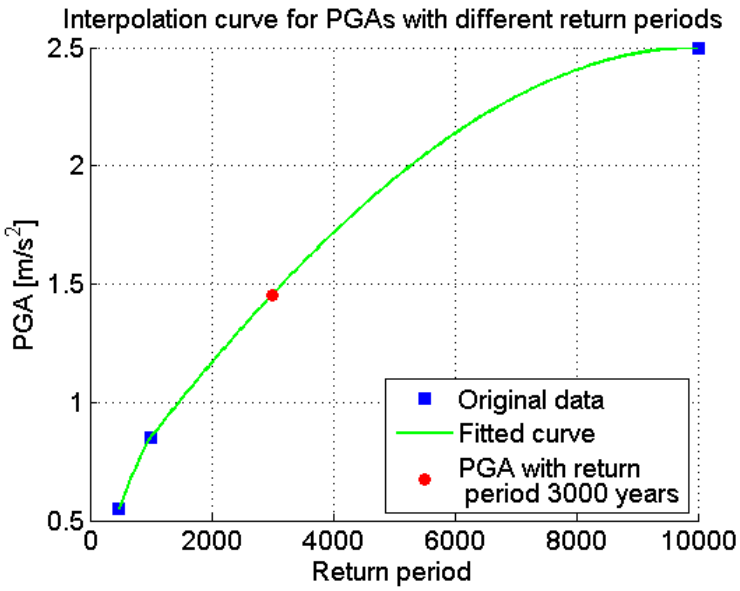

Figure 4.26: Interpolation of expected PGAs based on return periods

Doing this a PGA of 1.45 m/s^2 is obtained. Using the formulas described in Section 3.3, the following scaled PGA is obtained:

$$a_g S = 1.45\ m/s^2 \cdot 0.8 \cdot 1.6 \approx 1.86\ m/s^2 \tag{4.13}$$

The acceleration time histories for the Friuly earthquake is then scaled to this value, and the frequency content is modified as described in Section 3.3.

Table 4.16 shows the maximum base shear, base moment and displacements obtained from three different direct integration time history analyses using these acceleration time histories: linear, nonlinear without $P-\Delta$ effects and nonlinear including $P-\Delta$ effects.

Table 4.16: Results from linear and nonlinear direct integration acceleration time history analyses with PGA 1.86 m/s^2

			Linear	Nonlinear		Difference	Difference
				w/o $P-\Delta$	w/ $P-\Delta$	Lin. vs Nonlin.	w/o $P-\Delta$ vs. w/ $P-\Delta$
Max base shear	x-direction	$[N]$	9.77E+07	5.05E+07	5.09E+07	-48.3 %	0.6 %
	y-direction	$[N]$	1.14E+08	4.69E+07	4.78E+07	-58.8 %	2.0 %
Max base moment	About x	$[Nmm]$	4.94E+12	2.11E+12	2.12E+12	-57.4 %	0.9 %
	About y	$[Nmm]$	5.93E+12	3.32E+12	3.34E+12	-44.1 %	0.6 %
	About z	$[Nmm]$	3.24E+12	1.48E+12	1.54E+12	-54.2 %	3.6 %
Max displacement	x-direction	$[mm]$	665.6	530.4	535.7	-20.3 %	1.0 %
	y-direction	$[mm]$	425.8	442.9	444.3	4.0 %	0.3 %

As seen in Table 4.16, there are significant differences between the results obtained with linear and nonlinear analyses with a PGA of 1.86 m/s^2. The difference for the maximum base shears and base moments are between 44 % and 59 % and the difference for the maximum displacement in the x-direction is approximately 20 %. For the maximum displacement in the y-direction however, there is a minimal difference between the results obtained by linear and nonlinear analyses.

When it comes to $P-\Delta$ effects, the difference between including these and not including these is less than 4 % for all max base shears, base moments and displacements. This is more than the difference was for analyses with PGA 0.7 m/s^2, but the influence of $P-\Delta$ effects are still small with PGA 1.86 m/s^2.

Figure 4.27 shows the maximum displacement of each story in the x- and y-direction for the three different analyses previously described. As seen, the displacement of each story during nonlinear analyses are substantially smaller than during linear analyses for the x-direction, while for the y-direction the displacements are almost the same.

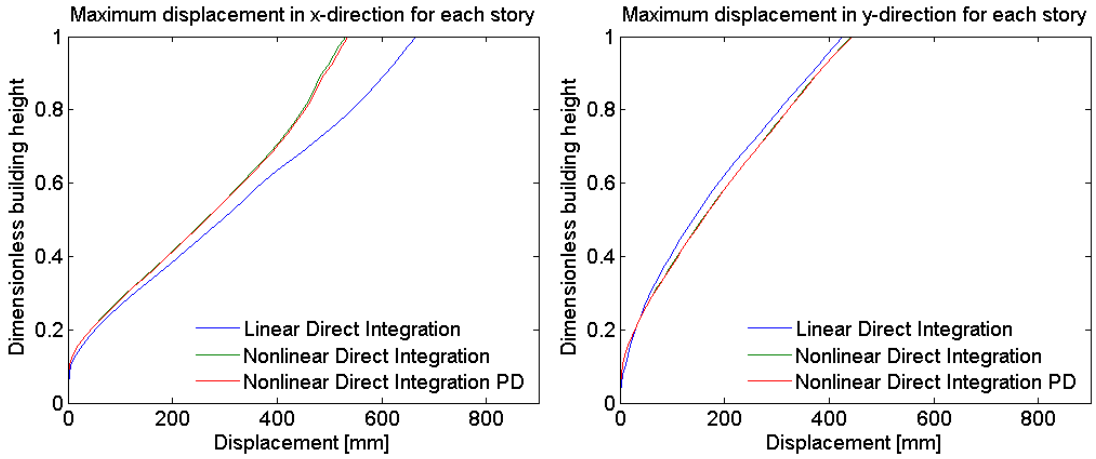

(a) Maximum displacement of each story in the x-direction

(b) Maximum displacement of each story in the y-direction

Figure 4.27: Maximum displacement of each story in the x- and y-direction for linear direct integration time history analysis compared to nonlinear direct integration time history analysis with PGA 1.86 m/s^2. PD in the legend means that $P-\Delta$ effects are included in this analysis

Maximum and minimum stresses in the rebar and concrete layers for the shear wall and elevator shafts for the analyses with PGA 1.86 m/s^2 are shown in appendix F.2. Figure 4.28 shows the minimum stresses in the rebar layer obtained during the analyses. The yield stress of the rebar material is reached in the lower stories of the building, while the stresses in the rest of the building remain small compared to the yield stress. This shows the same tendency as in Section 4.4.2 and Section 4.5; plasticity occurs in the lower stories of the structure.

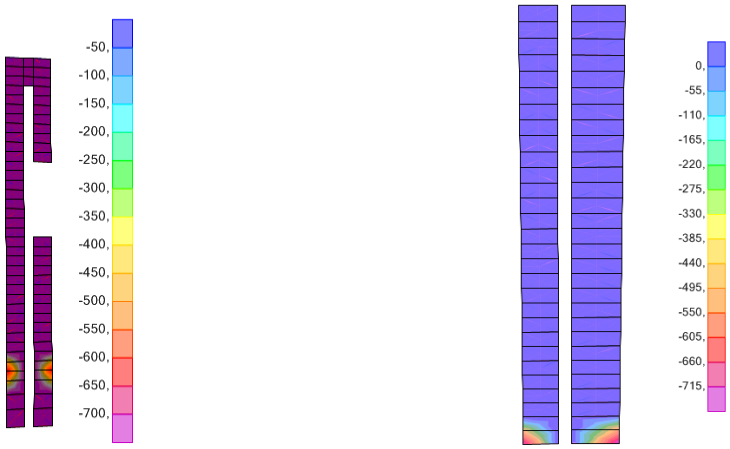

(a) Stresses in x-direction $[MPa]$

(b) Stresses in y-direction $[MPa]$

Figure 4.28: Minimum stresses in the rebar obtained from nonlinear direct integration time history analysis with PGA 1.86 m/s^2. PD in the legend means that $P-\Delta$ effects are included in this analysis

5 Comparisons and discussion

5.1 Natural periods of the building

A fourier transform of the roof displacement over time is performed for the results obtained by linear modal, linear direct integration and nonlinear direct integration time history analyses to obtain the frequency spectrum of the output motion. This is done in order to compare how the fundamental periods of the building changes as nonlinear effects occur. The matlab script used for this operation is shown in appendix G. Figure 5.1 shows the result of the fourier transform for the displacements during the PGA 0.7 m/s^2 analyses, while Figure 5.2 shows the same for PGA 1.86 m/s^2.

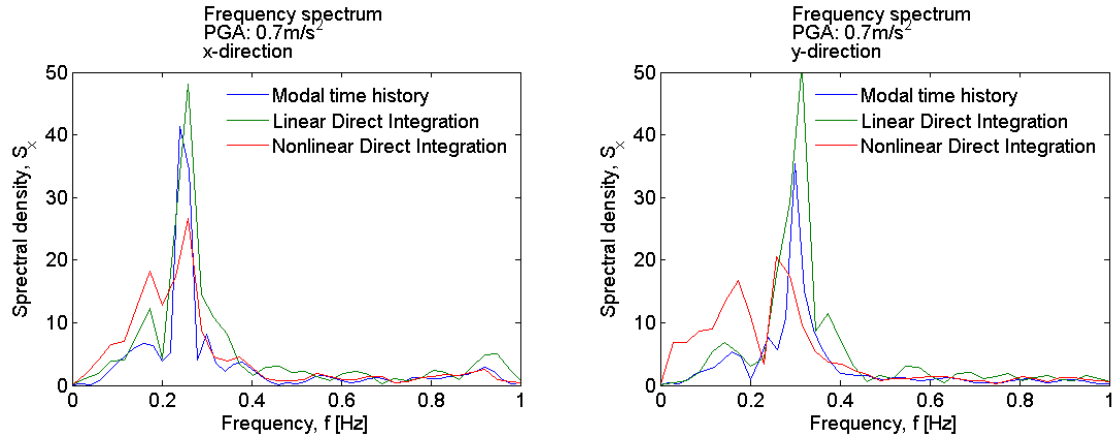

(a) Fourier transform of the displacement of the top story in the x-direction

(b) Fourier transform of the displacement of the top story in the y-direction

Figure 5.1: Fourier transform of the displacement of the top story in the x- and y-direction for modal, linear direct integration and nonlinear direct integration time history analyses with PGA 0.7 m/s^2

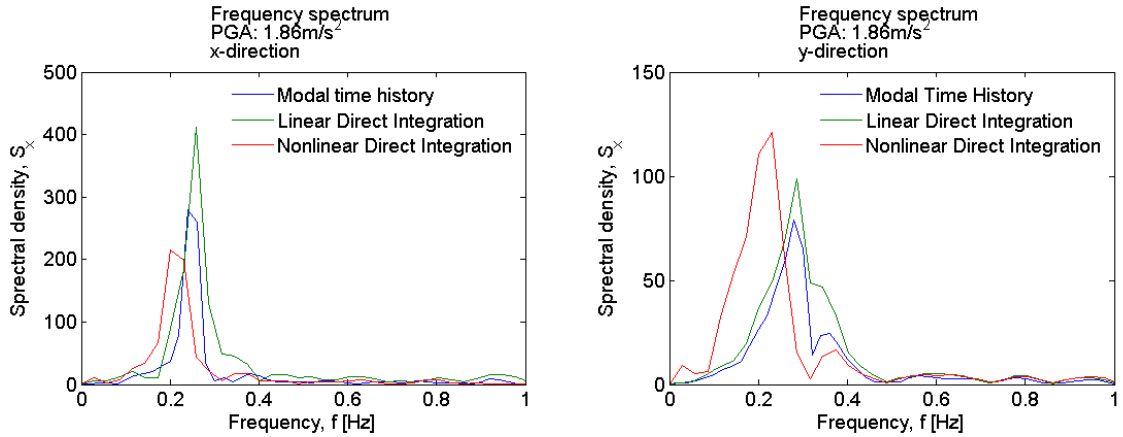

(a) Fourier transform of the displacement of the top story in the x-direction

(b) Fourier transform of the displacement of the top story in the y-direction

Figure 5.2: Fourier transform of the displacement of the top story in the x- and y-direction for modal, linear direct integration and nonlinear direct integration time history analyses with PGA 1.86 m/s^2

As seen in these figures, the location of the largest peak is the same for linear and nonlinear analyses in the x-direction with PGA 0.7 m/s^2, while the largest peak for the y-direction results is located at a smaller frequency for the nonlinear analysis than for linear analyses. The largest peak has a significantly smaller frequency for the nonlinear analysis with PGA 1.86 m/s^2. This is an indication that there are no major nonlinear effects occurring during earthquakes as small as 0.7 m/s^2 in the x-direction, but some nonlinear effects occur in the y-direction. For PGA 1.86 m/s^2, the behavior of the building changes drastically and the first and second natural period increases, as shown by the peak for the nonlinear analyses being located at significantly smaller frequencies.

Table 5.1 shows the natural periods of the system obtained from different types of analyses. The estimates of the system's natural periods, calculated in Section 4.2, enclose all the other natural periods obtained, but this is as expected, since they are very rough estimates and provide a huge difference between the upper and lower boundary for the eigenperiods. Worth noting, is that the natural periods obtained for the structural element model matches the natural periods obtained by fourier transforms of the output fairly well.

Table 5.1: Comparison of the first natural periods in the x- and y-direction of the building calculated with different methods

	Analysis	Linearity	PGA $[m/s^2]$	1st period $[s]$	2nd period $[s]$
Structural element model		w/o $P-\Delta$		3.99	3.36
		w/ $P-\Delta$		4.14	3.46
Element model simulation	Modal	Linear	0.70	4.16	3.33
			1.86	4.16	3.57
	Direct integration	Linear	0.70	3.87	3.16
			1.86	3.87	3.48
		Nonlinear	0.70	3.87	3.87
			1.86	4.97	4.35
Estimate	Rayleigh quotient			3.23	1.85
	Dunkerley-Mikhlin			9.19	4.82

5.2 Comparison of nonlinearity from pushover analysis and direct integration time history analysis

Figure 5.3 and Figure 5.4 show the pushover curves in the x- and y-direction, in addition to the maximum base shear, obtained by nonlinear direct integration time history analysis, plotted against the maximum displacements, obtained by the same analysis.

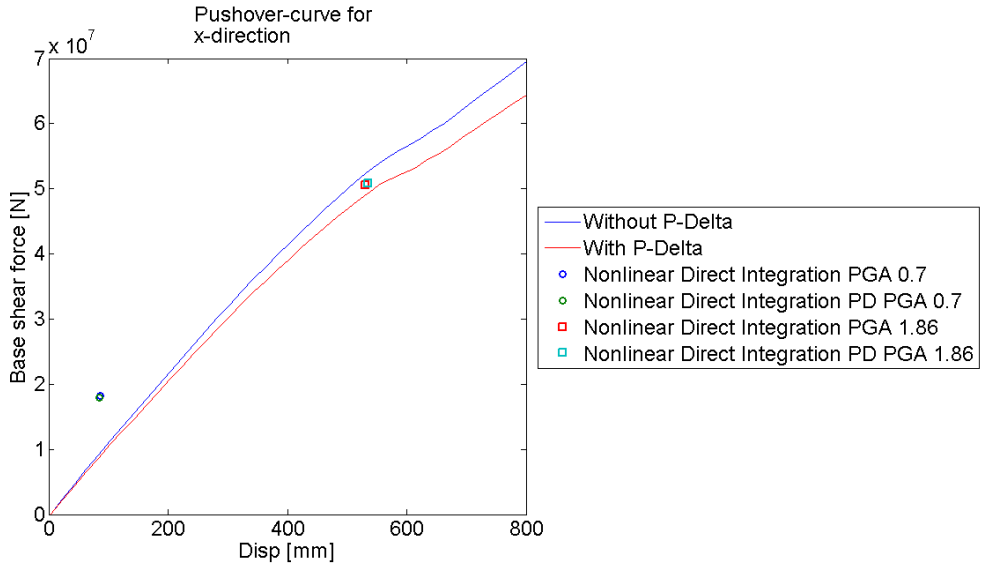

Figure 5.3: Pushover analysis in the x-direction compared to maximum values of displacement and base shear for the nonlinear direct integration time history analyses

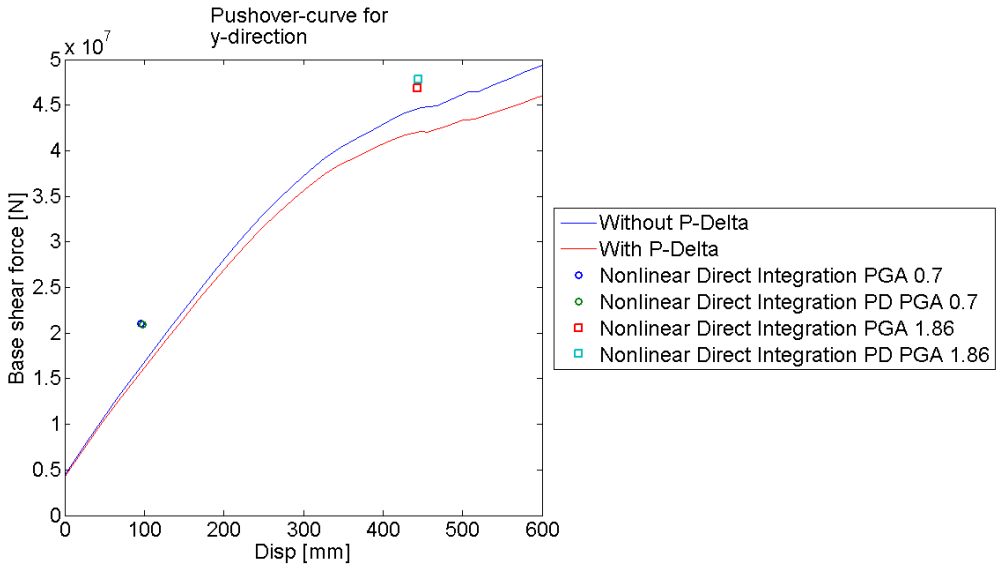

Figure 5.4: Pushover analysis in the y-direction compared to maximum values of displacement and base shear for the nonlinear direct integration time history analyses

As seen in these figures, the base shear for a specific displacement is generally higher for the time history analysis than it is for the same displacement in the pushover analysis. This has to do with the pushover analysis being a static analysis, whereas the time history analysis is a dynamic analysis. The base shear forces obtained from time history analysis will therefore have an added inertia force, or D'Alembert force, component and the absolute value of the force will naturally be larger than the one obtained from a static analysis.

The exception to this tendency is the x-direction results from nonlinear direct integration time history analysis with PGA 1.86 m/s^2. For these results, the base shear force from the dynamic analysis and the static analysis are far closer than in the other cases; the dynamic analysis actually results in a lower absolute value of the base shear force. This can be an indication that during dynamic analysis, plasticity in the x-direction is obtained for smaller displacements than would be expected from the static analysis results.

6 Concluding remarks

This thesis has focused on the analyses of a finite element model of Oslo Plaza using the analysis program SAP2000. This model was created from construction and architectural drawings of Oslo Plaza and several different types of analyses have been performed on the same model.

The natural periods and mode shapes of this model were calculated and compared to estimates of the natural periods. The impact of $P-\Delta$ effects on the natural periods were also discussed. The estimates of the eigenperiods were found to be very rough and it was concluded that these estimation techniques were not reliable for a system of this complexity. The $P-\Delta$ effect were found to have a bigger impact on the mode shapes with larger natural periods and the maximum differences between including and ignoring the $P-\Delta$ effects were found to be less than 4 %.

Ground motion data from three different earthquakes were used:

- the 1976 Friuly earthquake
- the 1985 Nahanni earthquake
- the 1987 Whittier earthquake

These acceleration time histories were scaled and modified to represent an expected earthquake in the Oslo area with a return period of 475 years. Modal time history analyses were performed on the FEM-model using load cases as described in Eurocode 8 for these earthquakes, and the Friuly records were found to give the largest responses for the building. These records were therefore used for the rest of the analyses performed. Linear direct integration time history analyses were performed and compared to the results from linear modal time history analyses. The two different types of analyses gave surprisingly different results when it came to maximum base shear forces, base moments and maximum displacements in the building. The results from the linear direct integration analysis were chosen as a basis for comparisons with later nonlinear analyses, while the results from the modal analysis were used for comparison with response spectrum analyses and to evaluate the effect of the swimming pool as a tuned liquid damper.

Modal pushover analyses were performed on the element model. From these analyses, it was concluded that plasticity was not expected in the building for smaller earthquakes, but for bigger earthquakes it is expected that plasticity occur in the longitudinal direction, when the displacement of the top-story reaches approximately 600 mm, while plasticity

is expected in the transverse direction when the top-story displacement in that direction reaches approximately 350 mm.

For response spectrum analyses performed according to EC8 with a ductility factor of $q = 1.0$, the maximum displacements, base shear forces and base moments were mostly larger than the ones obtained by modal time history analyses and this can therefore be assumed to be a conservative analysis method. The big advantage of this method is its simplicity and the very low calculation times. EC8 does allow for the use of a ductility factor of $q = 1.5$ for this type of building, but the results obtained from this analysis were found to be in the magnitude of 20 % smaller than the results obtained by the modal time history analysis and one should therefore be cautious to not set this factor too high.

Nonlinear direct integration time history analyses were performed on the model and the results were compared to the results obtained from linear direct integration time history analyses. As expected, there was found to be next to no nonlinearity in the building during an expected earthquake with a return period of 475 years in the Oslo area. The maximum displacement of the building for this type of earthquake is less than 100 mm, which has to be considered relatively small compared to the total height of the building.

Linear and nonlinear direct integration time history analyses were also performed for an expected earthquake in the Oslo area with a return period of 3000 years. For an earthquake of this size, displacements up to 700 mm were found and nonlinear effects can be expected to occur in the building, especially in the longitudinal direction of the building. Oslo Plaza should however still be safe from collapse even during an earthquake of this magnitude. The areas where plasticity is found to occur first in the building are in the lower stories of the shear walls and elevator shafts. These can therefore be considered weak spots, where the concrete might experience permanent deformations during an earthquake.

An interesting point discovered during the work with this thesis, is the possible behavior of the swimming pool in Oslo Plaza working as a liquid damper during earthquake excitation. With the dimensions of the pool, this effect is found to be next to non-existent, while it has been found that if the pool had been built only a few meters shorter, it could in fact reduce the longitudinal effects of an earthquake by as much as 25 %, especially as long as the behavior of the building is in the linear range.

$P-\Delta$ effects were found to have minimal influence on the behavior of the building during dynamic analyses. This conclusion is based on the differences in the obtained maximum base shear forces, base moments and displacements obtained from analyses with and without the inclusion of $P - \Delta$ effects.

7 Further work

This thesis has covered several of the most important aspects regarding response of a high-rise building during an earthquake. Different analysis methods have been compared and the effects of nonlinearity have been discussed.

This section provides suggestions for further work to better understand this area and better learn the seismic behavior of high-rise buildings in addition to earthquake design for Norwegian conditions.

- Perform continuous monitoring of the behavior of Oslo Plaza and other high-rise buildings with the use of accelerometers to better understand their true dynamic behavior. This can also better the understanding of the change in a structure's dynamic behavior over time.
- Obtain ground motion records for actual earthquakes in Norway and use these to perform FEM-analyses. This way one can control how accurate the modifications make the acceleration time histories represent Norwegian conditions in addition to providing statistical better insight into how high-rise buildings will behave during earthquakes representative for Norway.
- Model the actual ground conditions in the FEM-model to better understand how accurate the soil amplification factor provided by the Eurocode is.
- Perform seismic design of alternative structural systems in accordance with EC8 and compare to the structural system in Oslo Plaza.
- Monitor the dynamic behavior of the swimming pool and compare these results to the properties obtained using the theory explained in this thesis.

References

[1] NORSAR and Norwegian Geotechnical Institute. *Seismic Zonation of Norway*.

[2] Steven L. Kramer. *Geotechnical Earthquake Engineering*. Prentice Hall, 1996.

[3] Ray W. Clough and Joseph Penzien. *Dynamics of Structures*. McGraw-Hill Education, 2003.

[4] Edward J. Tarbuck and Frederick K. Lutgens. *Earth*. 10th ed. Prentice Hall, 2011.

[5] NORSAR. *jordskjelv.no: Seismiske bølger*. 2010. URL: http://www.jordskjelv.no/jordskjelv/bolger.html.

[6] Athol Carr. *Seminar on earthquake engineering*.

[7] Standard Norge. *Eurocode 8: Design of structures for earthquake resistance - Part 1: General rules, seismic actions and rules for buildings*.

[8] Eduardo Kausel. *Advanced Structural Dynamics*. MIT Copytech, 2009.

[9] Anil K. Chopra. *Dynamics of Structures*. Prentice Hall, 2011.

[10] Yun Zhao, Hua Wei, and Haijun Wang. "Simulation of Earthquake Response of High-rise Structure". In: *2nd International Conference on Electronic & Mechanical Engineering and Information Technology (EMEIT-2012)*. 2012.

[11] Edward L. Wilson. *Three-Dimensional Static and Dynamic Analysis of Structures*. Computers and Structures Inc, 2000.

[12] E. L. Wilson and A. Habibullah. "Static and Dynamic Analysis of Multi-Story Buildings Including P-Delta Effects". In: *Earthquake Spectra* 3 (1987).

[13] Karin Harnæs Hoel and Bjørn Thomas Svendsen. "The Effects of Near-fault Earthquakes On a High-rise Structure In The Oslo Area". MA thesis. NTNU. 2012.

[14] Hugo Bachmann. *Seismic Conceptual Design of Buildings – Basic principles for engineers, architects, building owners, and authorities*. Swiss Federal Office for Water and Geology, 2002.

[15] C. C. Chang and C. T. Hsu. "Control performance of liquid column vibration absorbers". In: *Engineering Structures* (1998).

[16] H. Gao and K. C. S. Kwok. "Optimization of tuned liquid column dampers". In: *Engineering Structures* (1997).

[17] Yukio Tamura et al. "Effectiveness of tuned liquid dampers under wind excitation". In: *Engineering Structures* (1995).

[18] Toshihiro Wakahara and Yoso Fujino. “A simple estimation of across-wind response of tall buildings with tuned liquid damper”. In: *Wind Engineering* (1998).

[19] E. W. Graham and A. M. Rodriguez. “‘The Characteristics of Fuel Motion Which Affect Airplane Dynamics”. In: *Journal of Applied Mechanics* (1952).

[20] Dorothy Reed et al. “Tuned liquid dampers under large amplitude excitation”. In: *Journal of Wind Engineering and Industrial Aerodynamics* (1998).

[21] L. M. Sun et al. “The Properties of Tuned Liquid Dampers using a TMD Analogy”. In: *Earthquake Engineering and Structural Dynamics* (1995).

[22] Linda Al Atik and Norman Abrahamson. “An Improved Method for Nonstationary Spectral Matching”. In: *Earthquake Spectra* (2010).

[23] N. A. Abrahamson. “Non-stationary Spectral Matching”. In: *Seismological Research Letters* (1992).

[24] G. T. Hahn, V. Bhargava, and Q. Chen. “The Cyclic Stress-Strain Properties, Hysteresis Loop Shape, and Kinematic Hardening of Two High-Strength Bearing Steels”. In: *Metallurgical Transactions* 21A (1990).

[25] Viviana Iris Novelli. “The Unloading Stiffness of Reinforced Concrete Members”. MA thesis. Università degli Studi di Pavia. 2008.

[26] R. D. Cook et al. *Concepts and Applications of Finite Element Analysis*. 4th ed. John Wiley & Sons, Inc, 2002.

[27] Computers and Structures Inc. *CSI Analysis Reference Manual For SAP2000®, ETABS®, SAFE® and CSiBridge™*.

[28] Klaus-Jürgen Bathe. *Finite Elements Procedures*. Prentice Hall, 1996.

[29] Y. M. Fahjan, J. Kubin, and M. T. Tan. “Nonlinear Analysis Methods for Reinforced Concrete Buildings with Shear walls”. In: *14th European Conference on Earthquake Engineering* (2010).

[30] Ashraf Habibullah and Stephen Pyle. “Practical Three Dimensional Nonlinear Static Pushover Analysis”. In: *Structure Magazine* (1998).

[31] Juan C. Reyes and Anil K. Chopra. “Three-dimensional Modal Pushover Analysis of Buildings subjected to two Components of Ground Motion, including its Evaluation for tall Buildings”. In: *Earthquake Engineering and Structural Dynamics* (2010).

A Matlab script to scale acceleration time histories

A.1 Main script

```
clc
close all
clear all

%%%%%%%%%%%%%%%%%%%%%%%%%%%%%%%%Input%%%%%%%%%%%%%%%%%%%%%%%%%%%%%%%%%%%%%%%%
Oslo_PGA = 0.7; %Desired PGA
%%%%%%%%%%%%%%%%%%%%%%%%%%%%%%%%%%%%%%%%%%%%%%%%%%%%%%%%%%%%%%%%%%%%%%%%%%%%%

%Reads time history data from text files
nahanni_NS = read_txt('recordhoeg1a.txt');
nahanni_EW = read_txt('recordhoeg1b.txt');
nahanni_V = read_txt('recordhoeg1c.txt');
nahanni_dt = 0.02;

whittier_NS = read_txt('recordhoeg2c.txt');
whittier_EW = read_txt('recordhoeg2a.txt');
whittier_V = read_txt('recordhoeg2b.txt');
whittier_dt = 0.02;

friuly_NS = read_txt('recordhoeg3a.txt');
friuly_EW = read_txt('recordhoeg3b.txt');
friuly_V = read_txt('recordhoeg3c.txt');
friuly_dt = 0.01;

%Finds the peak ground acceleration for the earthquakes
nahanni_PGA = PGA(nahanni_NS,nahanni_EW,nahanni_V);
whittier_PGA = PGA(whittier_NS,whittier_EW,whittier_V);
friuly_PGA = PGA(friuly_NS,friuly_EW,friuly_V);

%Scales the earthquakes to the desired PGA
nahanni_NS = (Oslo_PGA/nahanni_PGA).*nahanni_NS;
nahanni_EW = (Oslo_PGA/nahanni_PGA).*nahanni_EW;
nahanni_V = (Oslo_PGA/nahanni_PGA).*nahanni_V;

whittier_NS = (Oslo_PGA/whittier_PGA).*whittier_NS;
whittier_EW = (Oslo_PGA/whittier_PGA).*whittier_EW;
whittier_V = (Oslo_PGA/whittier_PGA).*whittier_V;
```

```
friuly_NS = (Oslo_PGA/friuly_PGA).*friuly_NS;
friuly_EW = (Oslo_PGA/friuly_PGA).*friuly_EW;
friuly_V = (Oslo_PGA/friuly_PGA).*friuly_V;

%Creates a vector containing the time in seconds for the time history
%and prints the time vector and time history to a file
nahanni_NS_t = find_t(nahanni_NS,nahanni_dt);
TS1=[nahanni_NS_t' nahanni_NS]; save Nahanni_NS.file TS1 –ASCII;
nahanni_EW_t = find_t(nahanni_EW,nahanni_dt);
TS2=[nahanni_EW_t' nahanni_EW]; save Nahanni_EW.file TS2 –ASCII;
nahanni_V_t = find_t(nahanni_V,nahanni_dt);
TS3=[nahanni_V_t' nahanni_V]; save Nahanni_V.file TS3 –ASCII;

whittier_NS_t = find_t(whittier_NS,whittier_dt);
TS4=[whittier_NS_t' whittier_NS]; save Whittier_NS.file TS4 –ASCII;
whittier_EW_t = find_t(whittier_EW,whittier_dt);
TS5=[whittier_EW_t' whittier_EW]; save Whittier_EW.file TS5 –ASCII;
whittier_V_t = find_t(whittier_V,whittier_dt);
TS6=[whittier_V_t' whittier_V]; save Whittier_V.file TS6 –ASCII;

friuly_NS_t = find_t(friuly_NS,friuly_dt);
TS7=[friuly_NS_t' friuly_NS]; save Friuly_NS.file TS7 –ASCII;
friuly_EW_t = find_t(friuly_EW,friuly_dt);
TS8=[friuly_EW_t' friuly_EW]; save Friuly_EW.file TS8 –ASCII;
friuly_V_t = find_t(friuly_V,friuly_dt);
TS9=[friuly_V_t' friuly_V]; save Friuly_V.file TS9 –ASCII;
```

A.2 Function *read_txt.m*

```
function ats = read_txt(txtname)
%Reads acceleration time histories from .txt files
%Input: txtname = the name of the .txt file
%Output: ats = a vector containing the time history value

A = fopen(txtname);
ats = textscan(A,'%f');
ats=ats{1};
fclose(A);

end
```

A.3 Function *PGA.m*

```
function pga = PGA(A,B,C)
%Finds the peak ground acceleration for an earthquake
%Input:     A:      time history in the North-south direction
%           B:      time history in the East-west direction
%           C:      time history in the Vertical direction
%Output:    pga:    the peak ground acceleration of the earthquake

maxA = max(A);
minA = abs(min(A));

maxB = max(B);
minB = abs(min(B));

maxC = max(C);
minC = abs(min(C));

maxes = [maxA,minA,maxB,minB,maxC,minC];

pga = max(maxes);

end
```

A.4 Function *find_t.m*

```
function t = find_t(A,dt)
%Creates a vector containing the time in seconds for the time history
%Input:     A:  Acceleration time history
%           dt: Time increment for the measurements
%Output:    t:  the time vector

maxtA = dt*(length(A)-1);
t=linspace(0,maxtA,length(A));

end
```

B Script for generating and plotting response spectra

```
%This script uses Newmarks Method to make a response spectrum. It
%also compares to the EC8 Response Spectrum.
clear all
clc
close all
% Importing data for the provided earthquake record.
input_txt
% Naming the earthquake for plotting later
quake_name = 'Friuly';
% Setting the font size for plots
f_size = 14;

% Defining variables
t_NS = friuly_NS_t;
P_NS = friuly_NS;
t_EW = friuly_EW_t;
P_EW = friuly_EW;
t_Z = friuly_V_t;
P_Z = friuly_V;
M = 1; gam = 0.5; beta = 0.25;
u0 = 0; udot0 = 0;
ksi = 0.05;
Tn = [0:0.01:5];
% Running Newmarks Method to generate response spectrum
for i = 1:length(Tn)
C = (2*ksi)*((2*pi)/Tn(i));
K = (2*pi/Tn(i))^2;
u_NS = Newmark_Method(t_NS,M,C,K,P_NS,gam,beta,u0,udot0);
u_EW = Newmark_Method(t_EW,M,C,K,P_EW,gam,beta,u0,udot0);
u_Z = Newmark_Method(t_Z,M,C,K,P_Z,gam,beta,u0,udot0);
PGD_NS(i) = abs(max(u_NS));
PGD_EW(i) = abs(max(u_EW));
PGD_Z(i) = abs(max(u_Z));
PGA_NS(i) = ((2*pi/Tn(i))^2)*PGD_NS(i);
PGA_EW(i) = ((2*pi/Tn(i))^2)*PGD_EW(i);
PGA_Z(i) = ((2*pi/Tn(i))^2)*PGD_Z(i);
end
```

```
% Creating the horizontal EC8 Response Spectrum
ag_40Hz = 0.55;
ag_R = 0.8*ag_40Hz;
vy_1 = 1.0;
ag = ag_R;
S = 1.6;
q = 1.0; % q can be set to a desired value here.
beta2 = 0.20;
Tb = 0.15; Tc = 0.45; Td = 1.50;
Sd = zeros(1,length(Tn));
% Calculating the horizontal elastic EC8 response spectrum
for j = 1:length(Tn)
if (Tn(j) >= 0) && (Tn(j) <= Tb)
Sd(j) = ag*S*((2/3) + ((Tn(j)/Tb)*((2.5/q)−(2/3))));
elseif (Tn(j) >= Tb) && (Tn(j) <= Tc)
Sd(j) = ag*S*(2.5/q);
elseif (Tn(j) >= Tc) && (Tn(j) <= Td)
Sd(j) = ag*S*(2.5/q)*(Tc/Tn(j));
if (Sd(j) <= (beta2*ag))
Sd(j) = beta2*ag;
end
else
Sd(j) = ag*S*(2.5/q)*((Tc*Td)/(Tn(j)^2));
if (Sd(j) <= (beta2*ag))
Sd(j) = beta2*ag;
end
end
end
% Calculating the vertical elastic EC8 response spectrum
a_vg = 0.6*ag;
vy_1 = 1.0;
S_vg = 1.0;
q_vg = 1.0; % q can be set to a desired value here.
beta2_vg = 0.20;
Tb_v = 0.05; Tc_v = 0.20; Td_v = 1.20;
S_ve = zeros(1,length(Tn));
for j = 1:length(Tn)
if (Tn(j) >= 0) && (Tn(j) <= Tb_v)
S_ve(j) = a_vg*S_vg*((2/3) + ((Tn(j)/Tb_v)*((2.5/q_vg)− (2/3))));
elseif (Tn(j) >= Tb_v) && (Tn(j) <= Tc_v)
S_ve(j) = a_vg*S_vg*(2.5/q_vg);
elseif (Tn(j) >= Tc_v) && (Tn(j) <= Td_v)
S_ve(j) = a_vg*S_vg*(2.5/q_vg)*(Tc_v/Tn(j));
if (S_ve(j) <= (beta2_vg*a_vg))
S_ve(j) = beta2_vg*a_vg;
```

```
end
else
S_ve(j) = a_vg*S_vg*(2.5/q_vg)*((Tc_v*Td_v)/(Tn(j)^2));
if (S_ve(j) <= (beta2_vg*a_vg))
S_ve(j) = beta2_vg*a_vg;
end
end
end

% Plotting the horizontal response spectrum comparison
figure(1)
%hold on
plot(Tn,PGA_NS,'b',Tn,PGA_EW,'r',Tn,Sd,'k')
%plot(Tn,Sd,'color',[0.765,0.765,0.765]);
title('Horizontal response spectrum comparison')
xlabel('Natural vibration period, T_n [s]');
ylabel('Acceleration, A [m/s^2]');
xlim([0 4]);
ylim([0 8]);
legend(['NS-component ' quake_name],['EW-component ' quake_name]...
,'EC8 Response Spectrum')
set(legend,'box','off')
set(findall(gcf,'type','axes'),'fontsize',f_size)
set(findall(gcf,'type','text'),'fontSize',f_size)
% Plotting the vertical response spectrum comparison
figure(2)
%hold on
plot(Tn,PGA_Z,'g',Tn,S_ve,'k')
%plot(Tn,Sd,'color',[0.765,0.765,0.765]);
title('Vertical response spectrum comparison')
xlabel('Natural vibration period, T_n [s]');
ylabel('Acceleration, A [m/s^2]');
xlim([0 4]);
ylim([0 2.5]);
legend(['Vertical-component ' quake_name],'EC8 Response Spectrum')
set(legend,'box','off')
set(findall(gcf,'type','axes'),'fontsize',f_size)
set(findall(gcf,'type','text'),'fontSize',f_size)
% Plotting the response spectrum for the earthquake
figure(3)
plot(Tn,PGA_NS,'b',Tn,PGA_EW,'r',Tn,PGA_Z,'g')
title(['Response spectrum ' quake_name ' earthquake'])
xlabel('Natural vibration period, T_n [s]');
ylabel('Acceleration, A [m/s^2]');
xlim([0 4]);
```

```
ylim([0 8]);
legend('NS-component','EW-component','Vertical-component')
set(legend,'box','off')
set(findall(gcf,'type','axes'),'fontsize',f_size)
set(findall(gcf,'type','text'),'fontSize',f_size)
% Plotting the EC8 Horizontal response spectrum
figure(4)
plot(Tn,Sd)
title('Horizontal elastic reponse spectrum EC8')
xlabel('Natural vibration period, T_n [s]');
xlim([0 4]);
ylim([0 2]);
ylabel('Acceleration, A [m/s^2]');
set(findall(gcf,'type','axes'),'fontsize',f_size)
set(findall(gcf,'type','text'),'fontSize',f_size)
% Plotting the EC8 Vertical response spectrum
figure(5)
plot(Tn,S_ve)
title('Vertical elastic response spectrum EC8')
xlabel('Natural vibration period, T_n [s]');
ylabel('Acceleration, A [m/s^2]');
xlim([0 4]);
ylim([0 2]);
set(findall(gcf,'type','axes'),'fontsize',f_size)
set(findall(gcf,'type','text'),'fontSize',f_size)
```

The function for Newmark's method

```
function u = Newmark_Method(t,M,C,K,P,gamma,beta,u0,udot0)
% Uses the Newmarks Direct Integration Method to find the displacement
% at each time-step for a 1-DOF system

% Input:    t: Time vector [1,n]
%           M: Mass matrix [1,1]
%           C: Damping matrix [1,1]
%           K: Stiffness matrix [1,1]
%           P: load vs. time [1,n]
%           gamma: Gamma (constant)
%           beta: Beta (constant)
%           u0: Initial displacements
%           udot0: Initial velocity
% Output:   u = Displacement Response [n,1], where n= number of time steps
```

```
% beta = 0, gamma = 1/2 -> explicit central difference method
% beta = 1/4, gamma = 1/2 -> undamped trapezoidal rule (implicit)
% Initial conditions
u = u0;
udot = udot0;
u2dot = (P(1) - (C*udot0) - (K*u0))/M;
dt = t(2) - t(1);
k_hat = K + (gamma*C)/(beta*dt) + M/(beta*(dt^2));
a = M/(beta*dt) + (gamma*C)/beta;
b = M/(2*beta) + (dt*C)*((gamma/(2*beta))-1);
% Calculations of the displacement, velocity and acceleration for each
% time-step, i
for i = 1:(length(t)-1)
dP = (P(i+1)-P(i)) + (a*udot) + (b*u2dot);
du_i = dP/k_hat;
dudot_i = ((gamma*du_i)/(beta*dt)) - ((gamma*udot)/beta)...
    + ((dt*u2dot)*(1-(gamma/(2*beta))));
du2dot_i = (du_i/(beta*(dt^2))) - (udot/(beta*dt)) - (u2dot/(2*beta));
u(i+1) = du_i + u(i);
udot = dudot_i + udot;
u2dot = du2dot_i + u2dot;
end
```

C Calculation of mass and second moment of inertia

In this section, the mass and and second moments of inertia used in the estimations of natural periods described in section 4.2 are calculated.

Calculation of mass of one story

It is assumed that the mass of each story consists of the mass of one slab, m_s, and walls, m_w. It is also assumed that each story is 2.75 m high, as this is the height of the majority of stories in the building.

The mass of each slab is calculated as

$$m_s = t_s \cdot x \cdot y \cdot \rho_{conc} \tag{C.1}$$

where t_s is the thickness of the slab, x the length of the slab, y the width of the slab and ρ_{conc} is the density of concrete.

$$m_s = 0.22m \cdot 54m \cdot 19m \cdot 2550kg/m^3 \approx 575\,000kg \tag{C.2}$$

The mass of the walls are calculated as

$$m_w = t_w \cdot y \cdot h_w \cdot \rho_{conc} \cdot n_w \tag{C.3}$$

where t_w is the thickness of one wall, h_w is the height on one story and n_w is the number of walls. n_w is chosen as 6 to account for shear walls and elevator shafts.

$$m_w = 0.3m \cdot 19m \cdot 2.75m \cdot 2550kg/m^3 \cdot 6 \approx 240\,000kg \tag{C.4}$$

This gives a total mass of each story equal to

$$m_{tot} = m_s + m_w = 815\,000kg \tag{C.5}$$

Calculation of second moment of inertia

The second moment of inertia around the x-axis, I_x has contributions from the shear walls and the elevator shafts in the x- and y-direction. The contribution from the shear walls are given by

$$I_1 = 4(\frac{1}{12} \cdot 0.3m \cdot (19m)^3) \approx 690m^4 \tag{C.6}$$

The contributions from the elevator shafts are calculated as

$$I_2 = 4(\frac{1}{12} \cdot 8m \cdot (0.25m)^3 + 0.25m \cdot 8m \cdot (6.5m)^2) \approx 340m^4 \tag{C.7}$$

$$I_3 = 12(\frac{1}{12} \cdot 0.2m \cdot (3m)^3 + 0.2m \cdot 3m \cdot (3m)^2) \approx 70m^4 \tag{C.8}$$

This gives a total estimated second moment of inertia around the x-axis of

$$I_x = I_1 + I_2 + I_3 = 1100mm^4 \tag{C.9}$$

The second moment of inertia around the y-axis, I_y has contributions from the shear walls and from the elevator shafts. The contributions from the shear walls are given by

$$I_1 = 2(\frac{1}{12} \cdot 19m \cdot (0.3m)^3 + 19m \cdot 0.3m \cdot (12m)^2) \approx 1640m^4 \tag{C.10}$$

$$I_2 = 2(\frac{1}{12} \cdot 19m \cdot (0.3m)^3 + 19m \cdot 0.3m \cdot (19m)^2) \approx 4110m^4 \tag{C.11}$$

The contribution from the elevator shafts can be calculated as

$$I_3 = 4(\frac{1}{12} \cdot 8m \cdot (0.25m)^3 + 8m \cdot 0.25m \cdot (5m)^2 \approx 200m^4 \tag{C.12}$$

The total second moment of inertia around the y-axis is then

$$I_y = I_1 + I_2 + I_3 = 5950m^4 \tag{C.13}$$

D Script for interpolating expected PGAs based on return periods

```
clc
clear all
close all

%Setting the text size
f_size = 14;

%Input
RP = [475 1000 10000]; %Return periods[years]
PGA = [0.55 0.85 2.50]; %Peak ground accelerations
year = 3000; %Return period for which we want to find the PGA

%Interpolation
years = 475:25:10000;
PGAs = interp1(RP,PGA,years,'pchip');
wantedPGA = interp1(RP,PGA,year,'pchip');

%Printing the result to screen
fprintf(['For a return period of %d years the expected PGA is %4.2f ',...
    'm/s^2\n'],year,wantedPGA);

%Plotting the result
figure
hold on
plot(RP,PGA,'bs','MarkerSize',7,'MarkerFaceColor','b')
plot(years,PGAs,'g-','LineWidth',2)
plot(year,wantedPGA,'ro','MarkerSize',7,'MarkerFaceColor','r')
title('Interpolation curve for PGAs with different return periods')
legend('Original data','Fitted curve',...
    ['PGA with return \newline period ',num2str(year),' years'],...
    'Location','SouthEast');
xlabel('Return period')
ylabel('PGA [m/s^2]')
grid on
set(findall(gcf,'type','axes'),'fontsize',f_size)
set(findall(gcf,'type','text'),'fontSize',f_size)
hold off
```

E Matlab script to calculate frequency spectrum of input time histories

```
clc
clear all
close all

% Setting the text size
f_size = 14;

% Input
filename = 'Modified_Friuly.xlsx';
direction = {'Friuly EW\newlinecomponent',...
    'Friuly NS\newlinecomponent'};
PGA = 'PGA: 0.7m/s^2';
dt = 0.01;
limy = [0 0.025];
limx = [0 10];
npeaks = 20;
Tn = [3.99 3.36]; % Natural frequencies of the building


% Defining variables
fs = 1./dt;
fn = [1/Tn(1) 1/Tn(1) 1/Tn(2) 1/Tn(2)];

% Input from excel
sheet = 1;
tmp1 = xlsread(filename,sheet);
sheet = 2;
tmp2 = xlsread(filename,sheet);
[n(1), m(1)] = size(tmp1);
[n(2), m(2)] = size(tmp2);
nmax = max(n);
data = zeros(nmax,4);
data(1:n(1),1:2) = tmp1;
data(1:n(2),3:4) = tmp2;


for k = 1:2
    % Calculating the spectral density
```

```
    num = n(k);
    acc = data(1:num,2*k);
    nyf = fs/2;
    f = linspace(0,nyf,num/2);
    aVf = acc - mean(acc);
    fftavf = (2*(fft(aVf)))/num;
    ck = abs(fftavf);

    % Plotting the spectral density against frequency
    figure(1)
    plot(f,ck(1:num/2,:))
    hold all
    title(['Frequency spectrum ','\newline',PGA,...
        '\newlineinput time history'])
    xlim(limx);
    ylim(limy);
    xlabel('Frequency, f [Hz]')
    ylabel('Sprectral density, S_x')
    legend(direction,'Location','NorthEast')
    set(legend,'box','off');
    set(findall(gcf,'type','axes'),'fontsize',f_size)
    set(findall(gcf,'type','text'),'fontSize',f_size)

    % Zoomed in plot
    figure(2)
    plot(f,ck(1:num/2,:))
    hold all
    title(['Frequency spectrum ','\newline',PGA,...
        '\newlineinput time history\newline'])
    xlim([0 0.5]);
    ylim(limy);
    xlabel('Frequency, f [Hz]')
    ylabel('Sprectral density, S_x')


%Finding peaks and corresponding values to render eigenfrequencies
    [pks,loks] = findpeaks(ck(1:num/2),'npeaks',npeaks,...
        'SORTSTR','descend');
    frek(:,k) = f(loks);

% Displaying data
    fprintf(['The first %d peaks of the ',...
        direction{k},' input time history are:\n'],npeaks)
    for j = 1:npeaks
        fprintf(['%4.2fs\n'],1/frek(j,k))
```

```
    end
    fprintf('\n')
end

% Plotting the two first natural periods of the building
figure(2)
plot(fn(1:2),limy,'r--',fn(3:4),limy,'r--')
legend([direction,'Natural frequencies\newlineof the building'],...
    'Location','NorthEastOutside')
set(legend,'box','off');
set(findall(gcf,'type','axes'),'fontsize',f_size)
set(findall(gcf,'type','text'),'fontSize',f_size)

hold off
```

F Section stresses in shear walls and elevator shaft during nonlinear direct integration time history analysis and pushover analysis

F.1 Nonlinear direct integration time history analysis with PGA 0.7 m/s^2

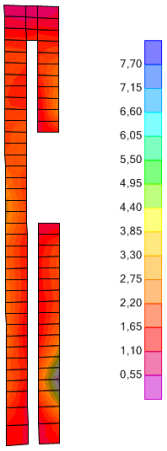

(a) Max stresses in the concrete in the x-direction $[MPa]$

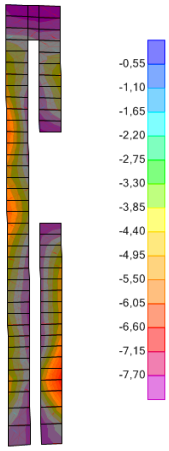

(b) Min stresses in the concrete in the x-direction $[MPa]$

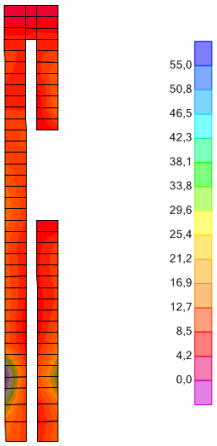

(c) Max stresses in the rebar in the x-direction $[MPa]$

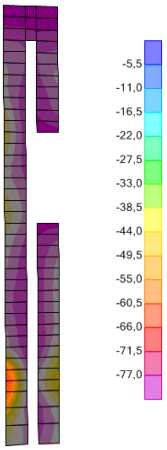

(d) Min stresses in the rebar in the x-direction $[MPa]$

Figure F.1: Maximum and minimum stresses in the concrete and rebar in the x-direction for nonlinear direct integration time history analysis with PGA 0.7 m/s^2

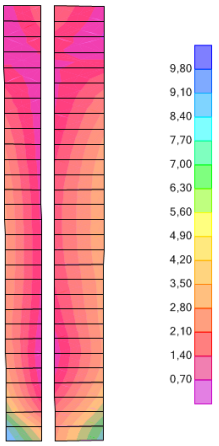

(a) Max stresses in the concrete in the y-direction $[MPa]$

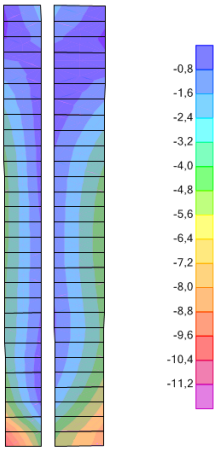

(b) Min stresses in the concrete in the y-direction $[MPa]$

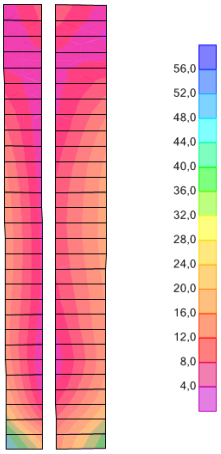

(c) Max stresses in the rebar in the y-direction $[MPa]$

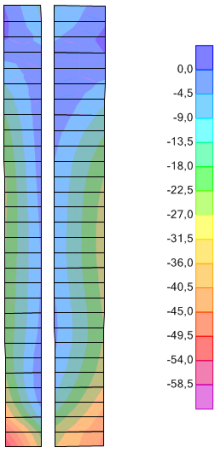

(d) Min stresses in the rebar in the y-direction $[MPa]$

Figure F.2: Maximum and minimum stresses in the concrete and rebar in the y-direction for nonlinear direct integration time history analysis with PGA 0.7 m/s^2

F.2 Nonlinear direct integration time history analysis with PGA 1.86 m/s^2

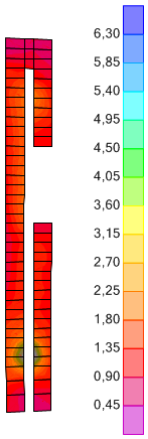

(a) Max stresses in the concrete in the x-direction $[MPa]$

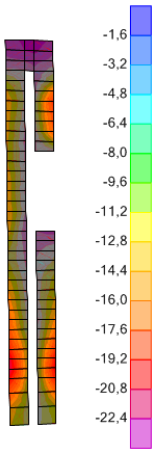

(b) Min stresses in the concrete in the x-direction $[MPa]$

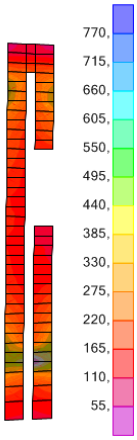

(c) Max stresses in the rebar in the x-direction $[MPa]$

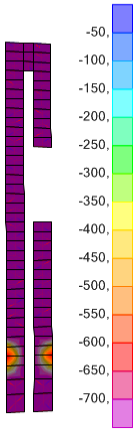

(d) Min stresses in the rebar in the x-direction $[MPa]$

Figure F.3: Maximum and minimum stresses in the concrete and rebar in the x-direction for nonlinear direct integration time history analysis with PGA 1.86 m/s^2

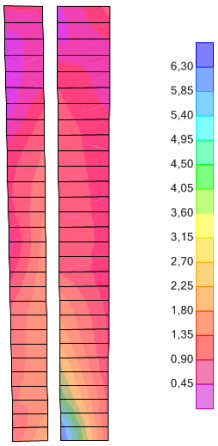

(a) Max stresses in the concrete in the y-direction $[MPa]$

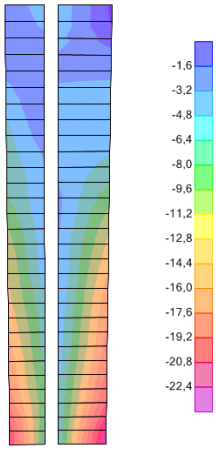

(b) Min stresses in the concrete in the y-direction $[MPa]$

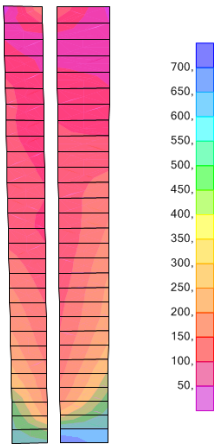

(c) Max stresses in the rebar in the y-direction $[MPa]$

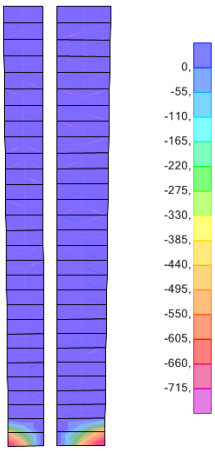

(d) Min stresses in the rebar in the y-direction $[MPa]$

Figure F.4: Maximum and minimum stresses in the concrete and rebar in the y-direction for nonlinear direct integration time history analysis with PGA 1.86 m/s^2

F.3 Pushover analysis

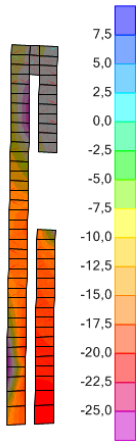

(a) Max stresses in the concrete in the x-direction $[MPa]$

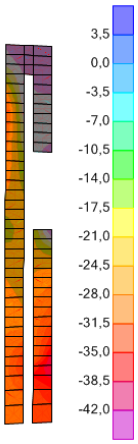

(b) Min stresses in the concrete in the x-direction $[MPa]$

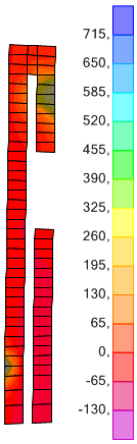

(c) Max stresses in the rebar in the x-direction $[MPa]$

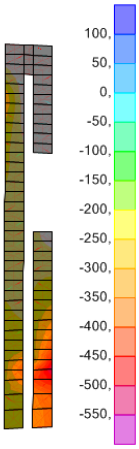

(d) Min stresses in the rebar in the x-direction $[MPa]$

Figure F.5: Maximum and minimum stresses in the concrete and rebar in the x-direction for pushover analysis

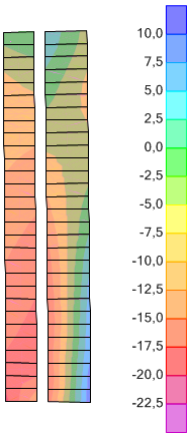

(a) Max stresses in the concrete in the y-direction $[MPa]$

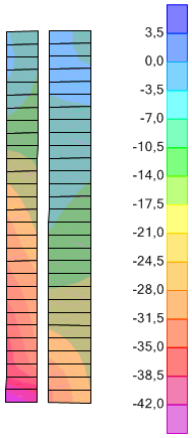

(b) Min stresses in the concrete in the y-direction $[MPa]$

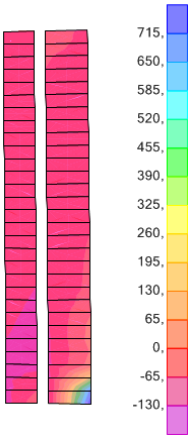

(c) Max stresses in the rebar in the y-direction $[MPa]$

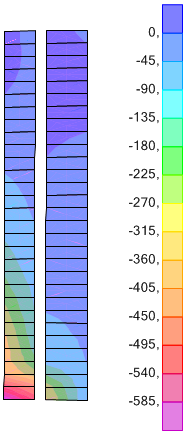

(d) Min stresses in the rebar in the y-direction $[MPa]$

Figure F.6: Maximum and minimum stresses in the concrete and rebar in the y-direction for pushover analysis

G Matlab script to calculate frequency spectrum of roof displacements over time

```
clc
clear all
close all

% Setting the text size
f_size = 14;

% Input
filename = 'ComparisonPGA0.7.xlsx';
direction = 'y';
case_num = [1 2 3];
PGA = 'PGA: 0.7m/s^2';
dt = [0.01 0.05 0.05];
limy = 50;


for k = 1:length(case_num)
    if dt(k) == 0.05
        steps(k) = 698;
    else steps(k) = 4998;
    end
end


% Defining variables
fs = 1./dt;

% Input from excel
if direction == 'x'
    sheet = 4;
elseif direction == 'y'
    sheet = 5;
else
    return
end
[tmpx, case_name] = xlsread(filename,sheet);
```

```
for k = 1:length(case_num)
    disp = tmpx(1:steps(k),case_num(k));
    [n, m] = size(disp);
    nyf = fs(k)/2;
    f = linspace(0,nyf,n/2);
    aVf = disp - mean(disp);
    fftavf = (2*(fft(aVf)))/n;
    ck = abs(fftavf);

    plot(f,ck(1:n/2,:))
    hold all
    title(['Frequency spectrum ','\newline',PGA,'\newline',direction,...
        '-direction'])
    xlim([0 1]);
    ylim([0 limy]);
    xlabel('Frequency, f [Hz]')
    ylabel('Sprectral density, S_x')
    legend(case_name{case_num},'Location','NorthEast')
    set(legend,'box','off');
    set(findall(gcf,'type','axes'),'fontsize',f_size)
    set(findall(gcf,'type','text'),'fontSize',f_size)

%Finding peaks and corresponding values to render eigenfrequencies
    [pks,loks] = findpeaks(ck(1:n/2),'minpeakdistance',10,'npeaks',1,...
        'SORTSTR','descend');
    frek(k) = f(loks);

% Displaying data
    fprintf(['The first natural period in the ',direction,...
        '-direction is %4.2fs\n'],1/frek(k))
end
hold off
```